UNIVERSIDAD DE ALCALÁ

Escuela Politécnica Superior

Departamento de Electrónica

Programa de Doctorado: Sistemas Electrónicos Avanzados. Sistemas Inteligentes

Tesis Doctoral

Estimation of Real Traffic Radiated Emissions from Electric Vehicles in terms of the Driving Profile using Neural Networks

Autor:

Ahmed Mohamed Wefky Elhadi Elezzazy

Director:

Dr. Felipe Espinosa Zapata

Madrid, España

2013

UNIVERSITY OF ALCALA

Higher Polytechnics School

Department of Electronics

PhD Program: Electronics: Advanced Electronic Systems. Intelligent Systems

PhD THESIS

Estimation of Real Traffic Radiated Emissions from Electric Vehicles in terms of the Driving Profile using Neural Networks

Author:

Ahmed Mohamed Wefky Elhadi Elezzazy

Supervisor:

Dr. Felipe Espinosa Zapata

<u>Committee:</u>

President: ……..

Secretary:……

Vocal 1: ……..

Vocal 2: …… ……

Vocal 3:……..

QUALIFICATION **DATE**

…….. ……..

DEPARTAMENTO DE ELECTRÓNICA
Campus Universitario s/n
28805 Alcalá de Henares (Madrid)
Teléfono: 918856540
Fax: 918856591

DEPARTAMENTO DE ELECTRÓNICA

Dr. Felipe Espinosa Zapata, Profesor Titular de la Universidad de Alcalá

INFORMA: Que la Tesis Doctoral titulada "Estimation of real traffic radiated emissions from electric vehicles in terms of the driving profile using neural networks", presentada por Ahmed Mohamed Wefky Elhadi Elezzazy, y realizada bajo mi dirección, reúne los méritos de calidad y originalidad para optar al Grado de Doctor.

Alcalá de Henares, a..... de..... de 2013

Fdo.: Dr. Felipe Espinosa Zapata

DEPARTAMENTO DE ELECTRÓNICA
Campus Universitario s/n
28805 Alcalá de Henares (Madrid)
Teléfono: 918856540
Fax: 918856591

DEPARTAMENTO DE ELECTRÓNICA

Dra. Sira E. Palazuelos Cagigas, Directora del Departamento de Electrónica de la Universidad de Alcalá

INFORMA: Que la Tesis Doctoral titulada "Estimation of real traffic radiated emissions from electric vehicles in terms of the driving profile using neural networks", presentada por Ahmed Mohamed Wefky Elhadi Elezzazy, y dirigida por el Dr. Felipe Espinosa Zapata, cumple con todos los requisitos científicos y metodologías para ser defendida ante un tribunal.

Alcalá de Henares, a …… de…… de 2013

Fdo.: Dra. Sira E. Palazuelos Cagigas

Abstract

The increment of the use of electric vehicles leads to a worry about measuring its principal source of environmental pollution: electromagnetic emissions. Given the complexity of directly measuring vehicular radiated emissions in real traffic, the main contribution of this PhD thesis is to propose an indirect solution to estimate such type of vehicular emissions. Relating the on-road vehicular radiated emissions with the driving profile is a complicated task. This is because it is not possible to directly measure the vehicular radiated interferences in real traffic due to potential interferences from another electromagnetic wave sources. This thesis presents a microscopic artificial intelligence model based on neural networks to estimate real traffic radiated emissions of electric vehicles in terms of the driving dynamics. Instantaneous values of measured speed and calculated acceleration have been used to characterize the driving profile. Experimental electromagnetic interference tests have been carried out with a Vectrix electric motorcycle as well as Twizy electric cars in semi-anechoic chambers. Both the motorcycle and the car have been subjected to different urban and interurban driving profiles. Time Domain measurement methodology of electromagnetic radiated emissions has been adopted in this work to save the overall measurement time. The relationship between the magnetic radiated emissions of the Twizy and the corresponding speed has been very noticeable. Maximum magnetic field levels have been observed during high speed cruising in extra-urban driving and acceleration in urban environments. A comparative study of the prediction performance between various static and dynamic neural models has been introduced. The Multilayer Perceptron feedforward neural network trained with Extreme Learning Machines has achieved the best estimation results of magnetic radiated disturbances as function of instantaneous speed and acceleration. In this way, on-road magnetic radiated interferences from an electric vehicle equipped with a Global Positioning System can be estimated. This research line will allow quantify the pollutant electromagnetic emissions of electric vehicles and study new policies to preserve the environment.

Acknowledgments

I am deeply indebted to the Spanish Ministry of Education for funding the work presented in this thesis through a four-year FPU scholarship.

The results obtained from this work would not have been possible without the scientific guidance of Dr. Felipe Espinosa and technical cooperation of Eng. Luis de Santiago.

I would like to highly acknowledge Eng. Miguel Martinez, Eng. Miguel Angel, Eng. Diego, Eng. Javier, Eng. David, Eng. Marta, Eng. Elena, Eng. Angel, and the rest of the personnel of the CATECHOM in the University of Alcala in Spain for their technical collaboration and support.

I'm really most grateful to Prof. Frank Leferink, Eng. Robert, Eng. Edward, Mrs. Lilian, Eng. Olga, Eng. Frits and the rest of the Electromagnetic Compatibility group in the University of Twente in the Netherlands for their enthusiastic participation.

I also wish to thank Eng. Pedro Revenga & Eng. Carlos Girón in the University of Alcala for offering me their electric motorcycle as well as Renault in the Netherlands for lending their Renault Twizy.

I also would like to express my appreciation to my professors in the University of Alcala, University of Zagazig in Egypt as well as in the primary, preparatory, and secondary schools.

Thanks a lot to my parents and sisters for their permanent guidance and encouragement.

I am really thankful to my beloved wife for her patience, continuous help, and sustaining all troubles and problems until I finished this work.

Glossary

ADC
analog to digital converter 24
ANN
artificial neural networks 15, 16, 44, 64
BP
backpropagation 44
CEM
computational electromagnetics 15, 37
CF
cascade forward 40
DFT
discrete fourier transform 24
DGPS
DIFFERENTIAL GLOBAL POSITIONING SYSTEM 70
DHLF
DOUBLE HIDDEN LAYERS FEEDFORWARD 39
DTD
distributed time delay 41
DUT
device under test 23
ELM
extreme learning machine 44, 45, 66, 67
EMC
electromagnetic compatibility 1, 6, 14, 15, 16, 19, 25
EMF
electromagnetic fields 3
EMI
electromagnetic interferences 9, 10, 13, 15, 16, 18, 23, 27, 33, 57, 59, 66, 74
FDTD
finite difference time domain 14
FEM
finite element method 15
FFT
fast fourier transform 26
GPS
global positioning system 9
ICNIRP
International Commission on Non-ionizing Radiation Protection 3
IDM
imbalance difference method 15
ITD
input time delay 41, 42
ITS
intelligent transport systems 21
LM
Levenberg-Marquardt 45
LMS
least mean square 44
LR
layer recurrent 18, 41
MLP
multilayer perceptron 17, 39, 40, 41, 46, 67
MUT
motor under test 30
NARX
nonlinear autoregressive with external inputs 18, 41, 67
OATS
open area test site 11

List of Figures

List of Tables

List of Equations

Table of Contents

1 INTRODUCTION

The recent trend to move from internal combustion to electric mobility poses many questions concerning Electromagnetic Compatibility (EMC) issues. The effect of traffic on vehicular emissions is one aspect that may be employed to reduce the vehicular pollution. It is important to know how to manage traffic in order to reduce the emissions of any given vehicle.

This introductory chapter points out the motivation of this PhD thesis and reviews the state of the art concerning vehicular emissions, radiated emissions due to electric vehicles as well as the driving profile parameters. Then, the thesis objectives are explained and its organization is described.

1.1. MOTIVATION

This section points out the scientific motivation behind the work documented in this PhD thesis by defending the choice of electric vehicles. It also discusses the problem of measuring radiated vehicular emissions in real traffic.

1.1.1. WHY ELECTRIC VEHICLES?

Electrification of road transport is being widely promoted by many governments all over the world. In the near future, the global population is expected to increase from 6 billion to 10 billion. Consequently, the number of vehicles would increase from 700 million to 2.5 billion approximately as can be seen in Figure 1 [1]. If all these vehicles are driven by spark-ignited engines, where would the oil come from? And where should the emissions be disseminated? For these problems, people have to think in electrification of transportation means for the 21st century. Thus, the progress of electric vehicle technology has taken an accelerated pace to fulfill the energy conservation as well as the environmental protection requirements. With respect to the energy conservation, electric-driven vehicles present a secure, economic, and efficient solution by the utilization of different types of renewable energy sources unlike the fossil fuel-based road

transport means. Concerning the environment protection, electric-propelled vehicles can provide exhaust-free urban transportation at least.

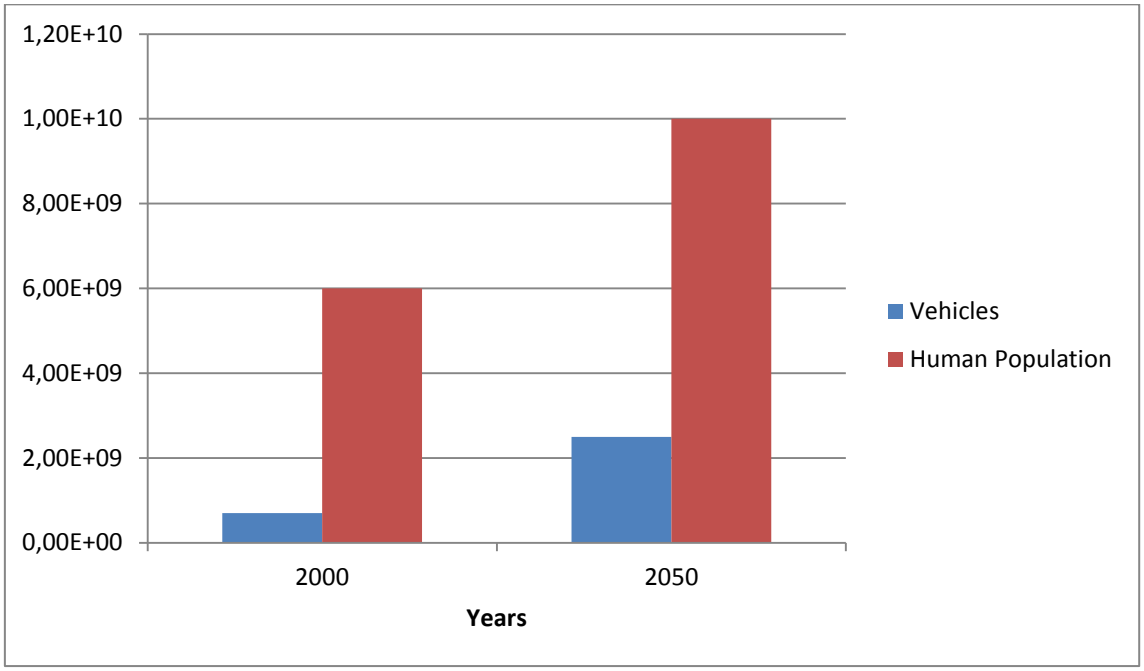

FIGURE 1, GROWTH OF POPULATION AND VEHICLES

The prevalence of electric automobiles in vehicle fleets across the world is steadily increasing. For example, in the United States (US), the share of electric vehicles is expected to rise from about 0.6% in 2010 to about 3.6% and 11.5% in 2015 and 2020, respectively. The number of electric vehicles on the road is estimated to increase from about 1.6 million in 2010 to about 10 and 34 million in 2015 and 2020, respectively [2]. Similar growth patterns are expected in other countries [3].

All electric powertrain vehicles, including fully electric, hybrid, and fuel cell vehicles, require significant electrical energy to be routed around the vehicle from the power sources (stored or generated) to the electric motors. High currents on the cables connecting the power source, power converter, and the electric motor generate low frequency magnetic fields. Given the size and space constraints of vehicles, the occupants may be in relatively close proximity to the electric powertrain. Consequently, during acceleration or regenerative braking, there might be large currents of hundreds amperes circulating a few centimeters away

from the passengers. Thus this could result in the penetration of the magnetic fields in the passenger compartment.

Bio-electromagnetics Aspect

Electromagnetic fields (EMF) generated by different sources are a subject of public concern because of the reported health problems related to the exposure to the fields a long time ago [4]. In April 1953, a conference was held in Bethesda, Maryland, to assess the state of scientific knowledge on radiofrequency (RF) and microwave (MW) bio-effects [5]. The main sources of exposure for the general public are: household electric appliances, transmission power lines, transformer stations, wiring of buildings, and electric transportation systems. At present, there are no specific standards related to electromagnetic field exposure associated with electric vehicle powertrain. Nonetheless, general recommendations for limiting the occupational and general public exposure to EMF have been developed by World Health Organization (WHO), European Union [6, 7], IEEE (C95.6 standard) [8], and the International Commission on Non-ionizing Radiation Protection (ICNIRP) [9-11], that should be taken into account during vehicle development. These standards not only established recommended exposure limits to EMF, but also included explanations concerning the ways these fields could affect human health.

One emerging source of magnetic fields is electrically powered vehicles. Several researchers have been addressing the hazards of long-term exposure to low frequency magnetic fields in electric/hybrid vehicles. The magnetic fields inside a sample of nine different electric vehicles from major US manufacturers have been evaluated at different operating conditions on the four seats [12]. This study showed that a maximum field intensity of 12 mille Gauss (mG) has been registered in the driver's seat during regenerative braking and maximum acceleration.

Another study of a wide range of transport systems conducted by the US department of transportation (Cambridge, MA) included measurement of magnetic fields at the head, waist, ankles and knees in conventional and electric cars, trucks and buses as well as other conveyances such as escalators and moving walkways, a

jetliner and an electric commuter train [13]. Maximum fields of 9–14 μT were reported from a variety of conventional vehicles for frequencies in the band 0.05–3 kHz, and maximum values of the order of 10 μT were reported for the same frequency band from the electric vehicle sample. This study also showed that there is no discernible evidence of electric fields that could be attributed to vehicular systems.

A study of a sample of fully electric as well as hybrid vehicles measured low frequency magnetic fields at 12 points representing various body parts from head to foot for each of the occupant locations [14]. A maximum value of around 15% of the ICNIRP reference levels for general public exposure has been registered in the vicinity of the front occupants' feet. Maximum exposure measures approaching 20% have been reported for head height in a hybrid bus [15]. A maximum exposure measure of almost 80% for the feet of a rear passenger in a hybrid car travelling at 80–100 km/h has been recorded in [16]. Maximum fields of 2.4 μT at seat level and 3.5 μT close to the floor in the 0.005–100 kHz frequency band have been measured in a hybrid car in [17]. Fields monitored over the entire day show a maximum value of 1.8 μT in a car of unspecified type recorded in the 40–800 Hz frequency range [18]. Maximum fields of 13.9–14.9 μT in the frequency band 0.01–5 kHz were recorded in a hybrid bus at the seat located closest to power cables during acceleration, deceleration and driving at 25 km/h given that the standard limit in this case is 26.6 μT [19].

Electromagnetic emissions radiated from DC and AC powered railway systems, metro, train, trolleybus, and tram have been analyzed in the 0.03 – 200 Hz frequency band [20]. Magnetic field intensities and spectral content have been related to the operational regimes of vehicles. Higher frequency components and amplitudes have been observed under high speeds. The highest magnetic fields have been recorded during maximum acceleration and regenerative braking.

Recently, a finite element model to evaluate the magnetic field created by a power electronics converter has been proposed and validated in [21]. The most critical directions regarding the magnetic field levels have been found to be the upper and one of the side faces. Consequently, putting the inverter inside an EV

under the rear seats as usual would imply that the passenger compartment would receive the most of the magnetic radiations. Maximum exposure value of 4.36 % has been recorded. A recent pilot study to assess magnetic field levels in the 40-1000 Hz frequency rang in 8 electric compared to 6 gasoline powered modern vehicles has been described in [22]. This study has also shown that the magnetic fields measured in electric vehicles were consistently greater than those measured in conventional gasoline-powered vehicles. No magnetic field in any vehicle has exceeded 1% of the ICNIRP limit in this study.

Table 1 has been reproduced from [23] giving a general idea about magnetic field levels in mG around various kinds of electrical equipment. It is important to take into account that different models of the same equipment can give different magnetic field intensities. This table says that: in extremely low frequencies, the magnetic field levels radiated from electric cars have more or less the same intensity as its combustion counterpart, findings similar to those reported in [13]. On the contrary, a recent study has revealed the opposite by concluding that electrically propelled vehicles emit more electromagnetic emissions than the spark-ignited ones [22]. Concerning electric fields, results in Table 2 published by the Federal Office for Radiation Safety gives typical electric field strengths measured near household appliances at a distance of 30 cm and at 50 Hz.

TABLE 1, EMF LEVELS DURING A WORKDAY FOR FREQUENCIES BELOW 3 KHZ

Industry	EMF Source	Magnetic Field Levels (mG)
Electrical equipment of machine manufacturing	Electric resistance heater	6.000 – 14.000
	Induction heater	10 – 460
TV Broadcasting	Video cameras	7.2 – 24
Hospitals	Intensive care unit	0.1 – 222
Transportation	Cars, minivans & trucks	0.1 – 125
	Diesel powered bus	0.5 – 146
	Electric cars	0.1 – 81
	Electric buses	0.1 – 88
	Electric train	0.1 – 330

TABLE 2, TYPICAL ELECTRIC FIELD STRENGTHS MEASURED NEAR HOUSEHOLD APPLIANCES

Appliance	Electric Field Strength (V/m)
Iron	120
Refrigerator	120
Hair dryer	80
Vacuum cleaner	8
Microwave oven	<1.5
ICNIRP reference level at 50 Hz	5000

All results show that the produced electromagnetic fields from electrified transport means remained far below the ICNIRP's reference values [24] for the general public for all driving conditions. Several studies have tried to prove the relationship between a long-term exposure to electromagnetic fields and different pathologies, e.g. cancer and leukemia, without finding evidence. Nevertheless, recent studies "suggest" a relationship between transport magnetic fields and certain adverse health effects. For example, an excess in male breast cancer among Norwegian Municipal Tram workers was reported in [25]. It's noteworthy that all studies determining whether or not the lengthy exposure to EMF from electric vehicles could be hazardous to the passengers have been conducted at low frequency ranges where the maximum frequency of interest was below 100 kHz.

EMC Aspect

On the other hand, serious problems already exist from the EMC point of view in electric drive vehicles. The Transport Research Laboratory in the United Kingdom has assessed the possible effects of electromagnetic emissions from electrically powered public and private transport on radio based services in the 20 Hz to 18 GHz frequency range. Almost all tests were carried out in accordance with the Automotive EMC Directive 95/54/EC with 10 m measuring distance. Results from peak level EMI tests in horizontal and vertical polarizations carried out on a hybrid vehicle, electric vehicle, heavy goods vehicle fitted with a data communications ring, and an electric train have revealed emissions from the vehicles exceeding CISPR 12 limits that could affect the radio spectrum [26].

Another study revealed that the results from the emissions testing carried out on 7 electric powered vehicles, with one exception, have been found to exceed the emission limits specified by 95/54/EC, CISPR 12, and 97/24/EC standards [27]. The maximum frequencies for these excessive emissions were 127 MHz for broadband and 144 MHz for narrowband. Some of the high frequency emissions (above 150 MHz) measured during charging of three electric vehicles have been found to exceed the CISPR 11 limits. Some measurements have been already done in the 9 KHz – 30 MHz frequency range showing that electric powertrain vehicles resulted in some slight increases over ambient levels by 2 to 3 dB. The only significant emissions below 30 MHz were observed from one of the hybrid vehicles with a reduced measurement distance from 10 to 3 m to obtain reliable signal levels. The highest levels detected with the reduced range configuration were a horizontal magnetic field of -3 dBuA/m and a vertical electric field of 50 dBuV/m at 29 MHz. The same study also showed some evidence for higher emission levels during acceleration and deceleration than under steady-state conditions. Moreover, two conventional internal combustion cars have been tested also for comparison purposes. Neither of them produced broad band emissions that exceeded 95/54/EC limits. This is another clear evidence of the logical claim that electrically driven vehicles will produce more radiated perturbations than its internal combustion counterpart.

Measured current waveforms from a hybrid vehicle inverter show evidence of very rapid current changes, particularly in the transitions between the drive and regeneration modes [28]. Current changes of the order of 100 A over about 0.4 ms can be seen for the drive mode, and around 150 A over perhaps 0.1 ms during the transition to regeneration. Conducted EMI of a power converter and its control as well as interface circuitry in the (30 MHz – 1 GHz) frequency range have already exceeded the EN-55022 limits [29]. Radiated EMI of a hybrid bus has been analyzed in different driving modes, e.g. pulling away, moving at 5 & 25 km/h, and regenerative braking, in the 10 kHz - 1 GHz frequency band using rod, loop, biconical, and log-periodic antennas in horizontal and vertical polarizations [19]. Below 30 MHz, authors reported that no electric field emissions were distinguished from the measured ambient level with a rod antenna.

Figures 2 & 3 show that conducted as well as magnetic field radiated emissions from a hybrid car have already exceeded the limits established by CISPR 25 [30]. It is the purpose of this PhD thesis to evaluate the radiated perturbations of electric vehicles in terms of the corresponding driving parameters.

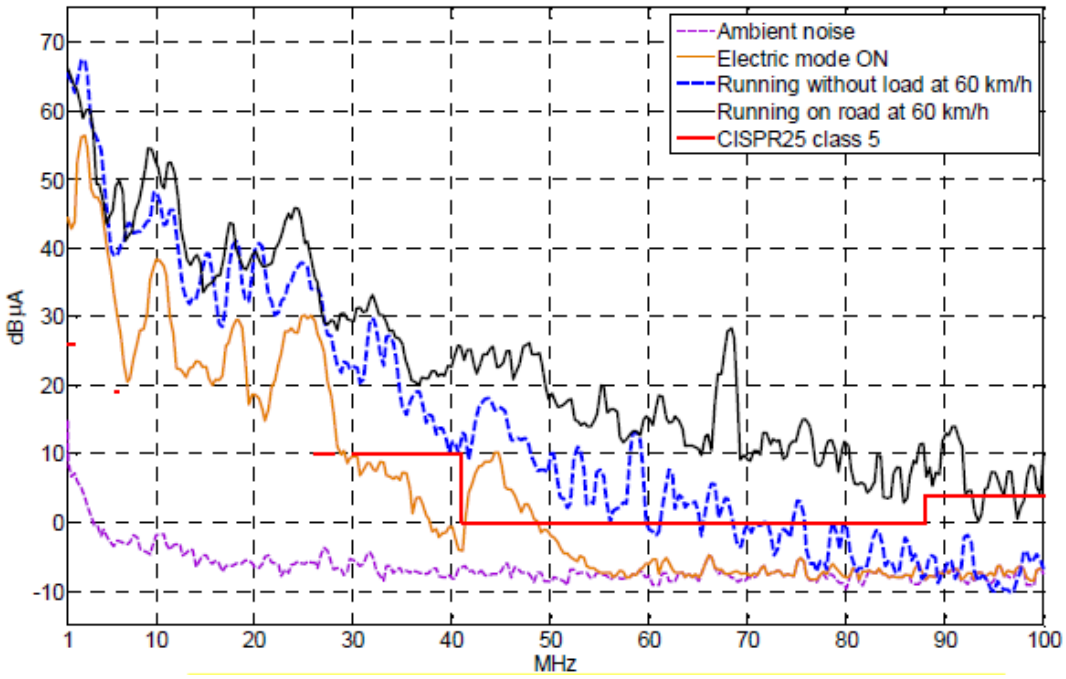

FIGURE 2, CURRENT MEASUREMENTS IN THE SHIELDED CABLE TO THE POSITIVE LINE OF THE ELECTRIC MOTOR

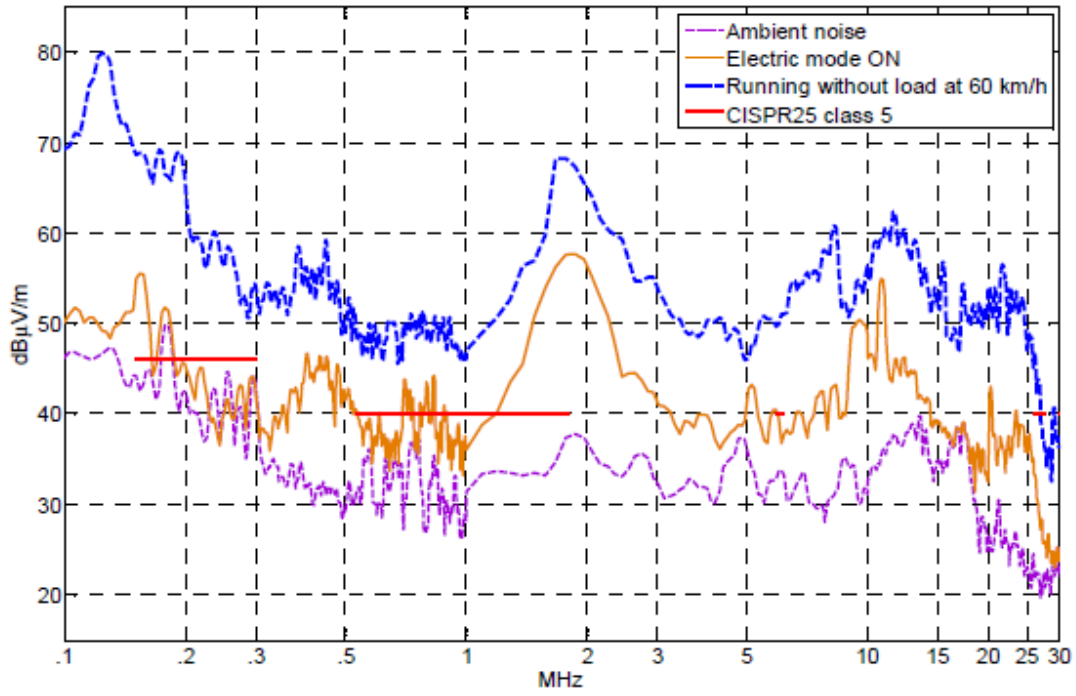

FIGURE 3, MAGNETIC FIELD MEASURED BY LOOP ANTENNA 1 M IN FRONT OF THE VEHICLE

1.1.2. MEASUREMENT OF RADIATED EMI IN REAL TRAFFIC

Real traffic electromagnetic radiated emissions due to vehicles have not been evaluated. Moreover, recent studies on automotive EMC have not adequately addressed the question of whether the driving regime affects the on-road radiated disturbances levels and frequency content. Furthermore, currently available automotive EMC standards, e.g. CISPR 12, SAE J551, 2004/104/EC ...etc., don't discuss the impact of the driving profile on the corresponding real world radiated interferences. Some EMC standards or directives, e.g. category 507 in the 4th edition of AECTP 500 [31], CISPR 12, and SAE J551, require measuring the radiated fields with the vehicle under test running at some constant speeds, i.e. steady state conditions. But, there are not standards requiring measurements during dynamic conditions like: starting-up, cruising (high constant speed), various rates of acceleration/ deceleration, normal braking, and regenerative braking. Besides, there are no models capable of accurately correlating the vehicular radiated electromagnetic fields in real world with the driving characteristics. Recent studies have shown that the frequency content and intensity of the magnetic fields inside electric [20, 32] and hybrid [17] vehicles as well as due to a DC motor drive [33] are continuously changing with the driving modes.

The problem is that measuring real traffic vehicular radiated fields in a direct way is a very complicated task because of the large size of antennas in low frequency ranges. Furthermore, such antenna would receive a lot of high level and continuously changing radiated waves from various interfering sources like: other vehicles, RFID, WiFi, GPS, Bluetooth, television broadcast, radio broadcast, mobile networks, satellite networks, and power lines. External magnetic radiated EMI from sources unrelated to the transportation system contributed to the measured fields along the roadway in this study [13]. It was relatively easy to distinguish the power line magnetic fields at 60 Hz. Nevertheless, the authors informed that people movers typically had stationary electric drive systems operating from 60 Hz power. Thus, it was impossible to distinguish its radiated magnetic fields in the presence of ambient power line fields from other sources.

1.2. STATE OF THE ART

This section discusses the following points: vehicular emissions, radiated interferences due to electric vehicles, Time and Frequency domain EMC measurements, and the driving profile parameters

1.2.1 VEHICULAR EMISSIONS

The vehicular emissions are being studied since the first cars appeared in the transport context. They can be subdivided into: acoustic, exhaust, i.e. gases & particles, and Electromagnetic Interferences (EMI).

Acoustic Emissions

There are several works analyzing the use of acoustic emissions or audible noise of vehicles for a lot of purposes like: classification and identification [34-37], speed estimation [38], and fault diagnosis [39]. Vehicle acoustic experiments have special test facilities and chambers as shown in Figure 4 exactly like automotive EMC tests.

FIGURE 4, ACOUSTIC TEST CHAMBER

Exhaust Emissions

Exhaust emissions rates are influenced by the way in which vehicles are operated. Several researchers have investigated the correlation of the driving behavior with exhaust emissions estimated from emission models or measured on a chassis dynamometer as described in Figure 5 rather than measuring in the field [40-48]. The effects of the driver behavior on real world exhaust emissions have

been characterized using onboard exhaust emission and engine operating data analyzers in [49, 50]. Recently, through the MIVECO project, the Electronics department at the University of Alcala (UAH) has developed an onboard measurement equipment to relate the driver activity, vehicle state and road conditions with exhaust emissions in real world conditions [51, 52]. This was the starting point of a research line at the UAH concerning the electromagnetic emissions of electric vehicles.

FIGURE 5, EXHAUST EMISSIONS MEASUREMENT ON A CHASSIS DYNAMOMETER

Electromagnetic Emissions

Electromagnetic disturbances in vehicles can be measured in a screened chamber as shown in Figure 6 or in an open area test site (OATS). Vehicular electromagnetic emissions can be divided into 2 major types: conducted and radiated emissions. This thesis focuses on the radiated emissions part of electromagnetic interferences.

FIGURE 6, EMC SEMI-ANECHOIC TEST CHAMBER

1.2.2 RADIATED INTERFERENCES DUE TO ELECTRIC VEHICLES

Nowadays, with new and more stringent EMC regulations, the EMI has become a major issue to deal with in every kind of application making use of electric and/or electronic devices. Every electric or electronic device should operate without introducing significant electromagnetic disturbances to the environment. This is particularly true in automotive applications; as today's vehicles are equipped with a large number of sensitive electronic communication and control systems for user's safety and comfort.

Electric vehicles have already been geared-up into mass production. Thus, the EMI issues could become more severe than ever. The developments that influence the electromagnetic emissions from modern electric vehicles arise from three technological trends in the automotive industry:

1. The replacement of the traditional mechanical systems with mechatronic alternative powertrain solutions.
2. The use of more sophisticated technologies to deliver existing functions, e.g. PWM control for vehicle lamps, stability control systems, and faster processors.
3. The introduction of new services based on wireless communications operating at increasingly high frequencies such as telematics, Bluetooth, and radar for adaptive cruise control.

1.2.2.1 MECHANISM, MEASUREMENT & ESTIMATION

This section reviews the radiation mechanisms and the previous works concerning the measurement, analysis, and estimation of radiated interferences in electric vehicles.

Mechanism

Power converters in the electric drives are the main source of high level low frequency electromagnetic pollution that can harmfully affect onboard small-signal devices [30, 53, 54]. This is because power electronic devices operate at high frequencies and switch on high voltages as well as currents [55-59]. Apart from environmental considerations, an electric driven vehicle may interfere with nearby ones in case of traffic jams for example.

The high voltage variations in electric drive vehicles can induce common mode currents in the parasitic capacitance between the high voltage rate nodes and the vehicle body frame as well as the small-signal circuits. On the other hand, the high current loops variations can induce inductive couplings to any other circuits in the vehicle. Another source of the inductive coupling is the leakage flux of magnetic components in power electronics circuits. Due to the huge magnitude difference between the power electronics currents and the small-signal currents, a very small inductive or capacitive coupling can harmfully influence the small-signal circuits like microprocessors existing in modern vehicles. Also the fast switching of the semiconductor devices causes ripples and current spikes, i.e. differential mode noise, in the main power paths. Moreover, digital circuits in automotive systems tend to radiated EMI due to their high clock frequency. Thus, there are two principal sources of radiated disturbances in automotive systems: conducted common mode currents and digital as well as RF circuits [59].

Measurement

Nowadays there are two main methods for measurement of EMI signals: traditional frequency domain measurements and its time domain counterpart. Drawbacks of the frequency domain measurement approach are: relatively long measurement time [60, 61] , missing of phase information for signal reconstruction in time domain [62]. Moreover, it is not guaranteed to measure the peak-radiated power when dealing with impulsive electromagnetic interferences [60, 63].

On the other hand, time domain EMI (TDEMI) measurement systems provide some capabilities that could never be achieved using the traditional frequency domain system like: improvement of impulsive emissions measurements, reduction of the measurement time, noise cancelation capability, as well as time domain visualization of the EMI signals. Nevertheless, there are two problems of the current time domain EMI measurement approaches: the limited dynamic range as well as the limited depth of memory to store a sufficient set of time domain data [63, 64]. The first trials of the work in the research line presented in this thesis have been done using frequency domain EMC measurement techniques [65]. The measurement methodology followed in this

thesis has been based on time domain measurements using digital oscilloscopes as explained in details in Chapter 2 to minimize the overall measurement time, and to enable the comparison to the ICNIRP limits as well as to enhance the capture of transient emissions.

Automotive EMC standards have already set the measurement procedure to be followed for recording the radiated electromagnetic emissions due to the whole conventional internal combustion vehicle, e.g. SAE J551, CISPR 12, 95/54/EC, 2004/104/EC, 2005/83/EC, and 2006/28/EC, as well as the onboard components, e.g. CISPR 25 and 97/24/EC. Several modifications to the currently available standards have been proposed concerning the EMC testing of electric vehicles expected to become more prevalent in the near future [26, 30, 66, 67]. Radiated emissions due to electrically powered vehicles have been measured and analyzed in several works. For example, implementation difficulties of measuring low frequency radiated interferences from an experimental electric vehicle were described in [55]. Furthermore, several EMI measurement tests have been carried out with seven models of different electric vehicles using a chassis dynamometer in [66]. Also, radiated electric as well as magnetic fields of a jacked up hybrid car have been measured in an anechoic chamber in [30]. Radiated magnetic fields inside and outside a hybrid bus have been analyzed in different driving modes in the 10 Hz – 1 GHz frequency band [19]. It is noteworthy that all of these works have not measured the electromagnetic radiated disturbances in real traffic conditions. Furthermore, no model has been developed yet about the relationship between the driving dynamics and the corresponding radiated electromagnetic fields.

Estimation

Several researchers have been interested in forecasting radiated emissions given the conductive ones. Equations are available at low frequencies to estimate the radiation from conducted emissions for very simple geometries [68]. The importance of modeling common mode currents to predict the radiation from printed circuit boards has been emphasized in [69]. The utility of finite difference time domain (FDTD) modeling for common mode radiation analysis has been

shown in [70]. An empirical strategy has been suggested to calculate the radiated disturbances in terms of measured common-mode currents in [71]. Moreover, prototype hybrid vehicle-level radiated interferences have been estimated using component-level conducted emissions and harness radiation coefficients in [72]. The transfer function of the full vehicle has been determined using FDTD modeling to anticipate the vehicle level radiated emissions from known module-level characteristics in [73]. Besides, radiated EMI generated by 42-V vehicle electronic-driven electrical loads have been predicted using FDTD method in [74]. These works haven't correlated the radiated electromagnetic waves with the corresponding driving profile. Moreover, the use of numerical electromagnetic techniques requires thorough knowledge of the physical electronic components and modules constituting the vehicle under test which is beyond the scope of the work presented in this thesis.

1.2.2.2 MODELING TECHNIQUES

Developing a model to estimate the radiated interferences of an electric vehicle can be accomplished using traditional computational electromagnetic (CEM) techniques or artificial neural networks (ANNs). This section analyzes the capability of these techniques to accomplish the goal of this PhD work.

Computational Electromagnetic Techniques

Usually Radiated emission problems are analyzed through numerical electromagnetic algorithms such as: finite element method (FEM) [75], FDTD [70, 73, 74], imbalance difference method (IDM) [76],…etc. Unfortunately, this approach can't be applied to solve the problem of estimating the real world radiated waves in terms of the driving characteristics. This is because all CEM solve Maxwell's equations for a specific configuration. Thus, the driving profile can't be an input for such type of models. Moreover, this solution requires thorough knowledge of the electronic systems comprising the vehicle while this thesis aims at developing a black-box model.

Artificial Neural Networks

Recently ANNs have been widely used in various applications like: aerospace [77], automotive [78], banking [79], defense [80], electronics [81],

entertainment [82], financial [83], industrial [84], insurance [85], manufacturing [86], medical [87], oil and gas [88], robotics [89], speech [90], security [91], telecommunications [92], transportation [93]. Thus, the number of neural network applications, the effort that has been exerted in neural network software & hardware, and the depth as well as breadth of interest in these devices have been growing rapidly [94].

ANNs have been exploited in different EMC problems such as detection and identification of vehicles based on their unintended radiated emissions [95], target discrimination [96, 97], calculation of multilayer magnetic shielding [98], estimating PCB configuration from EMI measurements [99], characterization and modeling of the susceptibility of integrated circuits to conducted electromagnetic disturbances [100], recognition and identification of radiated EMI for shielding apertures [101], prediction of electromagnetic field in metallic enclosures [102], adaptive beamforming [103, 104], integrated circuits pad modeling [105], cross talk on PCB & radar cross-section of cylinders with apertures [106], and detection of dielectric cylinders buried in a lossy half-space [107].

It's noteworthy that the computational capabilities of ANNs have been already utilized to estimate exhaust concentrations in terms of traffic and meteorological variables in [108]. Unlike the CEM tools, ANNs can provide time varying inputs and deal with the problem as a black box. This thesis takes advantage of ANNs to estimate radiated emissions from electric vehicles in terms of the corresponding driving variables. Chapter 3 presents the details of developing the ANN models used in this work.

Static as well as dynamic neural networks have been assessed in this thesis. The linear neuron (LN), multilayer perceptron (MLP), double hidden layers Feedforward (DHLF), and cascade feedforward (CF) networks represent the static neural models exploited in this thesis. On the other hand, input time delay (ITD), distributed time delay (DTD), layer recurrent (LR), nonlinear autoregressive with external inputs (NARX) models belong to the dynamic category of ANNs.

The MLP network is a modification of the standard linear perceptron and can distinguish nonlinearly separable data [109]. MLPs are the standard and most popular solution adopted for classification [110] and function approximation problems [111]. It has been exploited in diverse fields such as: heart disease diagnosis [112], low back pain diagnosis [113], banded chromosomes classification [114], bridges damage detection [115], air pollution forecast [116], gas mixture analysis [117], time series prediction [118], signal detection [119], cardiovascular risk prediction [120], solar radiation maps [121], crack detection in anisotropic laminated plates [122], transient stability analysis of power systems [123], speech recognition [124], character recognition [125], image recognition [126], data communications [127], machine translation software [128], atmospheric science [129], numerical solution of partial differential equations [130], and noisy fingerprint classification [131].

The DHLF neural network has been already employed in wood drying modeling [132] and air pollution forecasting [133]. In a complicated pattern recognition problem where number of classes exceeds 20, another hidden layer has already given more flexibility to the network [134]. The performance of an only one hidden layer network may be better than that of two hidden layers. For example, single hidden layer feedforward models were better than double hidden layer ones in detecting shelf life of kalakand stored at 6ºC [135]. On the contrary, it was found that in a bond classification problem, a network with two hidden layers outperformed the one with single hidden layer containing comparable number of hidden nodes [136]. This was because of the advantage obtained by the use of a subsequent hidden layer to provide another representation of useful classification information. Moreover, the classification accuracy of double hidden layer network was better than that of a single hidden layer one in detection of mammographic microcalcifications [137].

A recent study revealed that a cascade single hidden layer network gave better performance than double hidden layer networks for predicting sensory quality of roasted coffee flavored sterilized drink [138]. A cascade neural network model has been proposed for trajectory formation based on the minimum torque-

change criterion [139]. An integrated segmentation and recognition of handwritten numerals using a different type of cascade neural models has been proposed in [140]. A special training algorithm based on node-decoupled extended Kalman filtering for cascade networks has been proposed in [141]. Another interesting network growing learning methodology for cascade neural networks has been introduced in [142].

The ITD network has been utilized in many applications like rainfall forecasting [143], short term prediction of ionospheric parameters [144], isolated word recognition [145], power amplifier behavioral modeling [146], image sequence analysis [147], automated genome annotation [148], image recognition [149], character recognition [150], wastewater quality prediction [151].

The DTD network was firstly proposed in [152]. This type of dynamic networks has been used for time series prediction in [153]. The LR artificial intelligence model has been used to analyze the electromagnetic interference EMI between high voltage power lines and metallic underground pipelines for different problem geometries [154].

The computational capabilities of the NARX network have been reviewed in [155]. This artificial intelligence model has been extensively used in a lot of applications like: time series prediction [156], water resources prediction [157], modeling of hydraulic suspension dampers [158], adaptive control [159], thermodynamics [160], system identification [161], prediction of temperature and humidity [162].

1.2.3 DRIVING PROFILE

Driving behavior has an effect on the output power of the engine and consequently its electromagnetic emissions. Driving dynamics and the corresponding radiated electromagnetic waves due to a certain vehicle under test should be registered simultaneously to study the relationship between them. The driving style can be described by a lot of variables such as: vehicle velocity, engine speed, linear acceleration, frontal inclination, following distance, relative lane position, steering wheel angle, yaw angle, positions of pedals, use of accessories,

roadway grades (i.e., uphill or downhill), surface roughness, engine capacity, and so on [163]. These variables are related to either the driver activity, vehicle state or the traffic conditions. On-road measurement of the majority of these parameters is a straightforward task through the onboard diagnostic electronic system of the vehicle itself.

Concerning the driver behavior variables, neural models have been developed to estimate the pedals activity in terms of the engine RPM, vehicle velocity, linear acceleration, and the frontal inclination in [164]. In addition, the minimum set of variables, i.e. frontal inclination and engine RPM, needed to estimate the pedal activity has been presented in [165]. Moreover, neural estimator [166] and classifier [167] have been proposed to determine the gear position in terms of the vehicle speed and the engine RPM.

Some studies have used the vehicle velocity and acceleration to describe the operational modes of the vehicle [46-48, 50]. On the other hand, the driving profile has been described by the vehicle specific power [168] which integrates the vehicle speed, vehicle acceleration, road grade, aerodynamic drag, and tire rolling resistance, and it is generally defined as the instantaneous power per unit mass of the vehicle [169]. Whilst other researchers have combined both the velocity as well as the product of the velocity and acceleration as a rough estimation to the vehicle specific power in order to characterize the driving kinematics [41, 170]. In this thesis, the vehicle instantaneous speed and acceleration, calculated by differentiating the speed signal, have been considered as explanatory variables to represent the driving behavior.

1.3. THESIS OBJECTIVES

From the EMC point of view, the expected growth of electric vehicles is related to the increase of worry about the associated electromagnetic contamination. In this context, the main challenge of this PhD thesis is to present the novel proposal shown in Figure 7 to estimate the impact of a vehicle's operating mode on radiated electromagnetic emissions in real traffic using neural networks.

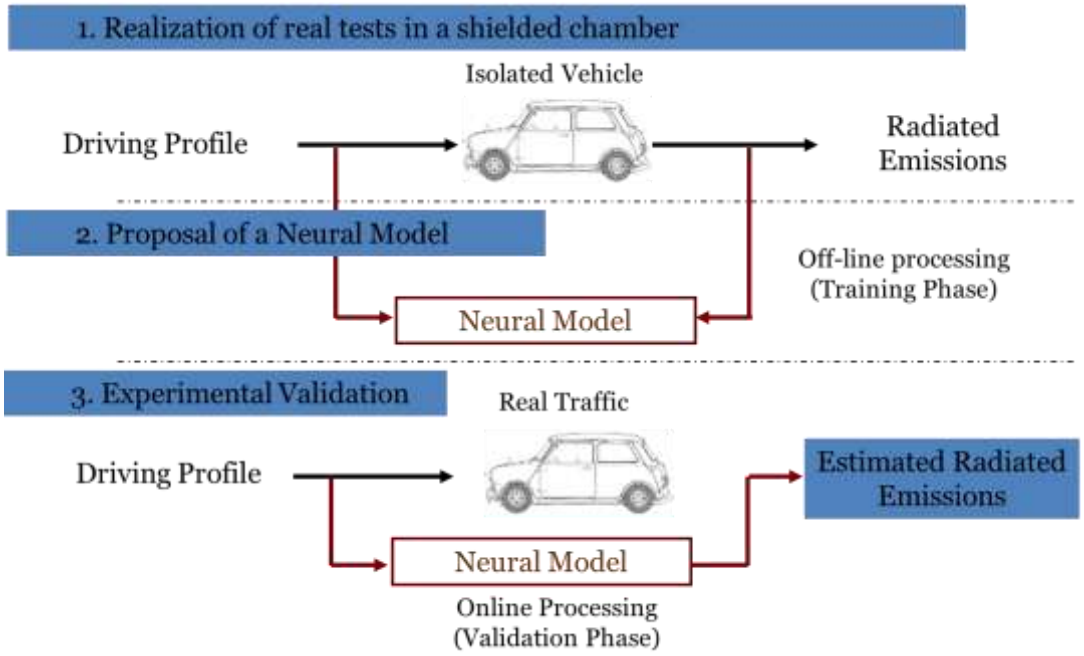

FIGURE 7, PROCEDURE FOR ESTIMATING REAL TRAFFIC VEHICULAR RADIATED EMISSIONS

Firstly, tests with the vehicle in a shielded chamber have to be done measuring the vehicle speed as well as the corresponding radiated emissions. Secondly, artificial neural networks should be exploited to develop the desired model using data registered from the previous stage. This model is a black-box one; that is the interference sources and the propagation paths in the vehicle under test as well as EMI suppression techniques are beyond the scope of this thesis. Finally, experiments have to be done in the field registering only the driving pattern signals that would be simultaneously applied to the obtained model estimating the real traffic radiated emissions.

The objective of that proposal is to quantify the change in real traffic radiated disturbances due to a corresponding perturbation in the driving dynamics. This can lead to:

- Quantifying the effect of environmental pollution of electric vehicles in real traffic conditions.
- Suggesting Eco-driving and Eco-routing guidelines in terms of minimizing the radiated electromagnetic fields. This idea can greatly help in the planning of highway facilities as well as the design of traffic management systems and procedures controlling the vehicle operation parameters. For example, model-

based traffic control determining the dynamic speed limits to reduce fuel consumption and emissions has been presented in [171].

- Comparing EMI emissions from trips, e.g. urban, extra-urban, rural, high-ways, and conventional roads with different driving parameters.
- Integrating such type of models into traffic network simulators to better understand the impact of traffic policies, including introduction of intelligent transport systems (ITS), on the electromagnetic environment. Thus, the development of this model attempts to bridge the existing gap between traffic simulation models as well as traditional transportation planning models, and electromagnetic compatibility impact models.

1.4. THESIS ORGANIZATION

This introduction chapter reviewed the state of the art and explained the motivation of this PhD dissertation. It also pointed out the theoretical basics employed in this thesis. Chapter 2 points out the measurement methodology followed in this work. Neural models development details are discussed in Chapter 3. Chapter 4 is dedicated to commenting the experimental results obtained from analyzing the raw data. Conclusions and future works are explained in Chapter 5.

2 MEASUREMENT METHODOLOGY

Vehicle manufacturers must satisfy legislative EMC requirements that include electric field narrowband and broadband radiated emissions measurements from 30 MHz to 1 GHz using an antenna at a fixed point relative to the vehicle. Broadband emissions are signals with bandwidth more than the receiver bandwidth and have pulse repetition frequencies smaller than the receiver bandwidth. On the other hand, narrowband emissions are signals with bandwidths smaller than the receiver bandwidth and have pulse repetition frequency greater than the receiver bandwidth. Unlike the emissions testing standards used by many other industries such as CISPR 22 and ANSI C63.4, there is no requirement for height scanning of the antenna and rotation of the test object in order to identify the maximum emission levels.

The most common test configuration is an open area test site or a semi-anechoic chamber with an antenna mounted 3 m high at a distance of 10 m from the side of the vehicle under test aligned with the front axle. Standards also permit measurements at a distance of only 3 m with the antenna height reduced to 1.8 m. Both narrowband and broadband disturbances are measured with a receiver bandwidth of 120 kHz. Broadband measurements are commonly carried out using a quasi-peak or peak detector with the engine running at constant speed, e.g. 1500 rpm, to detect perturbations from the spark ignition system. Narrowband measurements are done using a quasi-peak or peak detector with the vehicle's ignition switched on and the engine turned off to detect the emissions from onboard electronic modules.

These test procedures that have historically been applied were developed mainly for conventional spark-ignited engine vehicles. These techniques are therefore not well suited to electrically powered vehicles. This is because successful evaluation of the electromagnetic emissions from electric vehicles is likely to require the powertrain components to be exercised dynamically in order to mimic real operating conditions.

This chapter discusses the measurement methodology followed in the realized experimental tests. The first section will present the general ideas over which the measurement setup has been built. Next sections explain more details about the specifications with which the tests have been carried out with an electric motorcycle and an electric car. Additional measurements have been done below and above 30 MHz and interesting results have been found in the low frequency range below 30 MHz. That is why all the test results presented in this thesis have been concentrating on the 150 kHz – 30 MHz.

2.1. INTRODUCTION

Standards deemed to be relevant to whole vehicle emissions testing include 2004/104/EC and CISPR 12. The scope of these standards includes vehicles propelled by electrical means. However the emission limits, frequency band, and test procedure are the same as the 95/54/EC automotive EMC directive. However, the SAE J551-5 standard provides the measurement procedure as well as the emission limits for radiated electric and magnetic emissions due to electric vehicles in the 150 kHz – 30 MHz frequency range. This standard specifies a measurement methodology based on a traditional frequency stepping receiver which is not the best solution for measuring and detecting transient radiated EMI. As explained earlier, the main aim of this PhD thesis is to develop a model relating the driving dynamics with the radiated EMI of electric vehicles. That's why the EMI tests carried out in this thesis have not strictly followed the measurement procedure specified in the SAE J551-5 standard.

This section outlines the approach adopted for measurements in this work and comments on the common part between all the realized experiments. The basic idea of the proposed measurement methodology for radiated emissions is shown in Figure 8. Firstly, the software program executed from the PC triggers the digital oscilloscope to start the experiment. The EMI signal of the device under test (DUT) is captured by an antenna, filtered by an anti-aliasing low pass filter,

sampled as well as quantized by the digital oscilloscope's ADC, and sent to the PC's USB port to be saved in a database for offline processing. The previous scenario is repeated until all the time domain sweeps are saved in the PC's database.

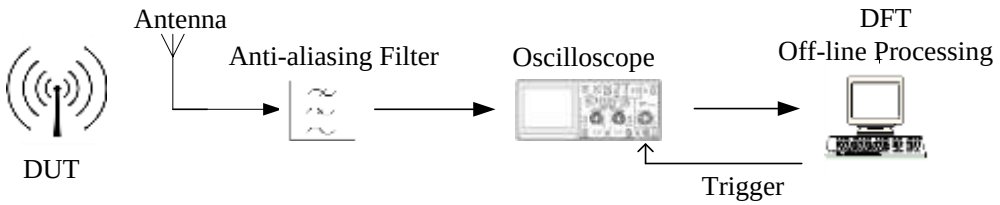

FIGURE 8, BLOCK DIAGRAM OF THE PROPOSED TDEMI MEASUREMENT SYSTEM

At the end of the experiment, spectrum and spectrogram of the device's EMI signal are computed via the Discrete Fourier Transform (DFT). Thus, the time domain evolution of the radiated emissions can be analyzed.

The following parameters of the oscilloscope should be properly adjusted: sampling time T_s (or the sampling frequency F_s), capture time T_c (duration of the time domain sweep of the oscilloscope), and sweeping time T_r (or the recording frequency). The relation between these times is illustrated in Figure 9.

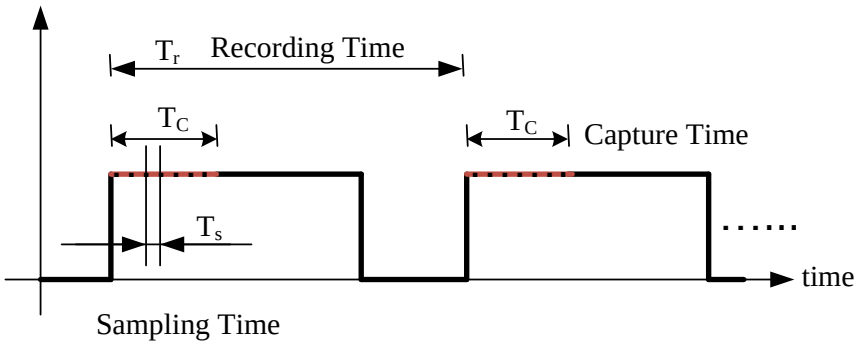

FIGURE 9, RELATION BETWEEN THE SAMPLING, RECORDING, AND CAPTURE TIMES

Sampling Time

According to the sampling theorem, the minimum sampling frequency equals twice the wanted maximum frequency, i.e. Nyquist frequency, of the calculated spectrum. To avoid aliasing errors, it's recommended to set the

sampling frequency 2 to 4 times higher than Nyquist frequency depending on the steepness of the antialiasing filter.

Capture Time

Besides, the capture time T_c depends on the distance between two neighboring frequency bins (frequency resolution, or frequency step) Δf which depends on the resolution bandwidth B_r as follows [61, 172]:

$$T_c = \frac{1}{\Delta f} = \frac{1}{1.06\ B_r} \qquad \text{EQN 1}$$

Record Length

As a result of choosing these two parameters, i.e. F_s & T_c, the time domain record length N_r, or number of samples per record is determined as follows:

$$N_r = F_s \times T_c \qquad \text{EQN 2}$$

It's noteworthy that the record length is limited by the oscilloscope's available memory as well as the maximum data transmission speed between the oscilloscope and the personal computer. As can be seen from Eqn 2, the record length depends on both the sampling frequency and the capture time. The capture time is already set by the resolution bandwidth determined by the EMC standards as can be seen in Eqn 1. On the other hand, the sampling frequency can be more than twice the maximum measured signal bandwidth. Thus, the lower bound on the sampling frequency is already imposed by the sampling theorem. Consequently, the upper bound on the sampling frequency is the value at which the oscilloscope's memory saturates or the maximum transmission speed between the oscilloscope and the PC is reached.

Recording Time

Finally, the recording time T_r (time between the start of two consecutive records), or the recording frequency F_r, has to be adjusted based on the driving profile signals and the maximum transmission speed between the PC and the oscilloscope. In other words the details and changes included in the driving

dynamics impose an upper bound on the recording time. That is the maximum separation between the starting of consecutive records has to be less than the minimum separation between two successive important changes in the driving style signals.

Moreover, the maximum data transmission speed between the oscilloscope and the PC controls the lower limit on the recording time. In other words, the minimum recording time corresponds to the maximum data transmissions speed between the oscilloscope and the PC.

Spectrogram and Mean Record Intensity

Samples of electric or magnetic field recorded by a digital oscilloscope are measured in Volts. In order to take into account the errors due to the antenna factor and the cable losses, FFT is applied to each sweep to convert it from time to frequency domain. To calculate the field intensity in dBuV/m, Eqn 3 should be considered where **V** is the FFT point to be corrected, **F** is the antenna factor and **L** is the cable losses.

$$\mathbf{E}\ (\mathrm{dBuV/m}) = 20*\log(\mathbf{V}) + 120 + \mathbf{F}\ (\mathrm{dB/m}) + \mathbf{L}\ (\mathrm{dB}) \qquad \text{EQN 3}$$

A spectrogram plot can be produced by the matrix of corrected frequency domain field intensity points in dBuV/m. This type of figures can visualize the temporal progress of the spectral components of the radiated EMI. Then, important frequency bands are determined where a clear change of the intensity of the spectrum can be observed with the speed profile. Finally the mean value of each sweep is calculated and a plot of both speed as well as radiated EMI mean sweep power can be plotted versus time.

2.2. ELECTRIC MOTORCYCLE EMISSIONS

The key aspects of the methodology to evaluate the effect of the driving profile on the radiated electromagnetic emissions based on TDEMI measurement in the range 150 kHz – 30 MHz are shown in Figure 10 [173]. EMI Tests have been

carried out in the semi-anechoic chamber of the CATECHOM (Center of High Technology and Homologation in the UAH) accredited by ENAC (Spanish Entity of Accreditation). EMI measurement tests in higher frequency ranges have been conducted without detecting discernible levels of electric radiated perturbations. Only electric field radiated emissions have been considered here because of the lack of instrumentation required to implement the complete setup concerning magnetic field measurements. Electric field EMI signals have been captured by active biconical antennas, filtered by anti-aliasing low pass filters, sampled as well as quantized by a digital oscilloscope, and sent to the PC's USB port via the GPIB/USB converter to be saved in a database for offline processing. The previous scenario is repeated until all the time domain records are saved in the PC's database. At the end of the experiment, an adaptive noise cancelation algorithm is applied to filter out the electromagnetic noise due to the CAN bus used to measure the instantaneous speed of the electric motorcycle. Spectra of the noisy, filtered, and CAN bus noise signals are computed via FFT.

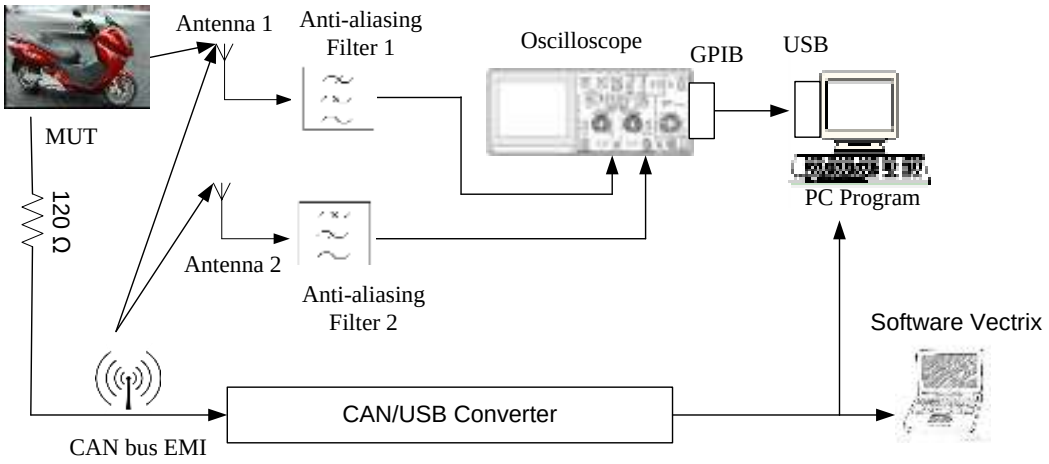

FIGURE 10, BLOCK DIAGRAM OF THE MEASUREMENT SETUP

According to Figure 10, antenna 1 is responsible for receiving the emissions of the Motorcycle under Test (MUT) as well as the CAN bus noise, and antenna 2 captures only the CAN bus noise correlated with the noise component in the signal received by antenna 1. Adaptive filtering techniques exploit the correlation between the noise component in the noisy EMI signal received by antenna 1 and

the reference noise signal received by antenna 2 to extract the EMI signal of the MUT.

Figure 11 shows the schematic diagram of a typical adaptive noise canceller. It receives two inputs: primary and reference. The primary input receives a signal *s* from the signal source corrupted by a noise *n* uncorrelated with the signal. The reference input receives a noise n_o uncorrelated with the signal but correlated with the noise *n*. The noise n_o passes through a filter to produce an estimate n_{est} of the primary input noise. This noise estimate is subtracted from the corrupted signal to produce an estimate of the signal (error). The objective of such a system is to produce a system output s_{est} that is the best fit in a least squares sense to the signal *s*. This is accomplished by feeding the system output back to the adaptive filter and adjusting the filter parameters through an LMS algorithm to minimize the total output system power. In other words, the system output serves as the error signal for the adaptive process. Assuming that *s*, n_o, *n* are statistically stationary signals and have zero means.

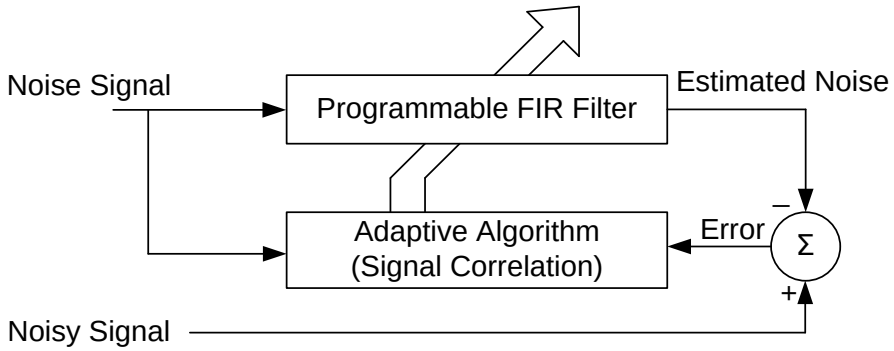

FIGURE 11, ADAPTIVE NOISE CANCELLER

$$s_{est} = s + n - n_{est}$$

$$s_{est}^2 = s^2 + (n - n_{est})^2 + 2 * s * (n - n_{est})$$

Taking expectation of both sides:

$$E[s_{est}^2] = E[s^2] + E[(n - n_{est})^2] + 2E[s(n - n_{est})]$$

$$E[s_{est}^2] = E[s^2] + E[(n - n_{est})^2]$$

The signal power E[s^2] will be unaffected as the filter is adjusted to minimize E[s_{est}^2]

$$\min E[s_{est}^2] = E[s^2] + \min(E(n - n_{est})^2)$$

Thus when the filter is optimized to minimize the output noise power $E[s_{est}^2]$, the output noise power $E(n - n_{est})^2$ is also minimized. Since the signal in the output remains constant, therefore minimizing the total output power maximizes the output signal-to-noise ratio. Since $(s_{est} - s) = (n - n_{est})$, this is equivalent to causing the output s_{est} to be a least squares estimate of the signal s. In this work, a frequency domain FIR adaptive filter using the DFT filtering algorithm has been used. The filter's length is 4000 and the step size is 0.01. These parameters gave the best performance in terms of noise suppression.

Figure 12 includes two photos of real test inside the semi-anechoic chamber of the UAH in Spain. The overall system has been calibrated against a periodically calibrated spectrum analyzer (ESIB26) measuring a square waveform; because a square waveform theoretically has many odd harmonics; consequently covering all the measurement range. An uncertainty analysis of the EMI measurement system has been done according to the CISPR 16-2-4 showing that the measurement accuracy of the whole system is ±7 dB (see Appendix A2).

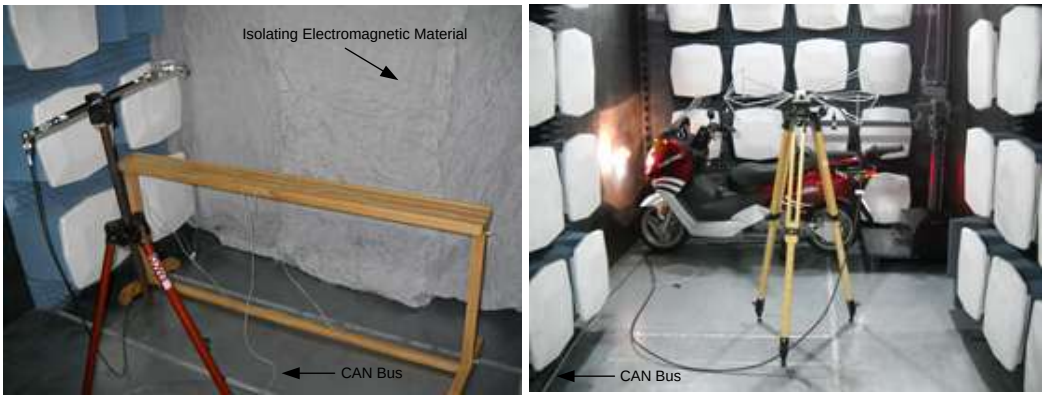

(a) Isolating material and antenna 2 (b) Motorcycle and antenna 1

FIGURE 12, REAL PHOTOS OF THE MEASUREMENT SETUP IN THE SEMI-ANECHOIC CHAMBER

Two speed profiles have been applied to the MUT: pulses and Urban European Driving Cycle (UEDC) as can be seen in Figures 13 & 14 respectively. The pulses profile has been considered as a rough approximation of extra-urban driving behavior. While the UEDC profile is a standard test cycle used to assess the exhaust emissions and fuel consumption of vehicles in urban environments.

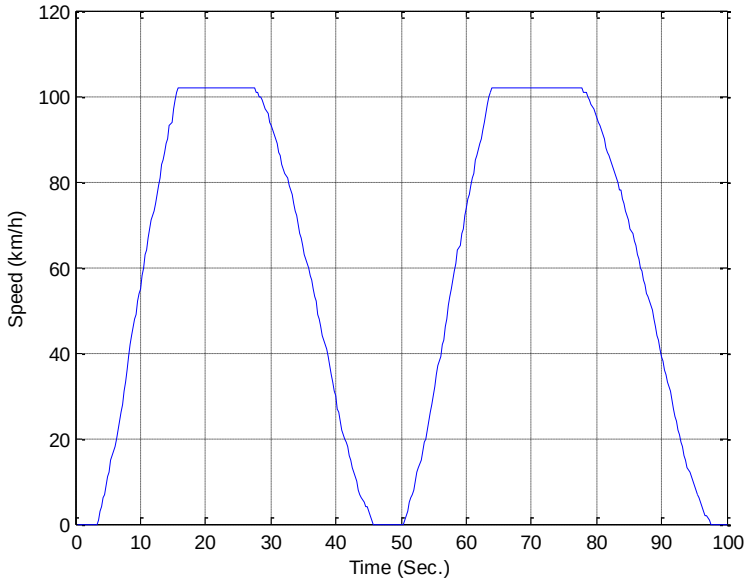

FIGURE 13, PULSES SPEED PROFILE

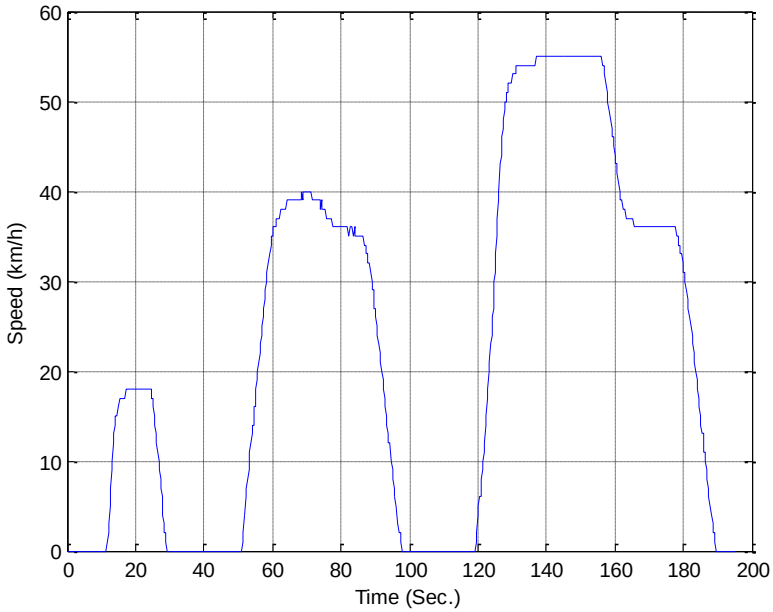

FIGURE 14, REAL UEDC SPEED PROFILE

2.3. ELECTRIC CAR EMISSIONS

The arrangement of the measurement system used in this test is outlined in Figure 15. Tests have been done inside a semi-anechoic chamber in Thales in Hengelo (the Netherlands) [174] in the 150 kHz – 30 MHz range. Most researchers interested in the measurement and analysis of electromagnetic emissions from electric driven vehicles concentrated on the magnetic field data [12, 16, 20, 21, 175, 176]. Because there is a metallic structure between the electric system and the passenger compartment on board the vehicle, it is reasonable to assume that at least the interior electric field will be minimal. Moreover, recent measurements of electromagnetic emissions from a hybrid vehicle showed that the level of the electric radiated disturbances has been below the limits established by the CISPR 25 [30]. Also, measurements below 30 MHz of radiated EMI due to a hybrid bus have shown that electric fields in that range are not discernible and can't be distinguished from ambient noise [19]. Furthermore, experimental and epidemiological data, as well as theoretical arguments, suggest that the magnetic rather than the electric component of the electromagnetic field can be relevant to the human organism; because magnetic field can penetrate freely within tissues. This is why in this test, only the magnetic field data has been employed for training and testing the neural networks. Magnetic radiated EMI has been measured by means of a loop antenna as shown in Figure 16. The antenna has been put at a distance of 1 m behind the car under test; because in this case, the motor was in the rear part of the car. The Agilent technologies DSO-X 3024A digital oscilloscope has been employed to register the EMI signals.

Anti-aliasing filters weren't needed because the bandwidth of the antenna was 9 kHz – 30 MHz. According to the sampling theorem, the sampling frequency must be at least twice the maximum signal frequency which is 30 MHz in this case. Therefore, EMI signals have been sampled at 125 MHz. The sweep duration (capture time) was 100 μs; because this is the reciprocal of the resolution bandwidth as explained in [61].

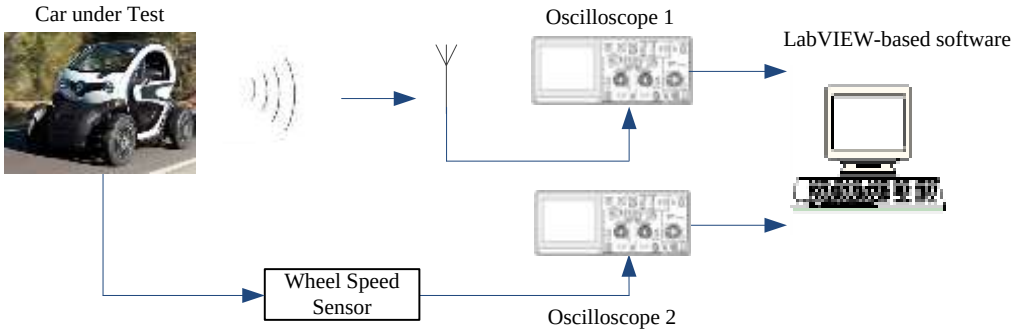

FIGURE 15, SCHEMATIC DIAGRAM OF THE MEASUREMENT SETUP

FIGURE 16, ROHDE & SCHWARZ LOOP ANTENNA DURING EXPERIMENTS WITH A RENAULT TWIZY

The driving profile has been registered by measuring the wheel rotational speed. The vehicle has been jacked up some centimeters from the ground by means of wood axle stands. So the electric car has been working under “free-wheeling” conditions. The problem of this condition is that the consumption of the electrical engine is very low. In this case, the interference levels measured will be lower than the emissions produced by the vehicle in a realistic situation. A rely as can be seen in Figure 17 (a) has been used to design the speed measurement

system. More details of the wheel speed measurement circuit are illustrated in Figure 17 (b). The velocity of the car has been changed manually. Six magnets have been fixed along the circumference of one of the rear wheels with a separation of 60 degrees approximately. This electronic system has been fixed near the wheel such that the rely conducts when a magnet passes. Because of different sampling times, the wheel speed signal has been registered by another oscilloscope at a rate of 10 kHz. It is already much more than twice the maximum frequency of the wheel speed signal. The sweep duration was 500 ms, and time between sweeps was also 1 second. These values for the speed measurement system have been ad-hoc adjusted.

The shielded cable measuring the wheel speed signal connected between the rely circuit inside the chamber and the scope outside the chamber didn't carry current because of the high input resistance of the scope channel. Only current pulses of 0.5 mA peak have been passing from the DC power supply to the ground passing by the pull-up resistor when the rely turns on. After analyzing different pulse trains from various speed profiles, the maximum pulse width has been found to be 5 ms approximately and the minimum rise/fall time was around 2-3 ms. Normally the spectrum of a digital switching waveform has a series of frequency components spaced at the reciprocal of the pulse repetition frequency and a first null at the reciprocal of the rise/fall time. Consequently, the spectrum of such current pulses is limited to 0.5 kHz approximately. The loop antenna used in this work usually measures in the 9 kHz – 30 MHz range, and the raw data have been analyzed in the 150 kHz – 30 MHz frequency range. Thus the speed measurement system has almost no effect on the measured magnetic emissions of the electric car.

A labVIEW software application has been designed to synchronize and save the sweeps of the EMI and speed signals. At the end of each experiment, two matrices are available in the database of the PC: EMI matrix and speed matrix. The rows represent the time-domain sweeps and the columns represent the samples within sweeps (12500 samples).

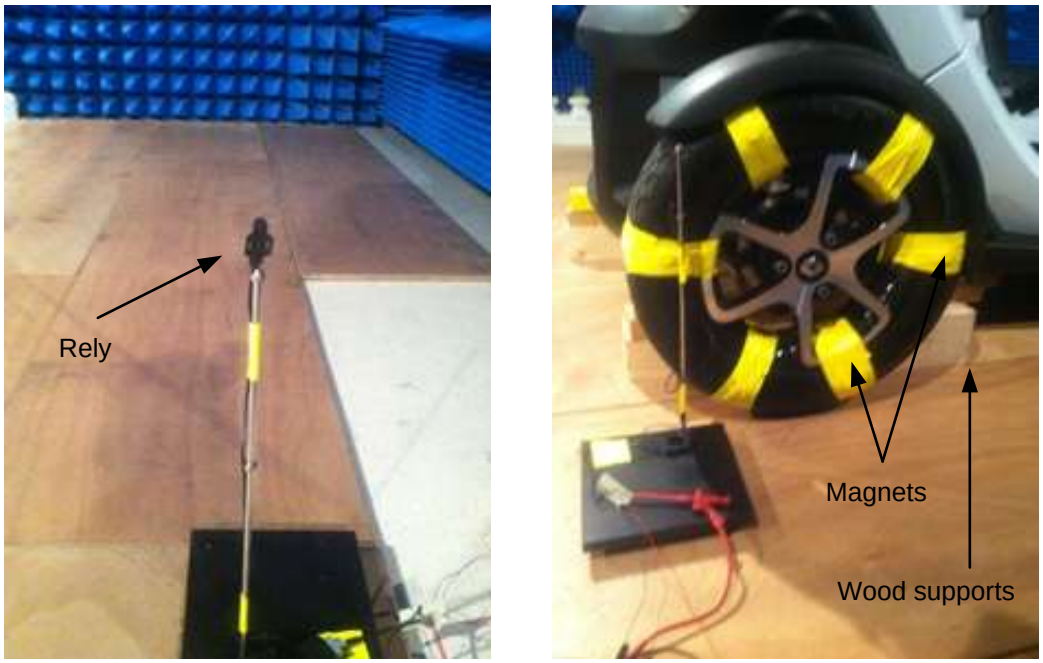

(A) MAGNETIC SENSOR (RELY) (B) SPEED MEASUREMENT CIRCUIT

FIGURE 17, ELECTRIC CAR WHEEL SPEED MEASUREMENT SYSTEM

On the other hand, the speed matrix contains samples of the digital signal resulting from the sensor. To calculate the sweep instantaneous speed, Eqn 4 should be considered where **D** is the wheel diameter in meters, **C** is the number of pulses per sweep, **N** is the number of pulses per turn, in this case 6, and **T** is the sweep duration in seconds. With the acquired instantaneous speed data, instantaneous acceleration has been calculated by forward finite difference method.

$$\text{Speed}\left({}^{\text{km}}/_{\text{h}}\right) = \frac{\mathbf{C}}{\mathbf{N}}\frac{1}{\mathbf{T}}\frac{\pi\mathbf{D}}{1000}3600 \qquad \text{EQN 4}$$

Three types of velocity profiles have been applied to the Renault Twizy: pulse, steps, and UEDC profiles as depicted in Figures 18, 19 & 20 respectively. The aim of the pulse profile is to analyze the effect of smooth acceleration and deceleration as well as cruising driving modes on the corresponding radiated interferences. The car has been also subjected to the steps profile in order to study the influence of the sharp accelerations and constant speeds on the corresponding radiated disturbances. The maximum velocity of the Renault Twizy is 80 km/h.

Both the steps and pulse patterns can simulate different driving behaviors up to 50 km/h. Moreover, the UEDC profile approximates the standard urban driving characteristics. Data of the UEDC style has been employed for training the neural network models, while data of the pulses and steps profiles have been used for the testing phase.

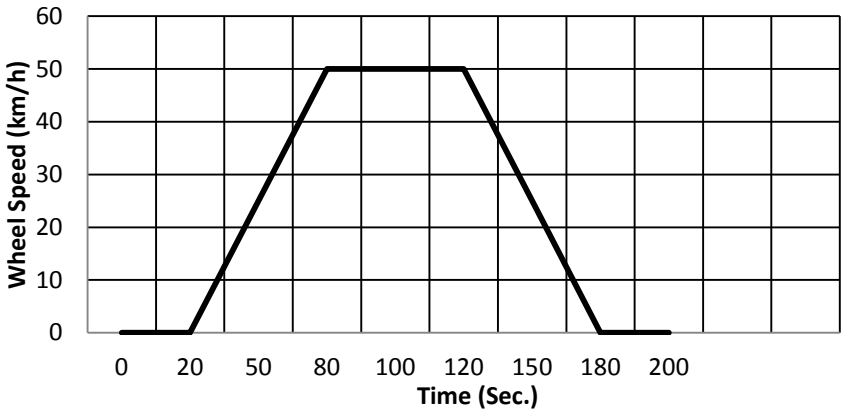

FIGURE 18, PULSE DRIVING PROFILE

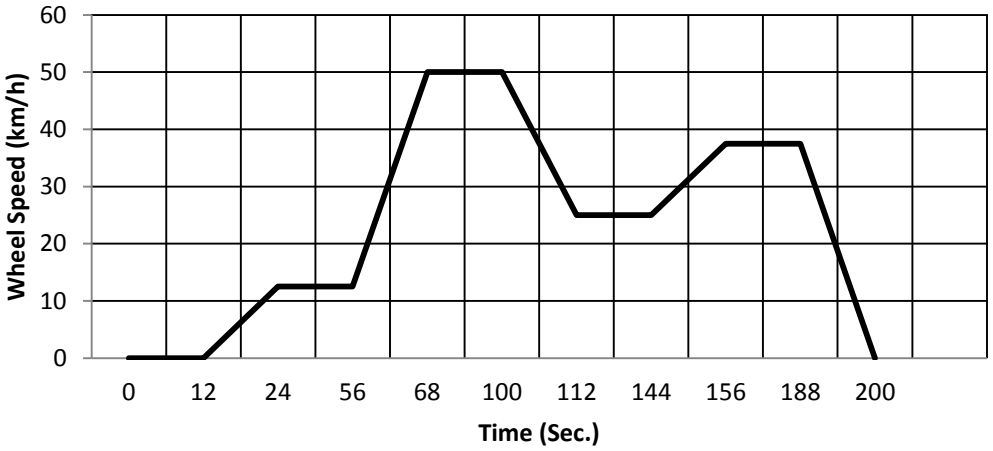

FIGURE 19, STEPS DRIVING PROFILE

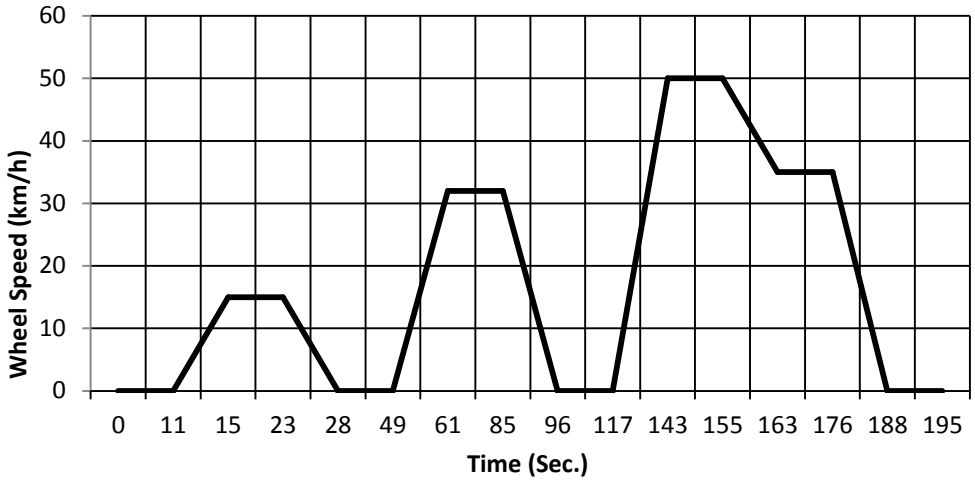

FIGURE 20, THEORITICAL UEDC DRIVING PROFILE

2.4. LIMITATIONS OF THE PROPOSED MEASUREMENT METHODOLOGY

The proposed EMI measurement technique in this thesis has the following limitations:

1. It doesn't follow a specific automotive EMC standard. This is because there is no standard, even SAE J551-5, which describes a procedure for measuring radiated disturbances from electric vehicles under transient driving modes.
2. Since the tests are performed inside shielded EMC chambers, the vehicles are tested without loading. Therefore the practical value of the model is limited.
3. A better approach to modeling should be done from measurements in open area test sites with the associated noise cancellation problems.
4. The vehicles under test were previously fully charged. In this way, the effect of the state of charge (SOC) of the power supply was not taken into account.

3 ARTIFICIAL NEURAL NETWORKS

ANNs are considered a kind of statistical modeling techniques offering several merits over the traditional CEM tools like: Rapid information processing, capability of providing mapping between input and output variables, requiring known input dataset without any assumptions, and automatic development of its own internal architecture.

3.1 NETWORK ARCHITECTURE

In this thesis a single output neural model is utilized to predict the vehicular radiated emissions in terms of the speed profile. The network output is the sweep mean level of radiated interferences in dBuV/m. Thus, all the networks described later will always contain one neuron in the output layer. Each layer of the neural models is fully connected to the next one. Different layers can have different number of neurons. This section presents the neural network topologies evaluated in this thesis. Based on the network layout, ANNs can be divided into two huge categories: static and dynamic networks.

3.1.1 STATIC NETWORKS

In some applications, the current value of the model output depends only on the current state of the inputs. This type of problems is usually called a static problem. In this thesis, four types of static networks have been analyzed: linear neuron, multilayer perceptron or single hidden layer feedforward, double hidden layer feedforward, and cascade. These artificial intelligence models have been selected for their wide range of applications as discussed previously in details in Section 1.2.2.2. The following sections give an overview of each type of these network topologies.

3.1.1.1 LINEAR NEURON (LN)

This network consists of a single linear neuron with *R* driving profile input variables as shown in Figure 21. The individual inputs p_1, p_2, …, p_R are each

weighted by corresponding elements $w_{1,1}$, $w_{1,2}$, …, $w_{1,R}$ of the weight matrix **W**. The first index of the elements in the weight matrix indicates the particular neuron destination for that weight. The second index indicates the source of the signal fed to the neuron. The neuron has a bias *b*, which is summed with the weighted inputs to form a net input *n* to the linear transfer function as shown in Eqn 5 where y_e is the model-estimated output.

$$y_e = n = w_{1,1}p_1 + w_{1,2}p_2 + \cdots + w_{1,R}p_R + b \qquad \text{EQN 5}$$

This expression can also be written in matrix form as described in Eqn 6, where **p** is the driving dynamics input column vector.

$$y_e = n = \mathbf{Wp} + b \qquad \text{EQN 6}$$

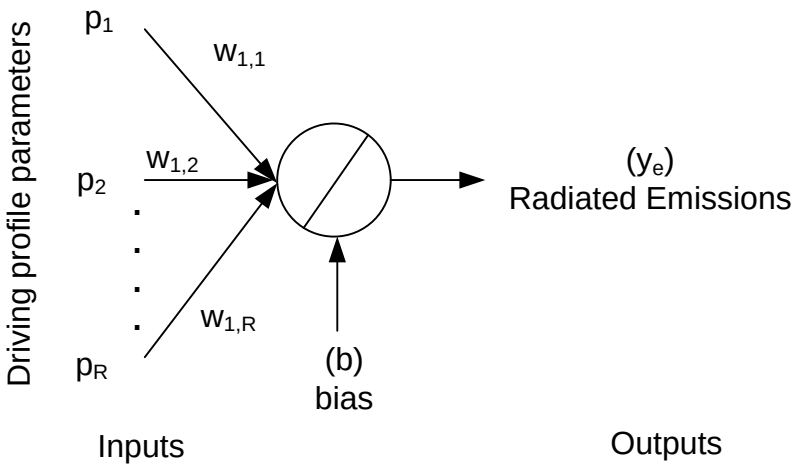

FIGURE 21, LINEAR NEURON NETWORK

3.1.1.2 MULTILAYER PERCEPTRON (MLP)

Figure 22 shows the topology of an R-input MLP network. It consists of two layers: "log-sig" hidden layer and linear output layer. So; it is also called single hidden layer feedforward network. Each layer has its own weight matrix **W**, bias vector *b*, net input vector *n*, and an output vector y_e. Superscript indices are used to distinguish between different layers. The estimated radiated emissions are calculated according to

$$y_e = n^2 = \mathbf{W}^2(\text{logsig}(\mathbf{W}^1\mathbf{p} + \text{b}^1)) + \text{b}^2 \quad \text{EQN 7}$$

In general, multi-layer networks are more powerful than single-layer ones. For instance, a network with sigmoid hidden layer and linear output layer can be trained to approximate most functions arbitrarily well, universal approximation property [177].

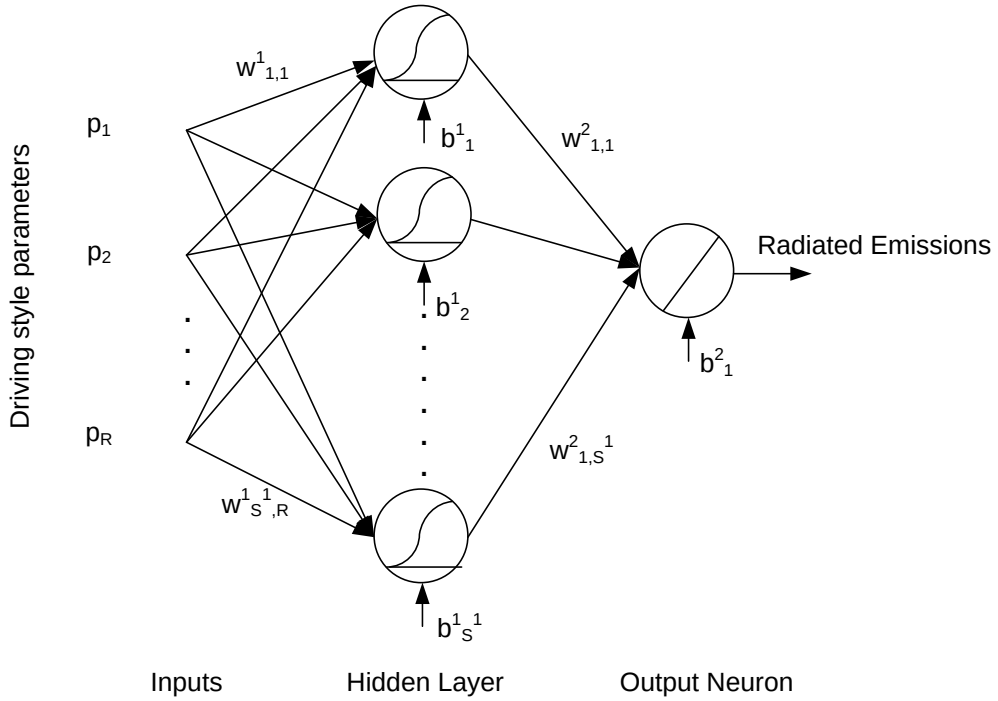

FIGURE 22, MLP NETWORK TOPOLOGY

3.1.1.3 DOUBLE HIDDEN LAYERS FEEDFORWARD (DHLF)

The internal structure of the DHLF network is illustrated in Figure 23. It is similar to the MLP network architecture but includes an additional hidden layer of sigmoid (log-sig) transfer function. The predicted radiated disturbances are calculated using Eqn 8. In general, one hidden layer is sufficient for the large majority of classification as well as regression problems.

$$y_e = n^3 = \mathbf{W}^3(\text{logsig}(\mathbf{W}^2(\text{logsig}(\mathbf{W}^1\mathbf{p} + \text{b}^1)) + \text{b}^2)) + \text{b}^3 \quad \text{EQN 8}$$

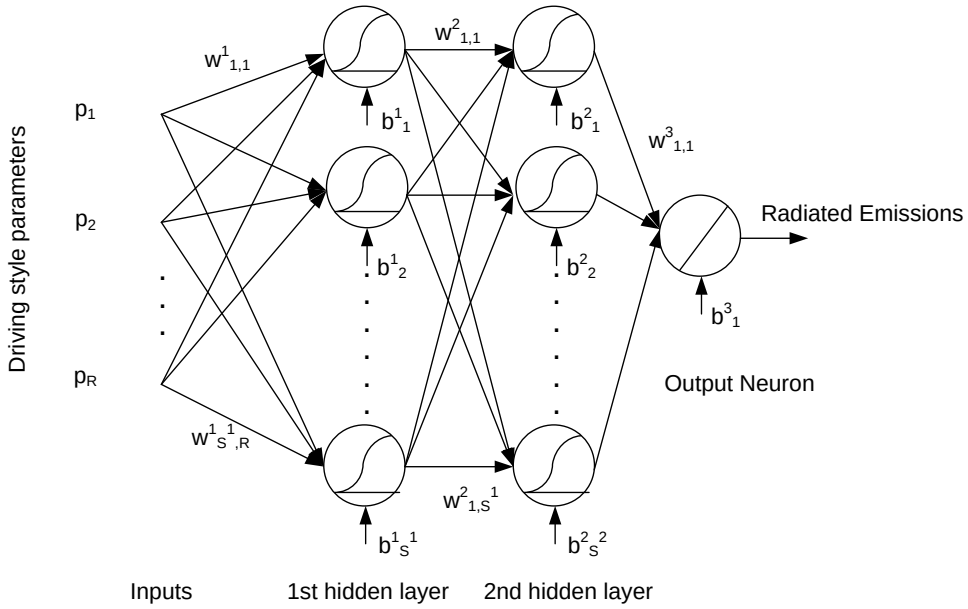

FIGURE 23, DOUBLE LAYER NETWORK ARCHITECTURE

3.1.1.4 CASCADE FEEDFORWARD (CF)

The CF network used in this dissertation is similar to the MLP neural network but includes a connection from the inputs to the output neuron as shown in Figure 24. The predicted magnetic fields are calculated according to Eqn 9.

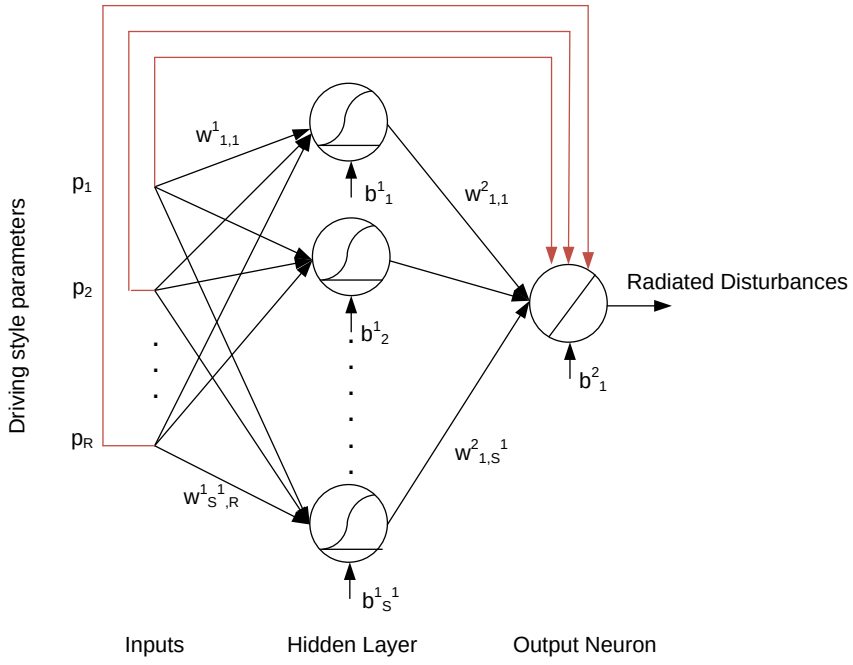

FIGURE 24, CASCADE FEEEDFORWARD NETWORK

$$\boldsymbol{y}_e = \boldsymbol{n}^2 = \mathbf{p} + \mathbf{W}^2\left(\text{logsig}(\mathbf{W}^1\mathbf{p} + \mathbf{b}^1)\right) + \mathbf{b}^2 \qquad \text{EQN 9}$$

3.1.2 DYNAMIC NETWORKS

In dynamic applications, the current value of the output variable depends on the current and past values of the input and/or output variable(s). In this thesis, four types of dynamic ANN models have been evaluated: Input Time Delay network (ITD), Distributed Time Delay network (DTD), Layer Recurrent (LR) network, Nonlinear Autoregressive with external inputs network (NARX). These neural models have been evaluated in this thesis for their various applications as explained in details in Section 1.2.2.2. This section introduces an overview of each neural network topology.

3.1.2.1 ITD NETWORK

The ITD neuro-computing model is the most straightforward dynamic neural network. It simply consists of a feedforward network with a tapped delay line at its inputs as shown in Figure 25. It is also called focused time delay network which is a part of a general class of dynamic networks labeled focused networks in which the dynamics appear only at the input of a static MLP network. The value of the magnetic radiated emissions estimated by this network is given by Eqn 10.

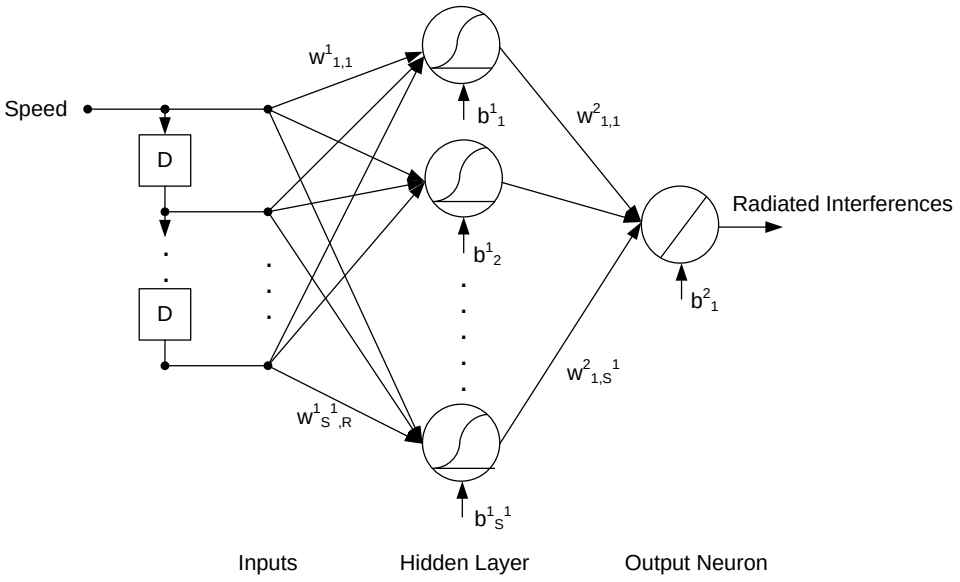

FIGURE 25, LAYOUT OF THE ITD NETWORK

$$y_e = n^2 = \mathbf{W}^2(\text{logsig}(\mathbf{W}^1.\boldsymbol{z}^{-1}.\mathbf{p} + \text{b}^1)) + \text{b}^2 \quad \text{EQN 10}$$

3.1.2.2 DTD NETWORK

The ITD network only has delay elements at the input of the hidden layer. Tapped delay lines can also be distributed throughout the network as can be seen in Figure 26. The behavior of the ITD model can be described by Eqn 11.

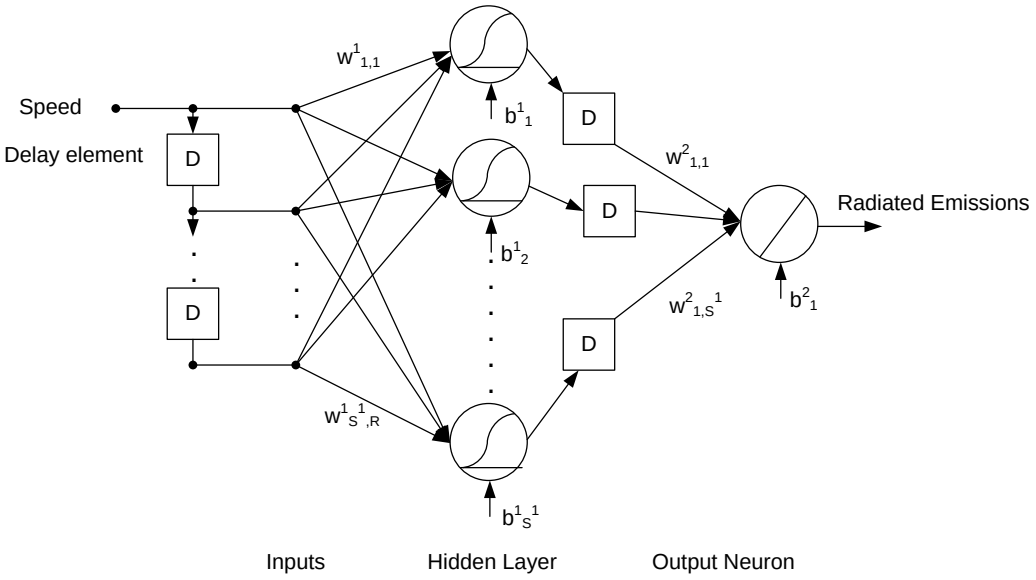

FIGURE 26, SCHEMATIC DIAGRAM OF THE DTD NETWORK

$$y_e = n^2 = \mathbf{W}^2(\boldsymbol{z}^{-1}.\text{logsig}(\mathbf{W}^1\mathbf{p} + \text{b}^1)) + \text{b}^2 \quad \text{EQN 11}$$

3.1.2.3 LR NETWORK

Layer recurrent neural networks are similar to feedforward networks, except that the hidden layer has a recurrent connection with a tap delay associated with it as can be seen in Figure 27. Eqn 12 depicts the behavior of the LR network.

3.1.2.4 NARX NETWORK

It is a recurrent dynamic network with feedback connections enclosing the hidden layer. The internal structure of this type of neural networks is shown in Figure 28. The current value of the output variable depends on its previous values as well as the current and previous values of the input signal. The behavior of this artificial intelligence model can be described by Eqn 13.

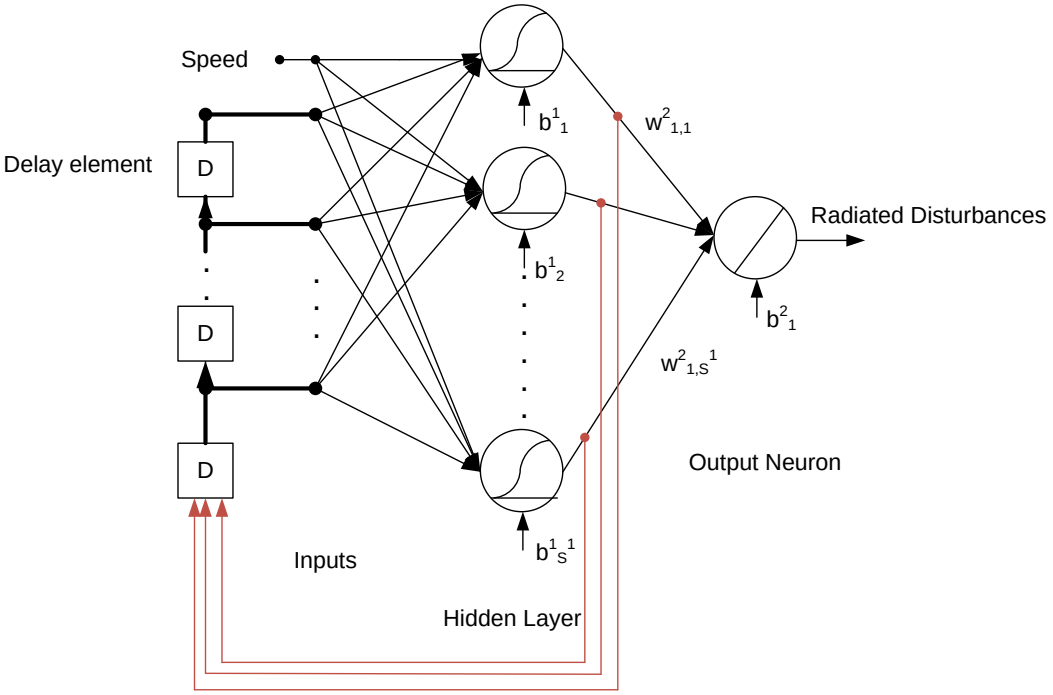

Figure 27, Layer recurrent network layout

$$y_e = n^2 = \mathbf{W}^2(\text{logsig}(\mathbf{W}^1.(\mathbf{p} + \boldsymbol{z}^{-1}.n^{\mathbf{1}}) + \mathrm{b}^1)) + \mathrm{b}^2 \qquad \text{EQN 12}$$

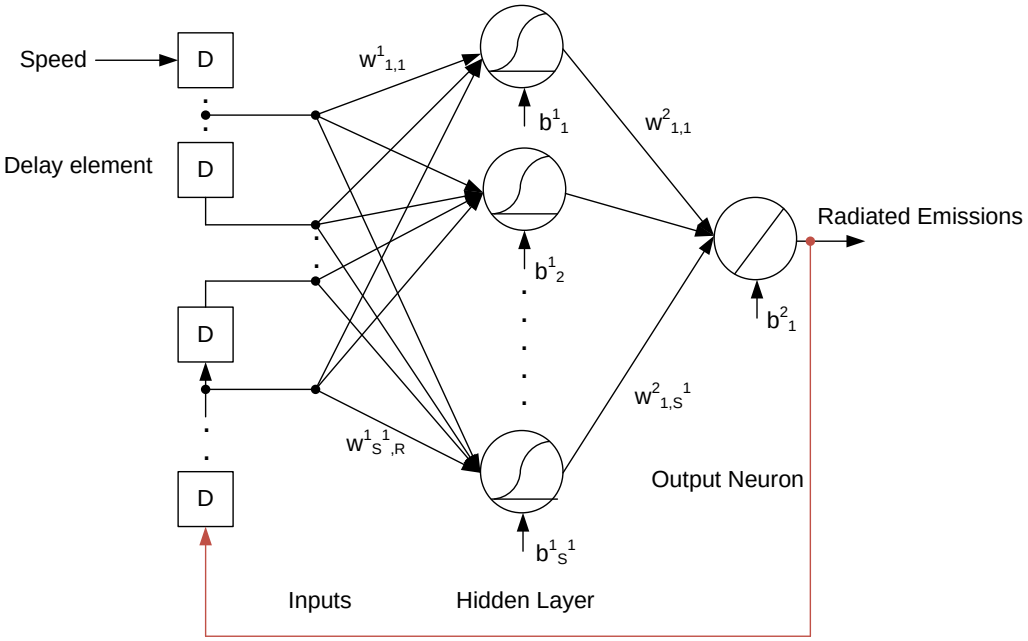

FIGURE 28, SCHEMATIC DIAGRAM OF NARX NETWORK

$$y_e = n^2 = \mathbf{W}^2(\text{logsig}(\mathbf{W}^1.\boldsymbol{z}^{-1}.(\mathbf{p} + y_e) + \text{b}^1)) + \text{b}^2 \quad \text{EQN 13}$$

3.2 TRAINING ALGORITHMS

Couple of reasons can lead to the failure of training a given ANN. Firstly; improper initialization can cause the model parameters to fail to converge to the proper values. On the other hand, an insufficient number of hidden neurons can lead to the inability of the given model to implement the desired function. In this work, to avoid the first possibility, each neural model was trained and tested 10 times. The network architecture with the lowest root mean square error (RMSE) on the testing data set has been chosen. The RMSE has been calculated according to Eqn 14 where **N** is the size of the testing dataset, y_e is the vector of estimated values by the model, y_m is the vector of measured values by the measurement system.

$$RMSE = \left[\frac{1}{N}\sum_{i=1}^{N}(y_e - y_m)^2\right]^{1/2} \quad \text{EQN 14}$$

With respect to the second reason, there is no theory yet to explain how to choose the optimal number of hidden neurons to approximate any given function. If the hidden neurons are too few, a high training error and high generalization error would result due to under-fitting. On the contrary, if the hidden neurons are too many, there would be a low training error, but there would still be a high generalization error due to over-fitting. In most situations, the best way to determine the optimum size of the hidden layer is to train several networks and estimate the generalization error of each [178, 179]. In this work, the network growing technique [178] has been applied by sequentially adding hidden neurons from 1 to 30 in the majority of cases comparing the testing RMSE.

Three main learning algorithms have been used to train the neural models employed in this thesis: Least Mean Square (LMS), backpropagation (BP), and Extreme Learning Machine (ELM). This section points out the key points of each one of these algorithms.

3.2.1. LEAST MEAN SQUARE

Eqn 15 makes up the LMS algorithm, delta rule, or Widrow-Hoff learning algorithm; where **W** is the network weights matrix, α is the learning rate, **P** is the input vector, $\boldsymbol{e}$ is the error vector, i.e. the difference between the network outputs and targets, and k is the iteration index. This algorithm has been used to train the linear neuron network discussed in Section 3.1.1.1.

$$\boldsymbol{W}(k+\mathbf{1}) = \boldsymbol{W}(k) + \mathbf{2}\alpha\boldsymbol{e}(k)\boldsymbol{P}(k) \qquad \text{EQN 15}$$

3.2.2. BACKPROPAGATION

The backpropagation algorithm for multilayer networks is a generalization of the LMS algorithm discussed in the previous section. Both algorithms use the same performance index or cost function: mean square error. The network parameters are updated using the BP algorithm according to Eqn 16 where *s* is the sensitivity matrix.

$$\boldsymbol{W}(k+\mathbf{1}) = \boldsymbol{W}(k) - \alpha\boldsymbol{s}^{\boldsymbol{m}}(\boldsymbol{a}^{\boldsymbol{m-1}})^{\boldsymbol{T}} \qquad \text{EQN 16}$$

Since the basic back-propagation learning algorithm is too slow for most practical applications, there have been extensive research efforts to accelerate its convergence. Different gradient-descent variations of the backpropagation algorithm have been considered in this work like: Levenberg-Marquardt (LM) [180], Scaled Conjugate Gradient (SCG) [181], One Step Secant (OSS) [182], and Quasi-Newton BFGS [183].

3.2.3. EXTREME LEARNING MACHINES

ELM is considered a recently emerging learning algorithm that overcomes some challenges faced by the conventional backpropagation training such as: slow learning speed, trivial human intervene, local minima, and poor computational scalability [184]. ELM is designed for single hidden layer feedforward neural network topology. The ELM-trained networks have been proven to satisfy the

universal approximation property [185]. This learning algorithm has been exploited to train the MLP neural network in this paper.

The ELM is one of the most powerful tools that has been widely used in recent years in various fields [186] such as: security assessment [187], data privacy [188], EEG and seizure detection [189], image quality assessment [190], implementation with FPGAs [191], face recognition [192], and human action recognition [193]. Function approximation is one of the basic learning tasks that an ELM can accomplish [194].

The ELM algorithm is based on an MLP network whose input weights are randomly initialized. The output of an MLP neural network is

$$y_e = \mathbf{W}^2(\text{logsig}(\mathbf{W}^1\mathbf{p} + \text{b}^1)) \quad \text{EQN 17}$$

To obtain a zero estimation error, the vector of estimated values should be equal to the vector of target values. That is:

$$y_m = \mathbf{W}^2\big(\text{logsig}(\mathbf{W}^1\mathbf{p} + \text{b}^1)\big) \quad \text{EQN 18}$$

where y_m is the measured or target vector. The last equation can be written in the matrix form as follows:

$$\mathbf{T} = \mathbf{H}\mathbf{W}^2 \quad \text{EQN 19}$$

where $\mathbf{H}$ is the output matrix of the hidden layer, $\mathbf{W}^2$ is the weight matrix of the output layer, and $\mathbf{T}$ is the target matrix. In this way, the training of the MLP becomes the solution of minimum squares problem defined by Eqn 19. In other words, the optimum weights of the output layer are:

$$\mathbf{W}^{2^*} = \mathbf{H}^\dagger\,\mathbf{T} \quad \text{EQN 20}$$

where $\mathbf{H}^\dagger$ is the Moore-Penrose pseudo inverse [195].

4 RESULTS & DISCUSSION

Measurement as well as estimation results of radiated emissions will be discussed in this chapter. The first section introduces the results obtained from the tests carried out with a Vectrix electric motorcycle. Afterwards, the results obtained from tests done with the Renault Twizy electric car are analyzed. The last section presents the estimated electromagnetic emissions derived from a Think City electric car in real traffic conditions.

4.1 ELECTRIC MOTORCYCLE

This section discusses the measurement results, neural model development details, and comments on the model-estimated radiated emissions of an electric motorcycle.

4.1.1. MEASUREMENT & ANALYSIS RESULTS

The results obtained from measuring the electric radiated emissions from an electric motorcycle are explained in this section as a result of applying the pulses and UEDC speed profiles described in Section 2.2.

4.1.1.1 PULSES PROFILE

Figure 29 shows the spectrogram of the electric field emissions corresponding to the pulses speed profile. The processing steps followed to obtain such Figure and the next one have been already explained in details at the end of Section 2.1. The horizontal axis of this Figure represents the time in seconds while the vertical one denotes the frequency components in the EMI signal. The intensity of the different spectral components is represented by the color as can be noted in the color bar at the right of the Figure. It's clear that emission levels in the 4 – 8 MHz range as well as around the 15.4 MHz frequency component change correspondingly with the applied speed excitation profile as shown in Figure 30. For example, the emissions level was minimum during the idling driving mode, i.e. when the speed was zero. On the other hand, emissions mean level reached the maximum value during the cruising driving mode at 100 km/h.

Emission levels below 3 MHz are significant but independent from the instantaneous velocity of the motorcycle. The radiated EMI levels decrease slightly when the motorcycle is in idling mode and remain virtually constant when the speed is not zero. At 16 MHz approximately, there is a clear constant spectral component of the emissions. Also from 23 to 30 MHz, a light radiated emission can be detected. In all these cases, it is difficult to relate the motorcycle radiated emissions to the applied speed profile.

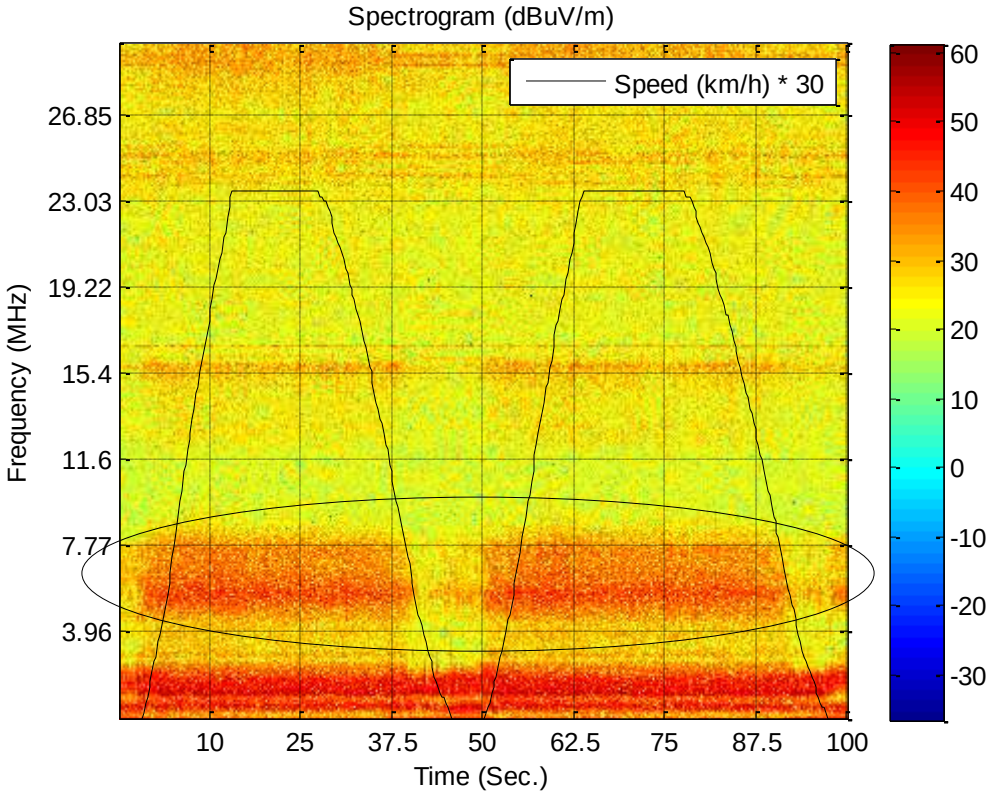

FIGURE 29, SPECTROGRAM OF THE EMISSIONS DUE TO THE PULSES PROFILE

Concentrating on the 4 – 8 MHz frequency range, there is a dead zone where the emissions can be noted when the speed exceeds 10 km/h approximately as can be seen in Figure 30. Then the emissions increase as a result of increasing the corresponding speed till 40 km/h where the emissions saturate more or less to the maximum level.

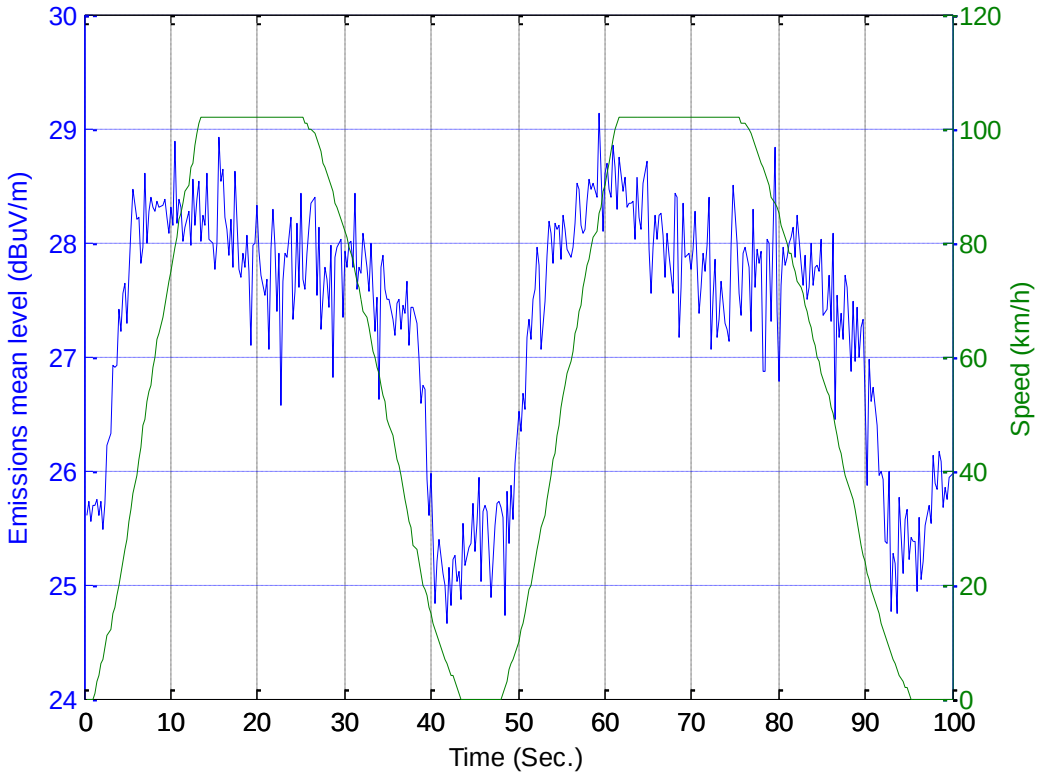

FIGURE 30, TEMPORAL EVOLUTION OF SPEED & EMISSIONS DUE TO THE PULSES PROFILE

4.1.1.2 UEDC PROFILE

The 4 – 8 MHz frequency range and at 15.4 MHz approximately again contained the time-varying spectral components of the radiated emissions as depicted in Figure 31.

The mean value of the emissions sweeps is changing with the instantaneous value of the motorcycle speed in the 4 - 8 MHz frequency range. Figure 32 shows that it is possible to distinguish between idling and cruising driving regimes. On the other hand, it's complicated to observe the difference in emission levels due to different cruising levels. Similar to the previous profile, three zones can be observed: a dead zone below 10 km/h, linear between 10 and 40 km/h, and a saturated one for velocities above 40 km/h.

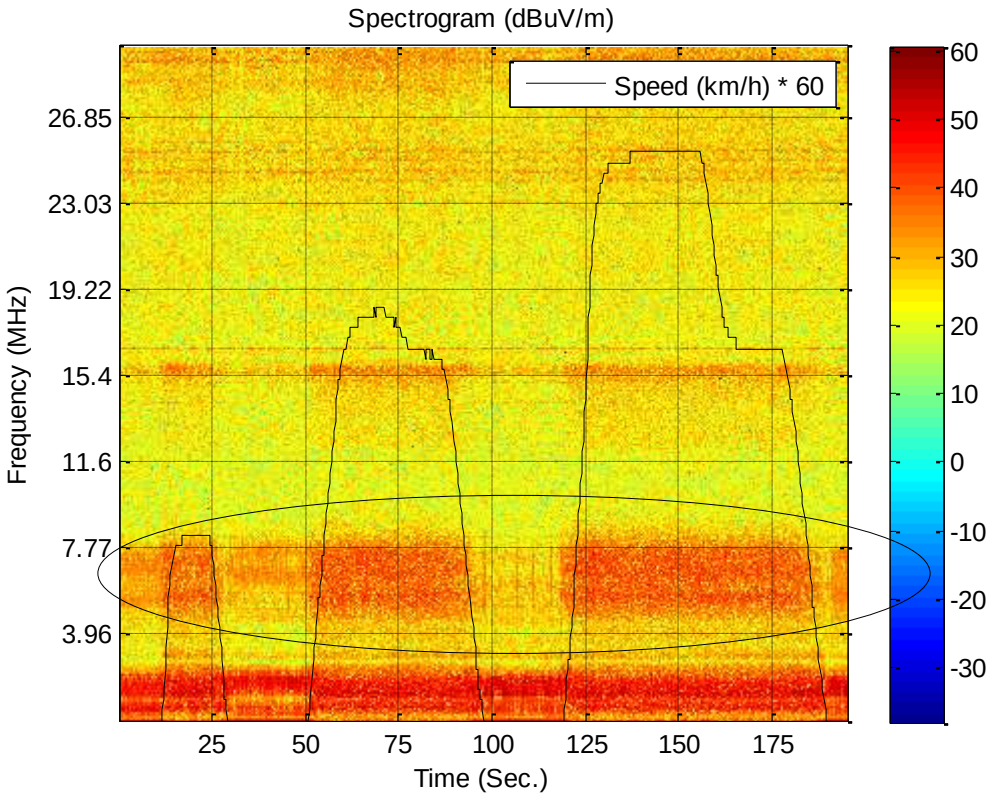

FIGURE 31, SPECTROGRAM OF THE EMISSIONS DUE TO THE UEDC PROFILE

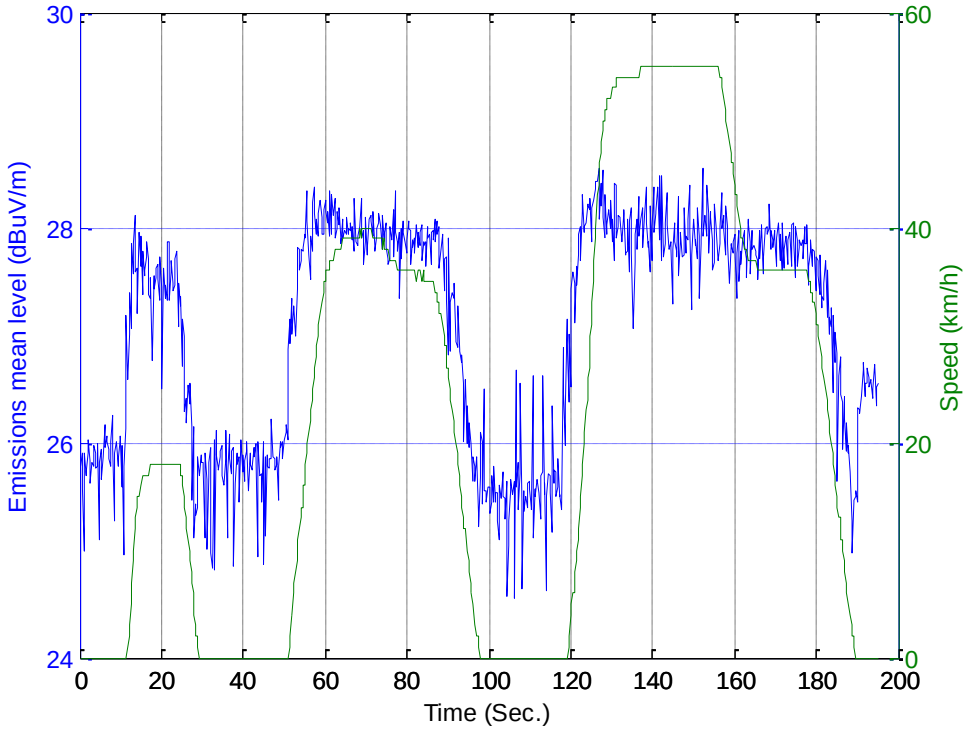

FIGURE 32, TEMPORAL EVOLUTION OF SPEED & EMISSIONS DUE TO THE UEDC PROFILE

It is noteworthy that the radiated perturbations of the electric motorcycle due to both the pulses and UEDC profiles have approached the limits established by the SAE J551-5 standard at 16, 24, and 30 MHz approximately as can be seen in Figure 33. It describes the peak detector results for all frequency bins from 150 kHz to 30 MHz. The peak at 15.4 MHz has also been noticed in the spectrogram in Figure 31. Also the same figure shows that the motorcycle emissions have already exceeded the limits specified by the MIL-STD-461F standard for ground applications. The measurement uncertainty of the electric motorcycle radiated disturbances is ±7 dB calculated according to CISPR 16-4-2 with the parameters tabulated in Appendix A2.

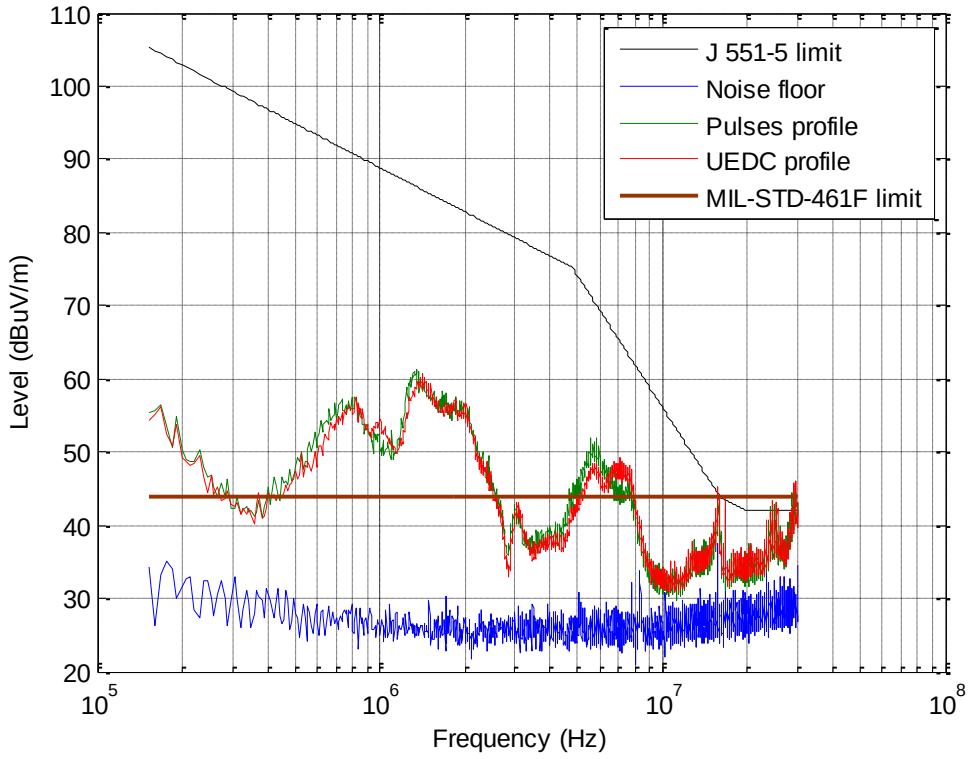

FIGURE 33, PEAK DETECTOR SPECTRA OF BOTH PROFILES

The SAE J551-5 standard has been selected as a reference because it provides limits for electric as well as magnetic radiated emissions below 30 MHz due to electric vehicles. Also the MIL-STD-461F specifies radiation limits for electric radiated emissions due to traditional non-electric vehicles in military applications below 30 MHz. The measurement distance between the antenna and

the vehicle under test should be 1m and 3m according to MIL-STD-461F and SAE J551-5 respectively. It's very important to take into account that these results have been obtained with a free running motorcycle. This means that with the same motorcycle running in real traffic conditions, which can be simulated by a dynamometer, the emissions will increase indeed.

The parameters of the two driving patterns applied to the electric motorcycle are illustrated in Table 3. The pulses style shown in Figures 13 & 30 mimic an interurban driving behavior and the standard UEDC depicted in Figures 14 & 31 roughly simulate an urban driving cycle as can be concluded from the maximum and average speed values recorded in Table 3. Although the maximum speeds in both profiles were completely different, i.e. 55 km/h and 102 km/h for UEDC as well as pulses driving styles respectively, the corresponding maximum level of emissions were approximately the same as can be seen also in Figures 30 & 32. This saturation of the emissions level although the instantaneous speed was changing may be because the level of the electric radiated emissions is more related to changes in speed than to the instantaneous speed value.

TABLE 3, STATISTICS OF THE DRIVING PROFILES

Driving Metrics	Pulses Profile	UEDC Profile
Maximum Speed (km/h)	102	55
Minimum Speed (km/h)	0	0
Average Speed (km/h)	59.0675	22.7231
Speed Standard Deviation	39.1965	20.2682
Maximum Acceleration (km/h/s)	4	3
Minimum Acceleration (km/h/s)	-3	-2
Average Acceleration (km/h/s)	0	0
Acceleration Standard Deviation	1.3946	0.6185
Maximum Emissions (dBuV/m)	29.1252	28.5492
Minimum Emissions (dBuV/m)	24.6598	24.5454
Average Emissions (dBuV/m)	27.2983	27.0594
Emissions Standard Deviation	1.0832	1.0382

4.1.2. MODEL DEVELOPMENT RESULTS

Concerning the data preparation task, the early stopping technique has been employed to improve the generalization performance. In this technique the entire normalized data set has been divided randomly into training (80%), validation (10%), and testing (10%) subsets. The validation subset is employed during the training phase by monitoring the validation set error. It normally decreases during the initial phase of the training, as does the training set error. However when the network begins to over-fit the data, the validation set error begins to rise [179]. When it increases for 10 iterations in this work, training stops and the network parameters are returned to the minimum validation set error state. The testing subset isn't used during training but the testing set error helps to compare different models based on the generalization performance.

The UEDC profile data has been utilized to train, validate and test the MLP neural model [196]. This type of ANNs has been selected for its simplicity, reliability, and wide range of applications. In this thesis, the MLP neural network has been trained with the LM numerical optimization method; because it is the fastest for function approximation problems of networks containing up to a few hundred weights [180]. The network growing technique has been adopted to increase the number of hidden elements from 1 to 30 gradually. Table 4 shows that 18 hidden neurons have achieved the best generalization performance in terms of the testing RMSE. Figure 34 shows the internal structure of the best MLP model. Only one type of ANNs has been taken into consideration to evaluate the data of the Vectrix; because the developed model has already gave reasonable and satisfactory results.

TABLE 4, GENERALIZATION RMSE CORRESPONDING TO DIFFERENT HIDDEN NEURONS

Hidden neurons	5	10	15	18	25	30
Testing RMSE * 1e-11	0.2289	0.2229	0.2763	0.2097	0.2362	0.2266

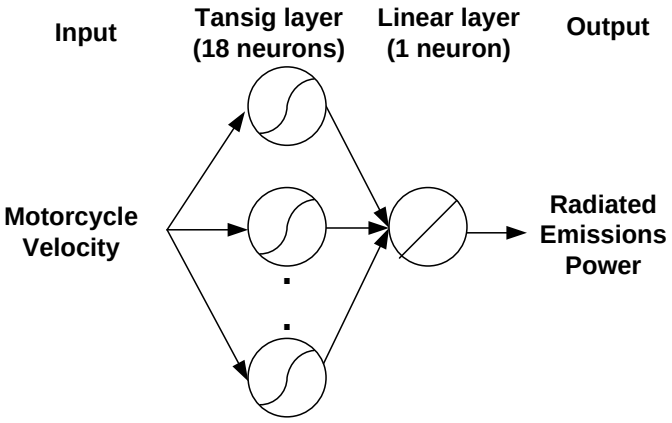

FIGURE 34, STRUCTURE OF THE PROPOSED MLP MODEL

4.1.3. ESTIMATION RESULTS

Figure 35 shows the spectra of noisy (received by antenna 1, refer to Figure 10), noise (received by antenna 2), and filtered (estimated by the adaptive noise canceller) signals. This figure clearly points out the capability of the proposed adaptive filter to cancel out or to reduce the additive CAN bus noise component on the motorcycle's EMI signal. For example, in the frequency ranges (1 - 2) and (7 – 8) MHz, although the reference CAN bus noise level was strong relative to the noisy signal level, the adaptive filter has successfully reduced the additive CAN bus noise.

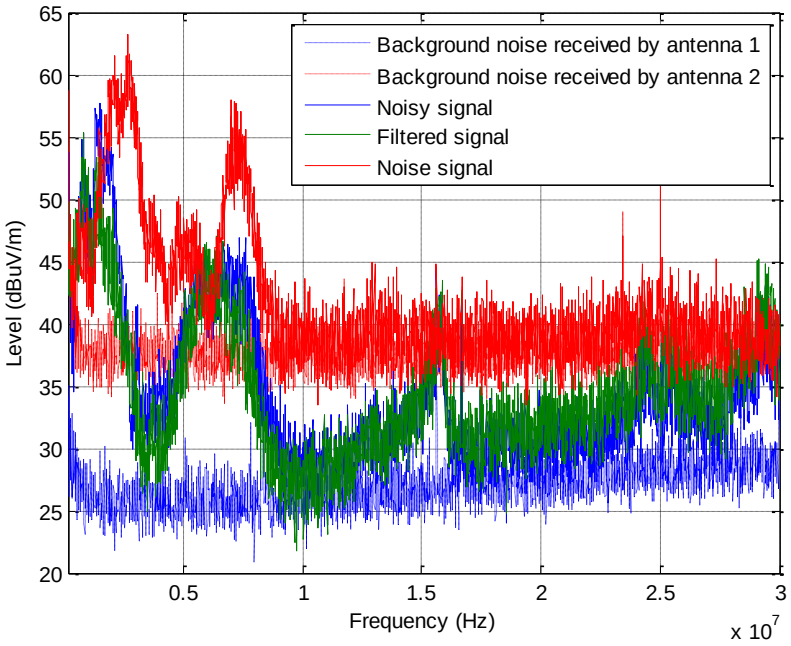

FIGURE 35, PEAK DETECTOR SPECTRA OF NOISY, NOISE, AND FILTERED (ESTIMATED) SIGNALS

Table 5 points out a comparison between the performance of different adaptive algorithms in terms of the root mean square difference (RMSD), see Eqn 14, between the noisy and estimated signals spectra where DFT is Discrete Fourier Transform [197], PBFD is Partitioned Block Frequency Domain [178], PBUFD is Partitioned Block Unconstrained Frequency Domain [178], NLMS is Normalized Least Mean Square [197], SDLMS is Sign Data Least Mean Square [198], SELMS is Sign Error Least Mean Square [198], *S* is the Step-size, and *BL* is Block Length. The more the RMSD, the more the capability of the adaptive noise canceler to reduce the additive CAN bus noise; because the RMSD in this case reflects the amount of noise suppression. The DFT adaptive algorithm achieved the best noise suppression performance in comparison with five different time as well as frequency domain adaptive algorithms.

TABLE 5, COMPARISON BETWEEN DIFFERENT ADAPTIVE ALGORITHMS

Algorithm & Parameters	RMSD
DFT (S=0.01)	4.3669
PBFD (S=0.01, BL=100)	3.8493
PBUFD (S=0.01, BL= 250)	1.0948
NLMS (S=0.5)	3.9104
SDLMS (S=0.05)	2.8912
SELMS (S=0.5)	4.0438

Figure 36 shows the estimated and measured radiated emissions as well as the motorcycle instantaneous speed. It clearly shows the nonlinear relationship between the motorcycle's velocity and the corresponding mean power of the radiated emissions. The level of the radiated disturbances increases with increasing the motorcycle's velocity. Also, the level of the radiated interferences remains at its minimum value when the motorcycle was idle. Moreover, it shows that the developed MLP model can successfully estimate the radiated emissions in terms of the applied velocity.

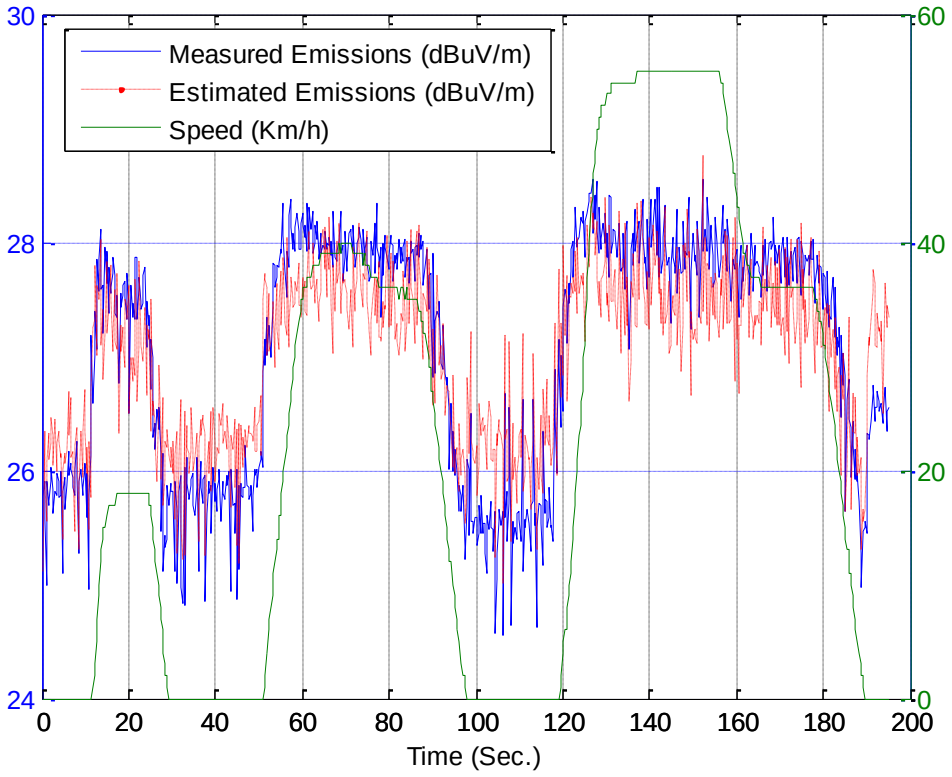

FIGURE 36, ESTIMATED & MEASURED EMISSIONS POWER

4.2 ELECTRIC CAR

The measurement results are analyzed and the neural model development details of the electric car are discussed here. Then the estimation accuracy of the selected model is described.

4.2.1. MEASUREMENT & ANALYSIS RESULTS

This section presents the results obtained from analyzing the data registered by applying three speed profiles: pulse, steps, and UEDC to a Twizy electric car.

4.2.1.1 PULSE PROFILE

This speed profile is a trapezoidal pulse in order to test the response of the radiated disturbances of the electric car to smooth acceleration and deceleration as well as high speed cruising driving modes. Figure 37 shows the temporal evolution

of the spectral components of the radiated emissions. The intensity of the low frequency components were relatively changing with time.

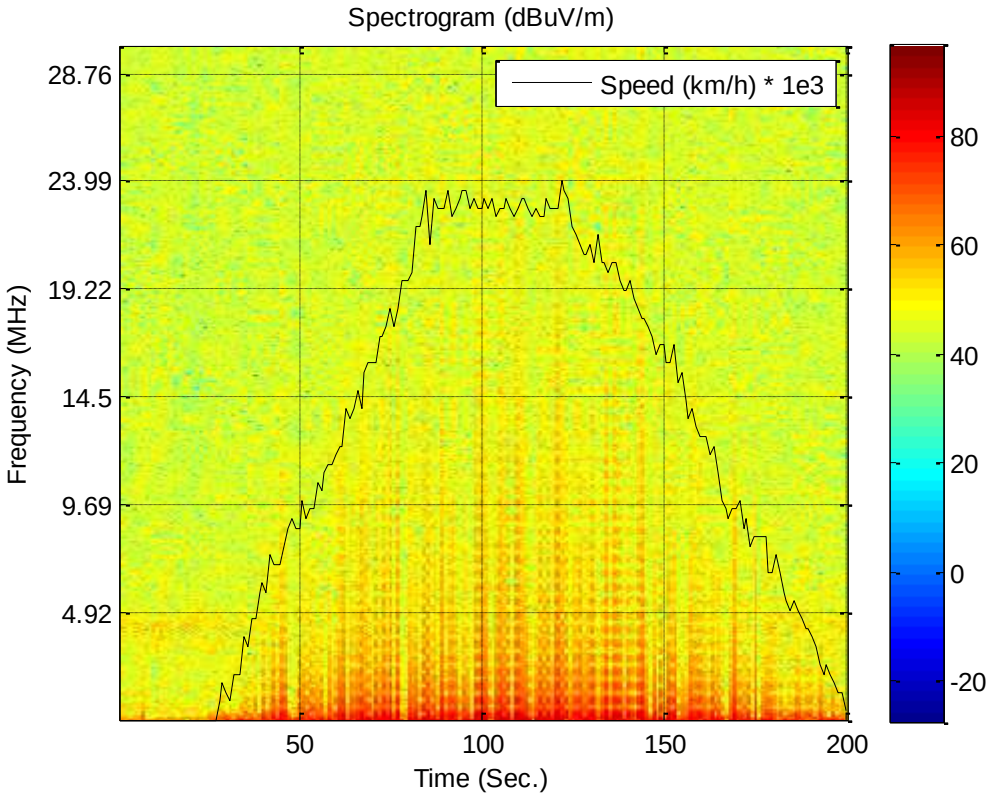

FIGURE 37, SPECTROGRAM OF THE EMISSIONS DUE TO THE PULSE PROFILE

A clear relationship between the sweep mean level of the radiated EMI and the corresponding speed profile can be noted in Figure 38. As expected, the minimum level of electromagnetic emissions has been detected during idling driving mode. On the other hand, the maximum emissions intensity has been recorded during cruising at 50 km/h.

The effect of the instantaneous acceleration on the intensity of the corresponding magnetic radiated interferences can be observed in Figure 39. Emissions have been increasing during acceleration, remaining approximately constant during cruising, and decreasing during deceleration.

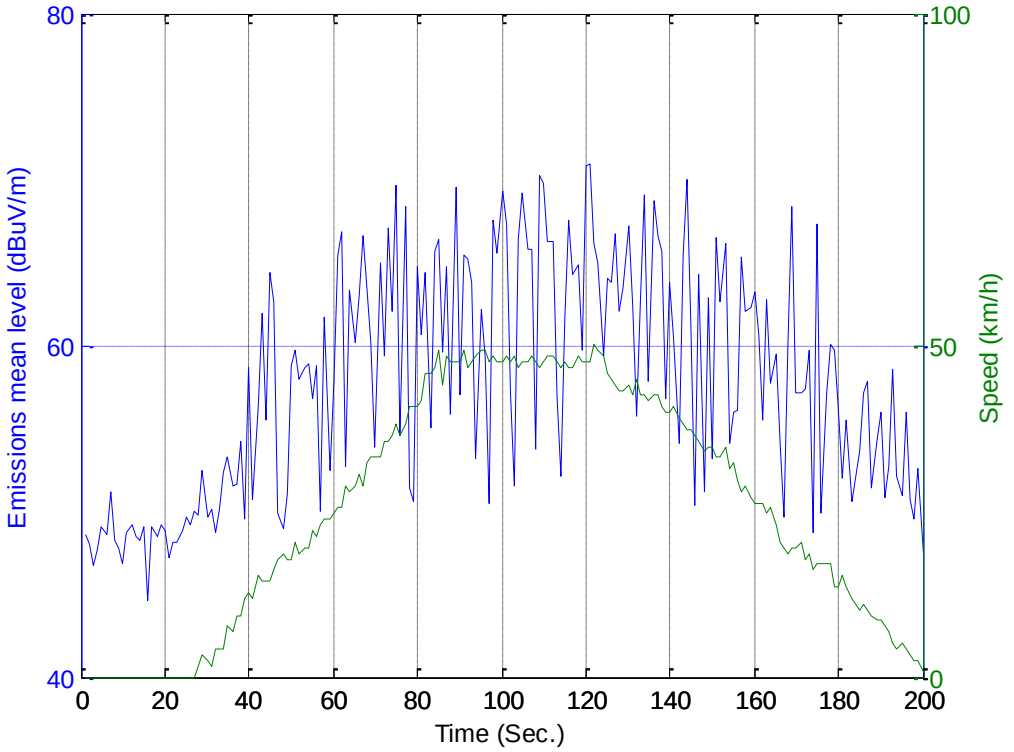

FIGURE 38, TEMPORAL EVOLUTION OF SPEED & EMISSIONS DUE TO THE PULSE PROFILE

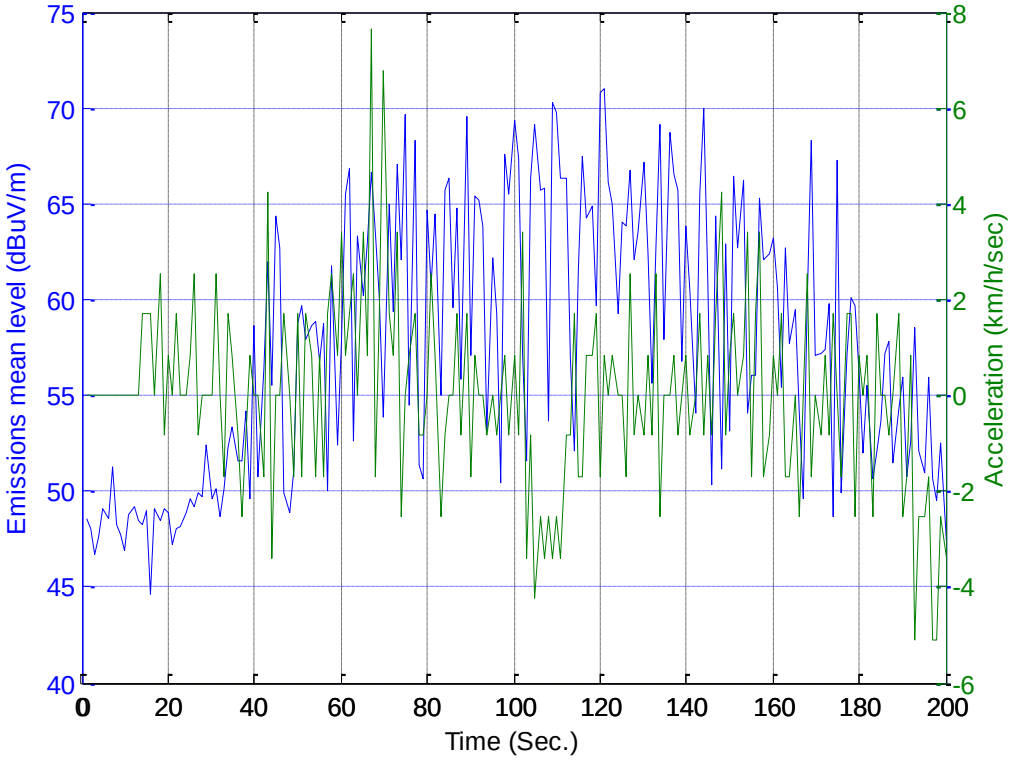

FIGURE 39, ACCELERATION & EMISSIONS VS TIME (PULSE PROFILE)

4.2.1.2 STEPS PROFILE

The aim of this driving cycle is to evaluate the effect of different constant speed values on the corresponding radiated electromagnetic fields. The spectrogram of the radiated EMI due to this profile is depicted in Figure 40. It also confirms that actually the time-varying spectral components are contained in lower frequencies. The higher the speed applied to the electric car, the higher the spectral components appearing in the spectrogram. Figure 41 shows that the sweep mean intensity of the radiated emissions have been changing increasingly and decreasingly with the instantaneous speed. It also shows the nonlinear cause-effect relationship where the emissions level at 50 km/h is not double times the emissions level at 25 km/h for instance. The impact of the instantaneous acceleration on the radiated magnetic waves can be seen in Figure 42. It shows that positive acceleration values correspond to an increase in radiated field level while negative acceleration values resulted in decreasing the intensity of the corresponding radiated magnetic fields.

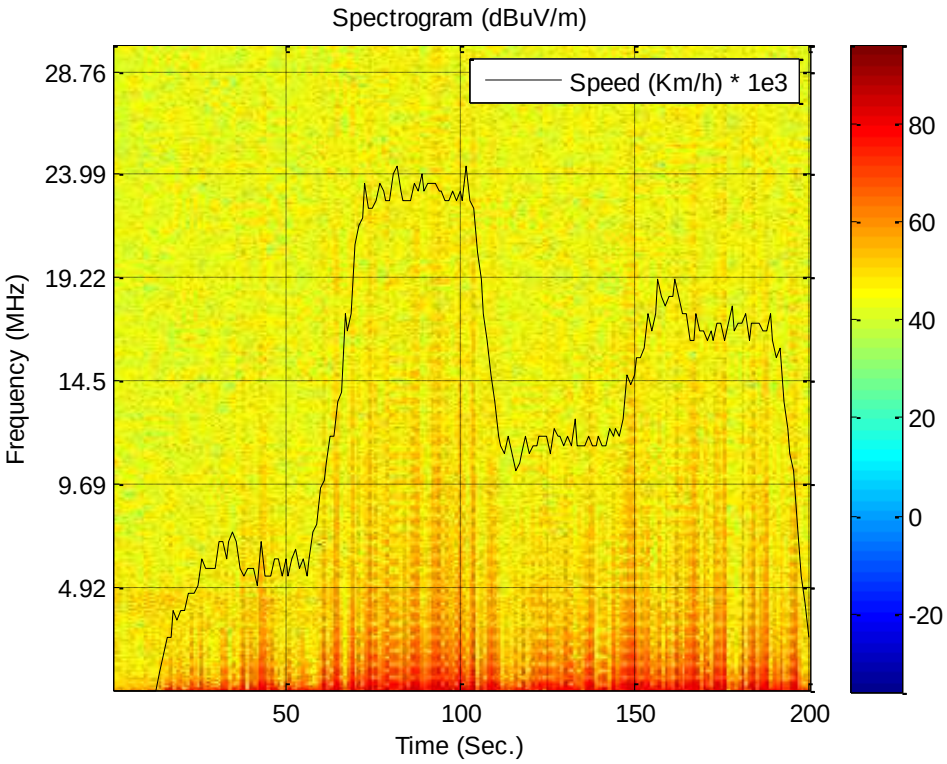

FIGURE 40, SPECTROGRAM OF THE EMISSIONS OF THE STEPS PROFILE

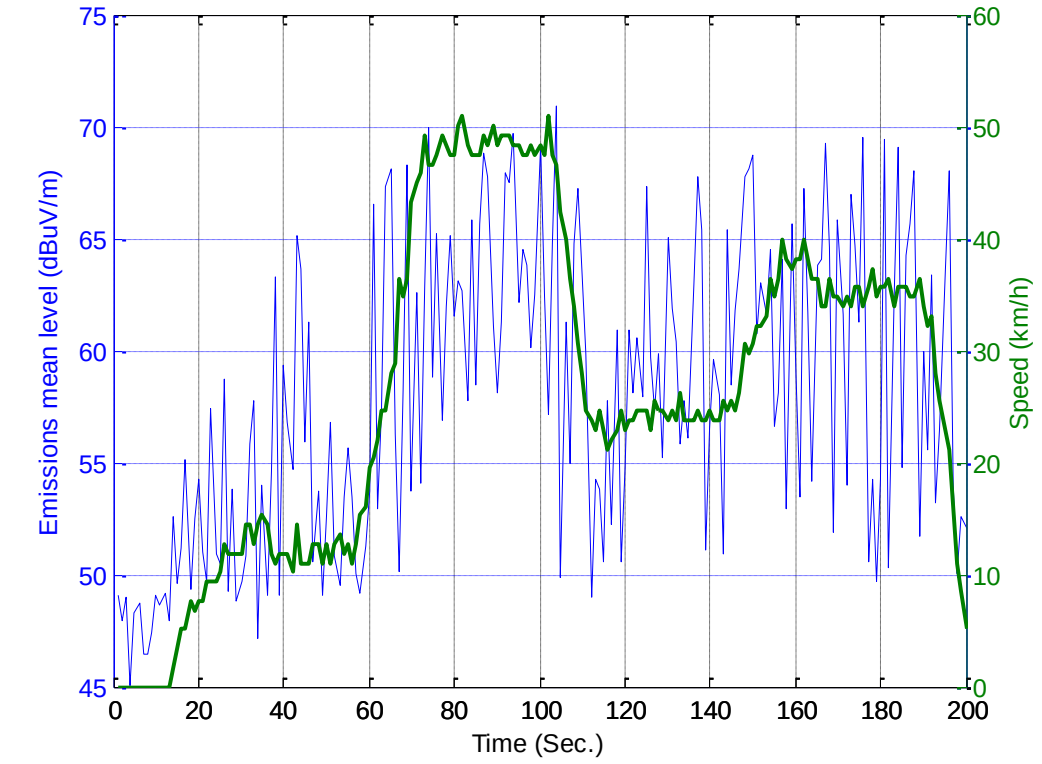

FIGURE 41, EMISSIONS & SPEED OF THE STEPS PROFILE

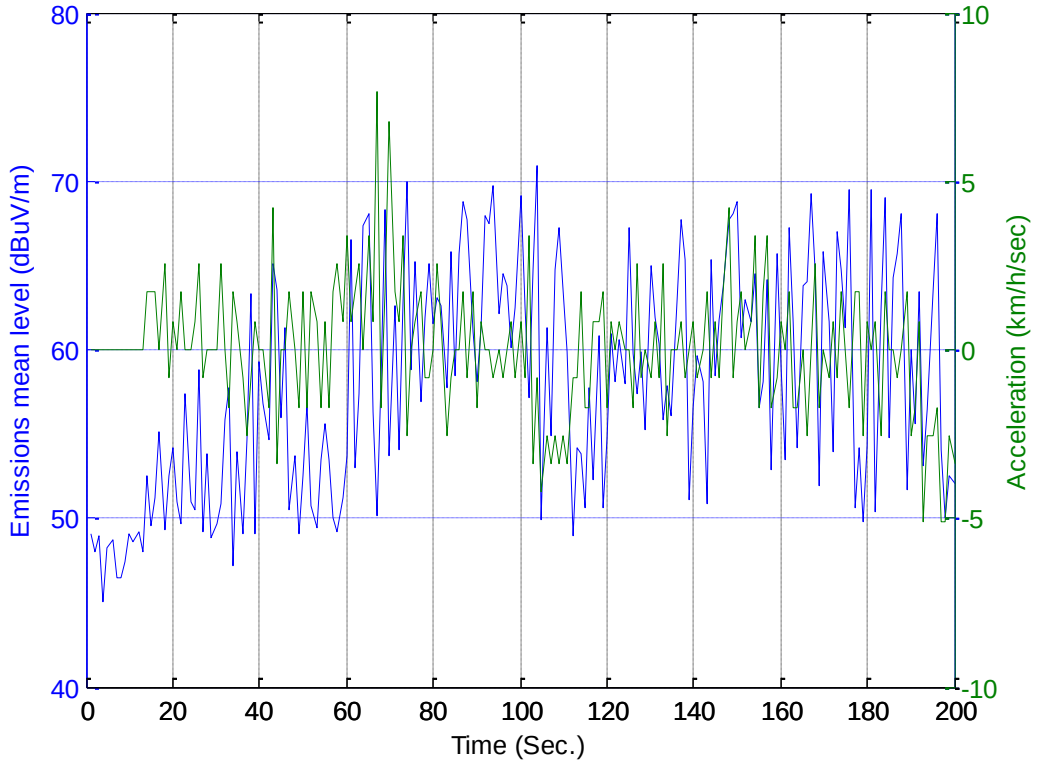

FIGURE 42, EMISSIONS & ACCELERATION OF THE STEPS PROFILE

4.2.1.3 UEDC PROFILE

The objective of applying this standard driving cycle to the Renault Twizy is to evaluate the influence of urban driving behavior on magnetic interferences. The spectrogram of the radiated magnetic disturbances is illustrated in Figure 43. Again, it confirms the fact that most of the time-varying spectral components of the radiated magnetic fields lie in lower frequency range. An obvious relationship between the record mean level of magnetic disturbances and instantaneous values of speed as well as acceleration can be noticed in Figures 44 & 45.

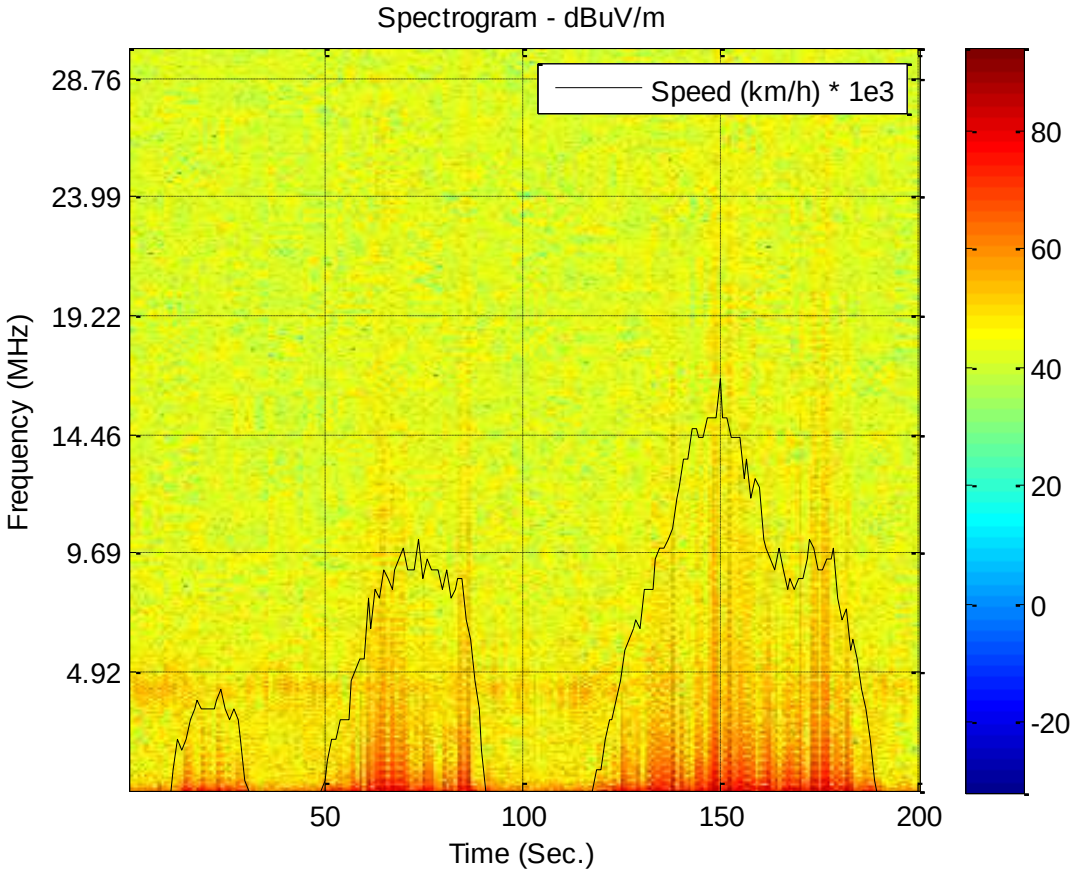

FIGURE 43, SPECTROGRAM OF THE EMISSIONS OF THE UEDC PROFILE

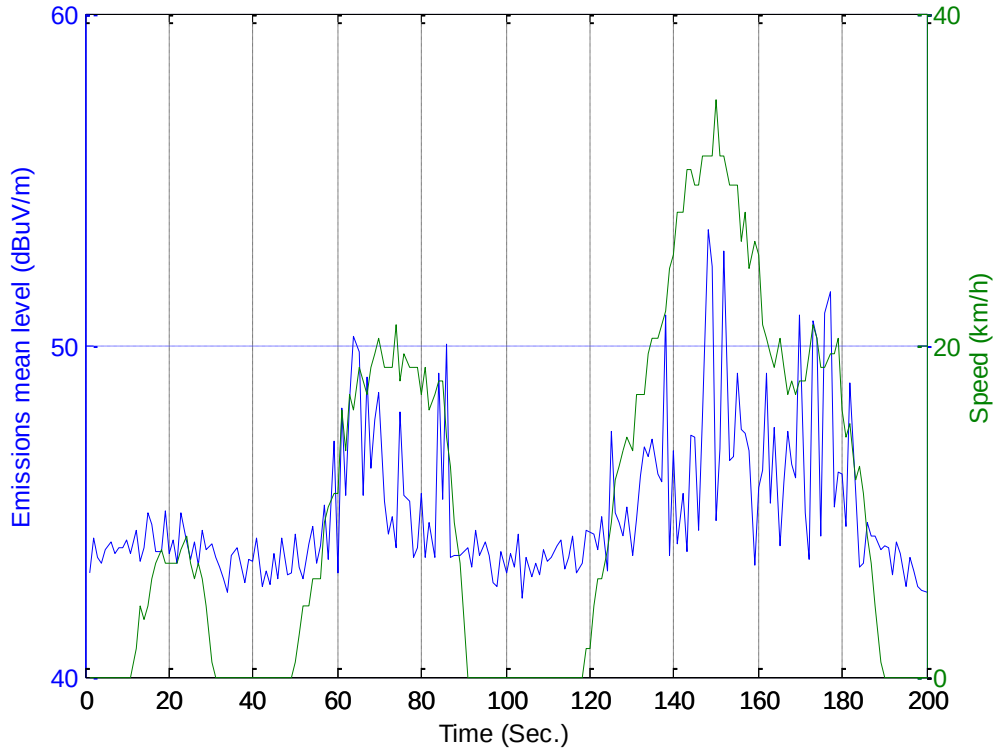

FIGURE 44, EMISSIONS & SPEED OF THE UEDC PROFILE

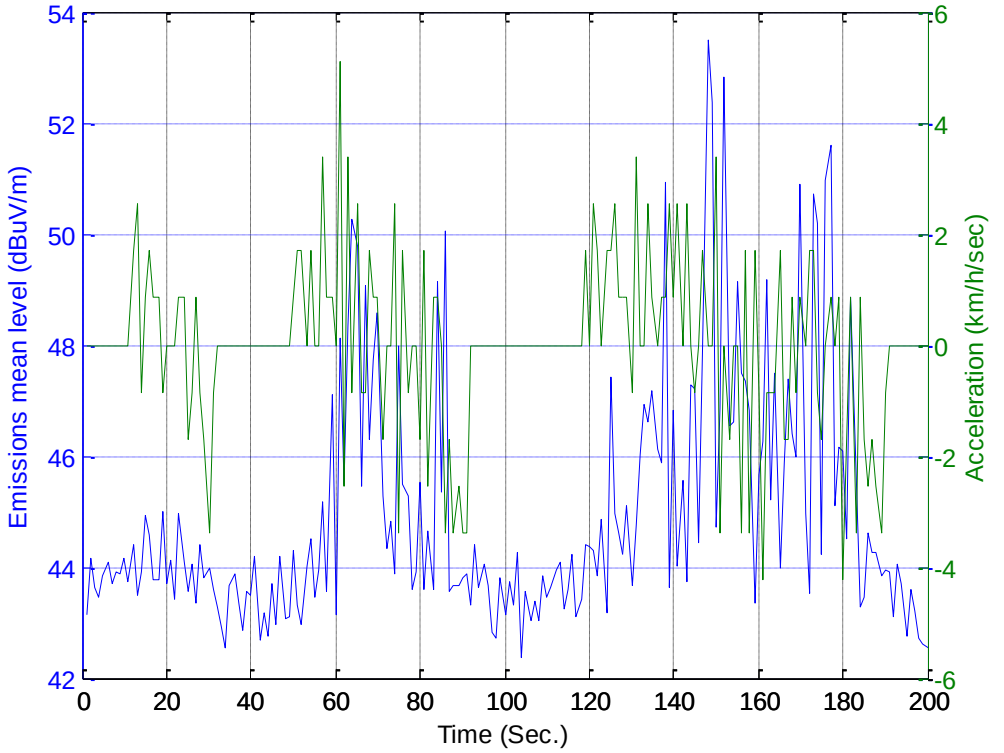

FIGURE 45, EMISSIONS & ACCELERATION OF THE UEDC PROFILE

It has been found that the radiated disturbances of the electric vehicle due to the three profiles have exceeded the limits specified by the SAE J 551-5 standard above 8 MHz as depicted in Figure 46. Limits for electric radiated emissions have been adopted as a reference although these are magnetic ones. This is because the standard provides reference limits of magnetic radiated emissions in dBuA/m while the magnetic emissions in this test has been recorded using a digital oscilloscope. A similar approach has been followed in [30] where authors have compared the magnetic emissions of a hybrid car in dBuV/m with the electric field reference limits provided by the CISPR 25 as shown in Figure 3 in this thesis. High background noise has been recorded by the loop antenna especially in the 20 – 30 MHz range although the noise floor should be at least 6 dB less than the reference limits established by the standard. Also the same figure points out that the emissions of the electric car are far above the limits set by the MIL-STD-461F for ground applications.

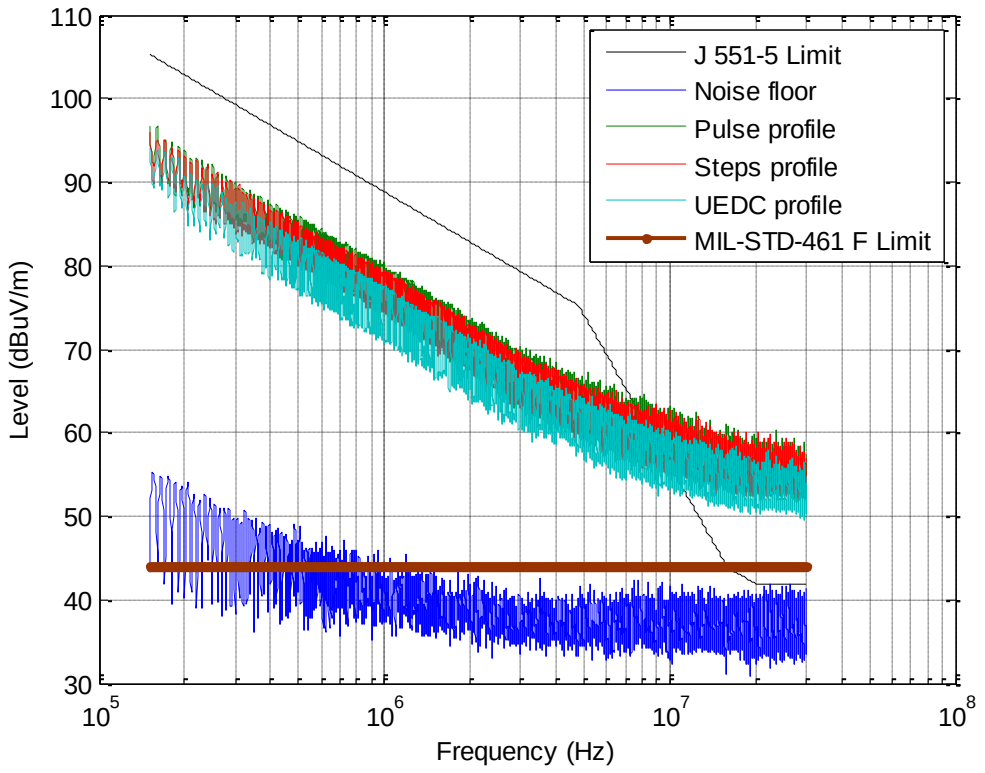

FIGURE 46, PEAK DETECTOR SPECTRA OF ALL PROFILES

With the expected widespread of the electric vehicles in the near future, these clear violations and severe breaches of the automotive EMC standards should be taken into account from the early design stage. It is worth mentioning that the same electric car running in the field will produce more radiated emissions than in the free running or unloaded condition. This can easily be simulated by tests done using a dynamometer-equipped EMC chamber.

The following general conclusions can be drawn after analyzing the results of the three driving profiles. Maximum levels of magnetic interferences have been detected during high speed driving modes as can be concluded from Figures 47 & 48. This is because to achieve high velocity, vehicles have to deliver more power thus generating more radiated emissions.

The data distribution in the training as well as testing subsets is depicted in Figure 47. It also shows that the idling emissions are the lowest as expected as a small amount of power is needed to maintain the engine operation. Mean magnetic emissions increased during acceleration, remained quite constant during cruising, and decreased during deceleration driving regimes. The testing subset contained unseen input values, e.g. speeds more than 35 km/h, during the training phase, thus testing the generalization of the proposed ANN models.

Table 6 shows the statistics related to the data of the three speed profiles picked up with the Renault Twizy. The UEDC standard test represents urban driving while the pulse & steps profiles can be considered as interurban driving profiles taking into consideration that the car maximum speed is 80 km/h.

As commented in previous paragraphs, the relationship between the instantaneous speed and the corresponding mean emission level is nonlinear. This could be also an additional justification for the choice of nonlinear ANNs for the modeling purpose.

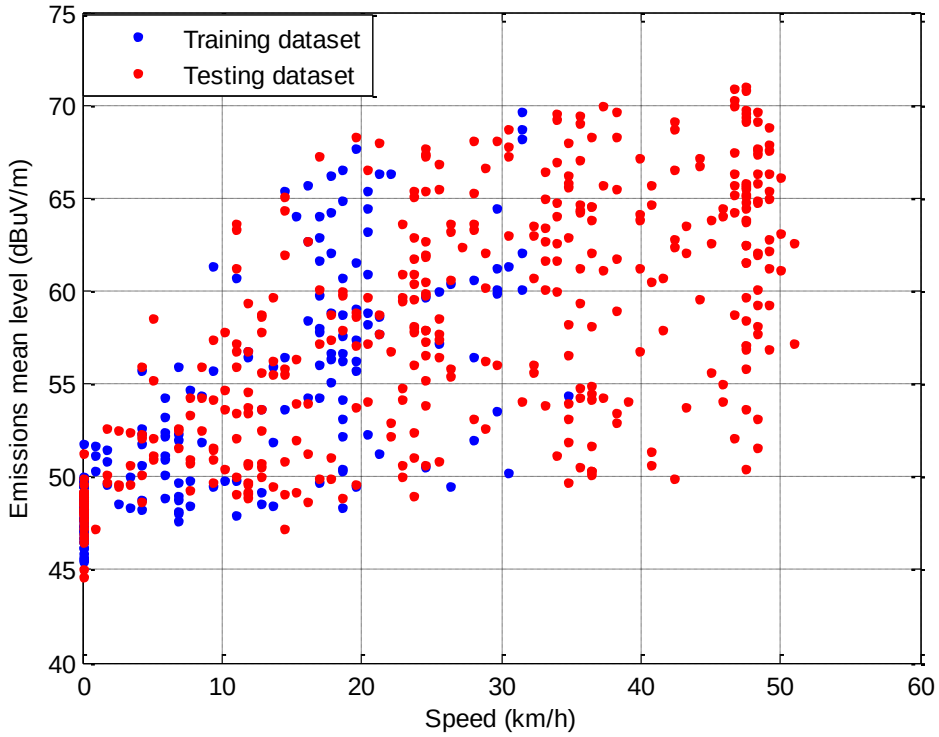

FIGURE 47, LEVELS OF MAGNETIC EMISSIONS VERSUS INSTANTANEOUS VEHICLE SPEED

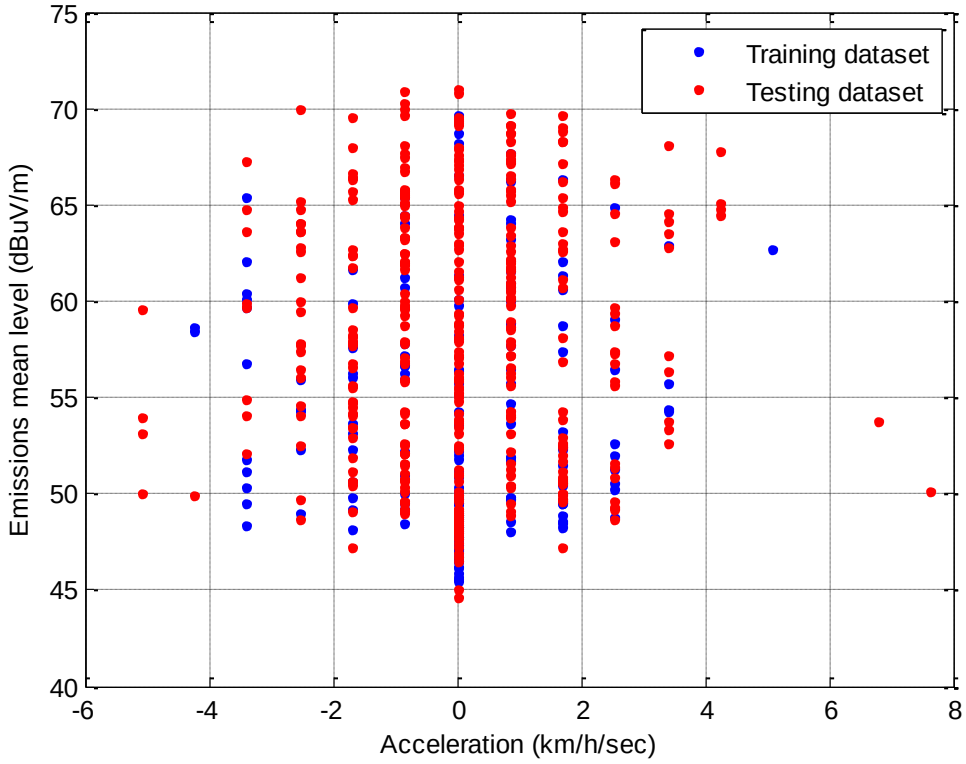

FIGURE 48, LEVELS OF MAGNETIC EMISSIONS VERSUS INSTANTANEOUS VEHICLE ACCELERATION

TABLE 6, STATISTICS OF THE DRIVING PROFILES

Driving Metrics	Pulse Profile	Steps Profile	UEDC Profile
Maximum Speed (km/h)	50.0456	50.8938	34.7774
Minimum Speed (km/h)	0	0	0
Average Speed (km/h)	25.5784	26.4521	10.1788
Speed Standard Deviation	17.5217	14.6538	10.0849
Maximum Acceleration (km/h/sec)	4.2412	7.6341	5.0894
Minimum Acceleration (km/h/sec)	-5.0894	-5.0894	-4.2412
Average Acceleration (km/h/sec)	0.0042	0.0254	0
Acceleration Standard Deviation	1.3934	1.8745	1.4924
Maximum Emissions (dBuV/m)	70.9753	70.9343	69.6102
Minimum Emissions (dBuV/m)	44.6315	45.0104	45.4302
Average Emissions (dBuV/m)	57.7686	58.0300	53.2129
Emissions Standard Deviation	6.9086	6.5825	5.9640

4.2.2. MODEL DEVELOPMENT RESULTS

Three types of neural models based on number of inputs have been tested. All models have only one output that is the level of radiated emissions in dBuV/m. The first type of models has only single input: the speed while the second model has two inputs: speed and acceleration. Both the instantaneous speed as well as the product of speed and acceleration have been considered as inputs for the third type of neural models [41].

Table 7 demonstrates the best results obtained from testing all the neural network topologies discussed in Section 3.1. It also points out that the relation between the instantaneous vehicle operational variables and the corresponding radiated EMI levels is nonlinear. This was observed from the previous analysis and now it is confirmed by the failure of the linear layer to map this relationship. Moreover, the effectiveness and robustness of the ELM algorithm can be noticed comparing the training times needed to achieve similar performance. Thorough analysis of the results given in this table suggests that two models can be candidates to be used for estimating the radiated emissions in terms of the driving

characteristics: the single input NARX model and the double inputs MLP model. This result is logical because the problem of interest is a dynamic one. That's the current level of the radiated emissions depends on the corresponding value of the speed as well as its history. Consequently, if only the speed signal is considered as an input, a dynamic model will give the best estimation results. However, if both the speed and its derivative are considered, a static model will give the best results. The double-input ELM-trained MLP model shown in Figure 49 is preferred because of its short training time relative to the single-input NARX model as can be seen in the latest column of Table 7. More detailed results about the performance of different neural networks have been included in Appendix A1.

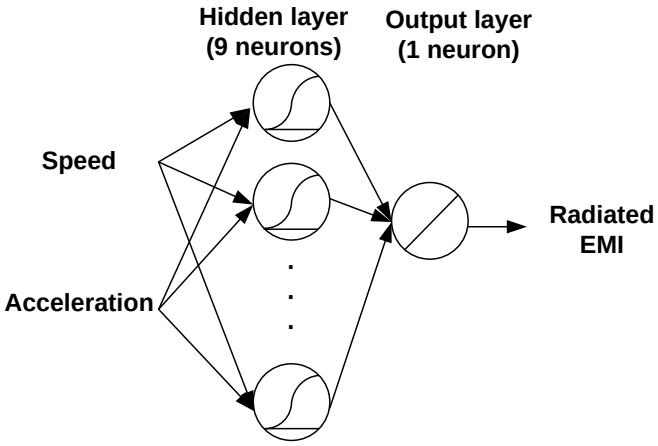

Figure 49, Topology of the selected model

TABLE 7, BEST TESTING RESULTS OF THE DIFFERENT NEURAL MODELS

Inputs	Network Type	Topology	Learning Function	Delays (Inp /Feedback)	Neurons (h1 / h2)	RMSE	Training Time
Speed	Static	LN	LMS		1	8.7245	40 m
		MLP	ELM		3	4.822	5 h 35 m
		DHLF	SCG		2 2	4.8361	2 d 20 h
		CF	BFGS		2	4.8290	2 h 6 m
	Dynamic	ITD	LM	1	5	4.8499	1 h 7 m
		DTD	LM	1 1	3	4.8503	5 d 1 h
		LR	SCG	1	2	4.8434	1 d 7 h
		NARX	BFGS	2 1	2	4.7934	5 h 56 m
Speed & Acceleration	Static	LN	LMS		1	8.8006	45 m
		MLP	ELM		9	4.7425	1 h 40 m
		DHLF	OSS		2 6	4.8388	19 h
		CF	SCG		2	4.8996	8 h

Dynamic	ITD	LM	1		4	4.8463	1 h 28 m
	DTD	OSS	1	1	2	4.8574	1 d 15 h
	LR	OSS	1		2	4.8481	1 d 22 h
	NARX	SCG	2	2	2	4.8625	20 h 35 m

4.2.3. ESTIMATION RESULTS

This section introduces the results estimated by the neural model. Firstly, the testing dataset of a Twizy electric car has been applied to the model. Then, speed information registered by an urban trip with a Think City electric car has been employed to predict the real time radiated emissions.

4.2.3.1. MODEL TESTING RESULTS

Figure 50 demonstrates the magnetic emission levels estimated by the model shown in Figure 49. The model can successfully distinguish between 4 different speeds as well as it responds reasonably to moderate and sharp accelerations. Moreover, the model generalizes very well, that's it could predict the magnetic field emissions associated with the unseen values of the instantaneous speed. This is because the pulse and steps profiles used in testing the proposed model have not been introduced to the model during the training phase.

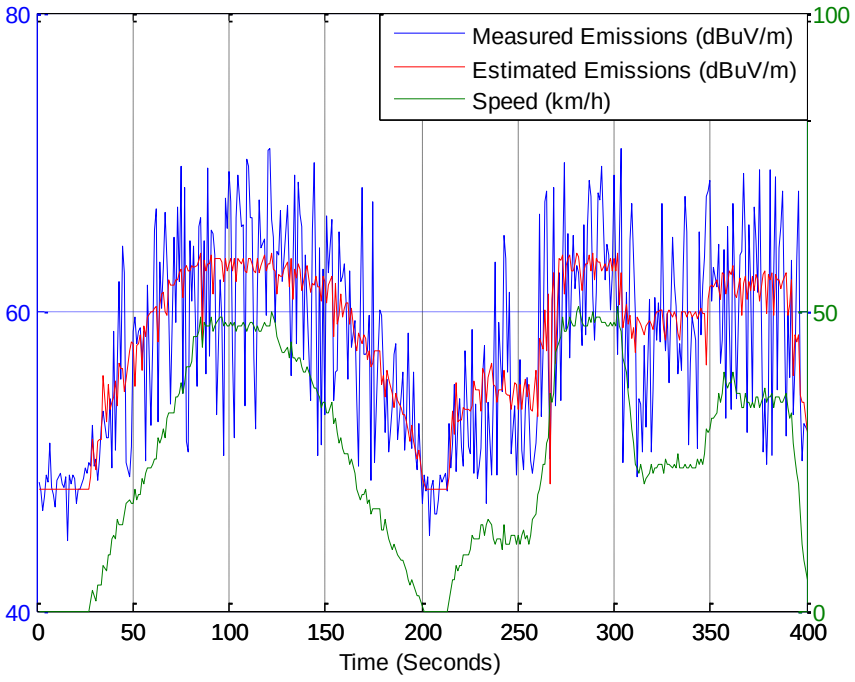

FIGURE 50, ESTIMATION RESULTS

A linear regression analysis as shown in Figure 51 has been done to study the relationship between the output of the network, i.e. estimated emissions, and the targets, i.e. measured emissions. The black line represents the perfect result, i.e. outputs = targets. The blue line is the optimum fitting linear regression line between measured and estimated magnetic field values. The regression coefficient (R) reflects the relationship between measured and estimated radiated emissions. If R = 1, then this means that there is an exact linear relationship between targets and outputs. On the other hand, if R is close to zero, then the relationship is nonlinear. The scatter plot is helpful in illustrating that certain data points have poor fit. For example, all data points whose measured emissions were above 65 dBuV/m approximately have corresponding estimated emission value saturated at 65 dBuV/m approximately. Consequently, samples of this range of magnetic field intensities should be considered while the training process. Thus, more data samples should be collected for the testing subset. The regression plot shown in Figure 51 indicates a good fit of the relationship between measured and estimated values the testing dataset.

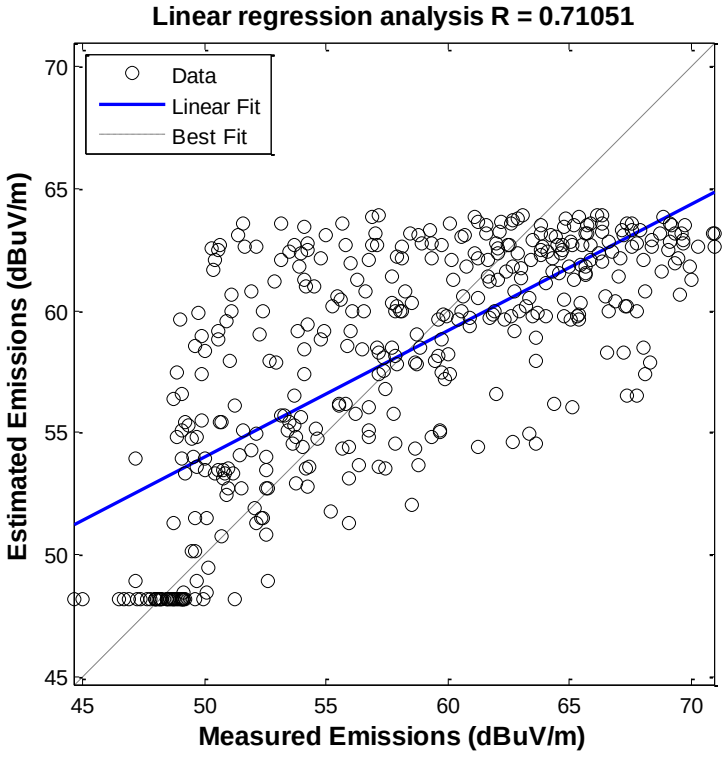

FIGURE 51, LINEAR REGRESSION ANALYSIS RESULTS

4.2.3.2. EXPERIMENTAL VALIDATION

In order to complete the proposed solution in Figure 7, the urban trip illustrated in Figure 52 has been realized with a Think City electric car in Alcala de Henares (Madrid) recording only the on-road car speed by means of an on-board Differential Global Positioning System (DGPS) device. Then the instantaneous speed and the calculated acceleration values during the trip have been applied to the proposed model in this work to predict the corresponding magnetic radiated emissions in the field as shown in Figure 53. The model responds well to changes in velocity as well as idling mode in urban driving mode. The mean value of the radiated magnetic interferences of 400 seconds trip is 58.02 dBuV/m (2.667e-5 mG).

FIGURE 52, MAP IMAGE OF THE TRIP IN ALCALA DE HENARES (MADRID)

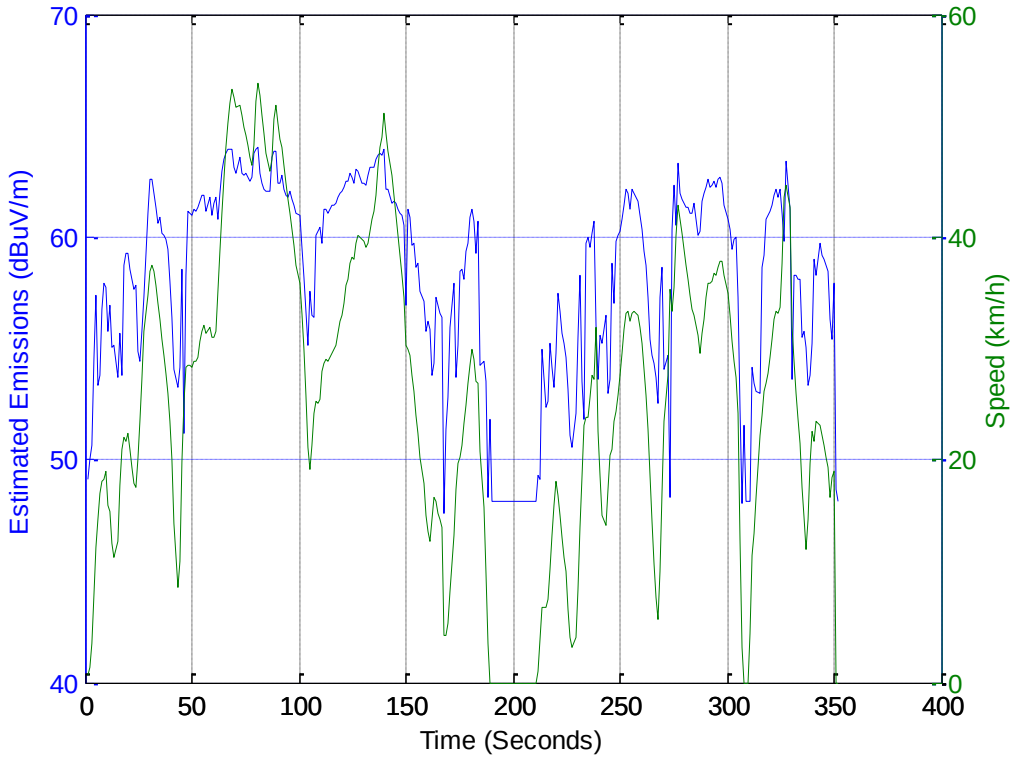

FIGURE 53, ESTIMATION OF THE THINK CITY RADIATED EMISSIONS

5. CONCLUSIONS & FUTURE WORKS

This chapter summarizes the main conclusions of the PhD work focusing on the way in which the objectives of the research work have been achieved. Then future research lines as well as recommendations are discussed.

5.1. CONCLUSIONS

With the expected growth of electric car and truck fleets across the globe, the acquisition of information concerning the electromagnetic environment associated with these vehicles is very timely. This thesis has proposed a modeling methodology for estimation of radiated emissions from electric vehicles based on driving dynamics. This methodology requires three successive steps. Firstly, radiated perturbations and the corresponding speed profile have to be recorded in a shielded EMC chamber. Then the capabilities of ANNs have to be exploited to model the relationship between them. Finally, the developed neural model can be employed to estimate the real traffic radiated disturbances if the instantaneous vehicle speed is being measured by a GPS for example. In the case of ambient electromagnetic noise, incorporating a second antenna enables the application of adaptive noise cancellation techniques using signal correlation. Among the analyzed ANN solutions, the MLP trained with ELM provided the best estimation results in terms of the minimum testing RMSE. The proposed methodology has been applied to two types of electrical vehicles: a motorcycle and a car.

In the motorcycle case, the emissions are not clearly dependent on the instantaneous value of the speed. Electric field emissions are produced once the speed exceeds a minimum threshold and a saturation effect occurs as can be seen in Figure 32. Moreover, the spectral components of the radiated disturbances are distributed to different frequency bands. According to Figure 33, the emission levels of the electric motorcycle under test have already exceeded the limits of MIL-STD-461F for ground applications for all frequencies and approached the limits established by the SAE J 551-5 standard at 16, 24, and 30 MHz.

In the case of the electric car, the magnetic radiated emissions are more linear with the instantaneous speed than the motorcycle case, but a saturation effect is also detected. The spectral components of these emissions were concentrated in the low frequency band. Higher frequency components appeared as a result to increasing the instantaneous velocity. In general, the magnetic radiated interference levels have been much more than the electric radiated disturbances emitted by the motorcycle for the same speed ranges. The measured radiated emissions from the electric vehicle were above the limits set by both MIL-STD-461F for ground applications for all frequencies and SAE J551-5 in the 8 – 30 MHz range.

It's noteworthy that all tests carried out in this work have been done with unloaded electric vehicles. This is because both the electric car and motorcycle have been jacked up inside the semi-anechoic chambers during all experiments. Of course a loaded electric vehicle is expected to radiate more electromagnetic emissions than unloaded one. On the other hand, it should be taken into account that the reference limits of the SAE J551-5 has been established for 3 m distance while the tests conducted in this thesis have been realized with 1m distance between the antenna and the vehicle under test. The MIL-STD-461 limits are provided for 1 m measurement distance for non-electric vehicles employed for military ground applications.

5.2. FUTURE WORKS

This section presents and discusses 10 main points regarding future research lines derived from the results of this PhD work.

1. Realizing a modal analysis of vehicular electromagnetic emissions, i.e. classification of emissions in terms of the driving mode [50].
2. Taking into account the frequency as an independent variable of the radiated electromagnetic waves, i.e. the output of the model.
3. Doing more urban and extra-urban tests with electric vehicles to produce a comprehensive emissions dataset for studying the effect of the average speed

as well as its standard deviation on the average emissions. In other words, it is important to study the effect of not only the instantaneous speed but also its fluctuations on the radiated vehicular emissions.

4. Realizing experiments in a shielded room equipped with a chassis dynamometer to see the effect of a loaded motor instead of a free running one. This allows the vehicle powertrain to be exercised under realistic load conditions without motion. The problem of such type of equipment is that it also introduces its own EMI interferences.
5. Analyzing whether a model of a vehicle matches the model of another one applying the same driving profile, and testing another types of electric vehicles such as electric buses, people movers, trams, and trains.
6. Studying the effect of more car related variables, i.e. motor temperature, battery state of health, battery state of charge, and vehicle accessories on the electromagnetic interferences.
7. Training recurrent networks with the reservoir computing algorithms like: echo state machine, backpropagation decorrelation, and liquid state machine.
8. Doing an interference evaluation study by assessing the impact of the measured emissions levels on wireless services below 30 MHz such as AM radio and RFID [67].
9. Thinking about the spatial distribution of the radiated disturbances. This provides the field intensities at the passenger seats for in-vehicle measurements. This information can be compared with limits established by health standards.
10. Relating the conducted disturbances to the driving profile as well. The advantage of this work is that the radiated emissions can be estimated in terms of its conductive counterpart later. Also in this case, the ambient interference problem will be avoided and thus real traffic tests with a loaded motor can be done in a straightforward way.

APPENDIX A1: ANNS TRAINING RESULTS

The following table gives more details about the brief training results showed in Table 7.

TABLE 8, MORE DETAILS ABOUT THE TESTING RESULTS OF DIFFERENT NEURAL MODELS

Inputs	Network Type	Topology	Training Function	Delays (Input / Feedback)	Neurons (h1 / h2)	Minimum Testing RMSE
Speed	Static	Linear layer	LMS		1	8.7245
		MLP	ELM		3	4.822
			LM		5	4.9558
			BFGS		3	4.9290
			SCG		2	4.8773
			OSS		2	4.8511
		Double layers	LM		2 3	4.8389
			BFGS		2 2	4.9143
			SCG		2 2	4.8361
			OSS		2 2	4.8622
		Cascade	LM		1	4.9117
			BFGS		2	4.8290
			SCG		2	4.8554
			OSS		3	4.8684
	Dynamic	FTDN	LM	1	5	4.8499
			BFGS	1	2	4.8923
			SCG	1	6	4.8503
			OSS	2	1	4.8596
		DTDN	LM	1 1	3	4.8503
			BFGS	1 1	3	4.8507
			SCG	1 1	2	4.8626
			OSS	1 1	2	4.8583
		LRNN	LM	2	1	4.8449
			BFGS	2	7	4.8662
			SCG	1	2	4.8434
			OSS	1	2	4.8442

		NARX	LM	2	1	3	4.8722
			BFGS	2	1	2	4.7934
			SCG	1	1	2	4.8415
			OSS	2	2	2	4.8539
Speed & Acceleration	Static	Linear layer	LMS			1	8.8006
		MLP	ELM			9	4.7425
			LM			3	4.9433
			BFGS			3	4.9345
			SCG			2	4.8876
			OSS			2	4.9039
		Double layer	LM			2 1	4.8657
			BFGS			2 1	4.9633
			SCG			7 2	4.8401
			OSS			2 6	4.8388
		Cascade	LM			3	4.9827
			BFGS			2	5.1002
			SCG			2	4.8996
			OSS			3	4.9725
	Dynamic	FTDN	LM	1		4	4.8463
			BFGS	1		2	4.9221
			SCG	2		2	4.8752
			OSS	1		2	4.8579
		DTDN	LM	2	2	3	4.8609
			BFGS	1	2	3	4.8950
			SCG	2	1	3	4.8703
			OSS	1	1	2	4.8574
		LRNN	LM	1		2	4.8635
			BFGS	1		4	4.9136
			SCG	1		2	4.8502
			OSS	1		2	4.8481
		NARX	LM	1	2	2	4.8783
			BFGS	3	3	2	4.9164
			SCG	2	2	2	4.8625
			OSS	1	1	1	5.1520

Speed & (Speed x Acceleration)	Static	Linear layer	LMS			1	8.8848
		MLP	ELM			7	4.7490
			LM			2	4.8708
			BFGS			2	4.9228
			SCG			2	4.7899
			OSS			5	5.3370
		Double layers	LM		1	7	4.8721
			BFGS		2	1	4.9308
			SCG		2	4	4.8388
			OSS		2	3	4.8355
		Cascade	LM			4	5.0916
			BFGS			1	5.3908
			SCG			4	5.2144
			OSS			7	5.0966
	Dynamic	FTDN	LM	1		2	4.8195
			BFGS	1		2	4.8581
			SCG	1		2	4.8563
			OSS	2		2	4.8318
		DTDN	LM	1	1	3	4.9133
			BFGS	1	2	2	4.9465
			SCG	1	1	2	4.8800
			OSS	1	1	2	4.8486
		LRNN	LM	1		2	4.9021
			BFGS	1		2	4.9307
			SCG	2		1	4.8575
			OSS	1		2	4.9512
		NARX	LM	2	1	2	4.8850
			BFGS	1	1	2	4.8899
			SCG	1	1	2	4.8724
			OSS	2	2	8	4.8675

APPENDIX A2: UNCERTAINTY OF EMI TESTS

Magnitude Xi	+ dB	- dB	PDF	k	value	u(xi)	ci	(ci*u(xi))^2
Receiver reading	-0,59	0,55	normal	1	-0,02	-0,02	1	0,001
Antenna-receiver attenuation	1,65	1,65	normal	2	0,825	0,825	1	0,681
Biconical antenna factor	1,5	1,5	normal	2	0,75	0,75	1	0,5625
Oscilloscope Corrections								
Exact voltage reading	3,90	3,90	rectangular	1,73	2,253	2,253	1	5,074
Measurement resolution	1,19	1,19	rectangular	1,73	0,688	0,688	1	0,473
Calibration uncertainty	1,19	1,19	normal	2	0,595	0,595	1	0,354
Antenna-receiver maladjustment	0,95	1,07	forma U	1,41	0,716	0,716	1	0,513
Antenna corrections								
Frequency interpolation of AF	0,3	0,3	rectangular	1,73	0,173	0,173	1	0,030
AF deviation with height	0,5	0,5	rectangular	1,73	0,289	0,289	1	0,084
Directivity difference	1	0	rectangular	1,73	0,289	0,289	1	0,084
Position of the phase center	1	1	rectangular	1,73	0,578	0,578	1	0,334
Cross polarization	0,9	0,9	rectangular	1,73	0,520	0,520	1	0,271
Site corrections								
NSA	4,75	4,75	triangular	2,45	1,938	1,939	1	3,759
Distance variation	0,28	0,28	rectangular	1,73	0,162	0,162	1	0,026
Table height	0,1	0,1	normal	2	0,05	0,05	1	0,003
Total								
Typical uncertainty (dB)								3,499
Expanded uncertainty (dB)			normal	2				6,999

Progress In Electromagnetics Research, Vol. 139, 671–687, 2013

ON-ROAD MAGNETIC EMISSIONS PREDICTION OF ELECTRIC CARS IN TERMS OF DRIVING DYNAMICS USING NEURAL NETWORKS

Ahmed M. Wefky[1, *], Felipe Espinosa[1], Frank Leferink[2], Alfredo Gardel[1], and Robert Vogt-Ardatjew[2]

[1]University of Alcala, Spain

[2]University of Twente, Netherlands

Abstract—This paper presents a novel artificial neural network (ANN) model estimating vehicle-level radiated magnetic emissions of an electric car as a function of the corresponding driving pattern. Real world electromagnetic interference (EMI) experiments have been realized in a semi-anechoic chamber using Renault Twizy. Time-domain electromagnetic interference (TDEMI) measurement techniques have been employed to record the radiated disturbances in the 150 kHz–30 MHz range. Interesting emissions have been found in the range 150 kHz–3.8 MHz approximately. The instantaneous vehicle speed and acceleration have been chosen to represent the vehicle operational modes. A comparative study of the prediction performance between different static and dynamic neural networks has been done. Results showed that a Multilayer Perceptron (MLP) model trained with extreme learning machines (ELM) has achieved the best prediction results. The proposed model has been used to estimate the radiated magnetic field levels of an urban trip carried out with a Think City electric car.

1. INTRODUCTION

Vehicular emissions can be divided into three major classes: acoustic (audible) noise, exhaust emissions, i.e., gases as well as particles, and electromagnetic disturbances, i.e., conducted & radiated emissions. Several works have correlated the driving profile with exhaust emissions estimated from emission models or measured on a chassis dynamometer [1–8]. The influence of the driver behavior on the real

Received 4 April 2013, Accepted 20 April 2013, Scheduled 19 May 2013

* Corresponding author: Ahmed Mohamed Wefky (awefky@depeca.uah.es).

Progress In Electromagnetics Research, Vol. 135, 231–244, 2013

MODELING RADIATED ELECTROMAGNETIC EMISSIONS OF ELECTRIC MOTORCYCLES IN TERMS OF DRIVING PROFILE USING MLP NEURAL NETWORKS

Ahmed M. Wefky, Felipe Espinosa*, Luis de Santiago, Alfredo Gardel, Pedro Revenga, and Miguel Martínez

Department of Electronics, University of Alcalá, Alcalá, Madrid, Spain

Abstract—Current automotive electromagnetic compatibility (EMC) standards do not discuss the effect of the driving profile on real traffic vehicular radiated emissions. This paper describes a modeling methodology to evaluate the radiated electromagnetic emissions of electric motorcycles in terms of the driving profile signals such as the vehicle velocity remotely controlled by means of a CAN bus. A time domain EMI measurement system has been used to measure the temporal evolution of the radiated emissions in a semi-anechoic chamber. The CAN bus noise has been reduced by means of adaptive frequency domain cancellation techniques. Experimental results demonstrate that there is a temporal relationship between the motorcycle velocity and the radiated emission power in some specific frequency ranges. A Multilayer Perceptron (MLP) neural model has been developed to estimate the radiated emissions power in terms of the motorcycle velocity. Details of the training and testing of the developed neural estimator are described.

1. INTRODUCTION

In the next 50 years, the global population is expected to increase from 6 billion to 10 billion and thus the number of vehicles is estimated to increase from 700 million to 2.5 billion. If all these vehicles are propelled by internal combustion engines, where will the oil come from? And where should the emissions be disseminated? Answers to these questions impose people to strive for sustainable road transportation for the 21st century [1]. In a world where energy conservation and

Received 25 October 2012, Accepted 17 December 2012, Scheduled 20 December 2012

* Corresponding author: Felipe Espinosa (espinosa@depeca.uah.es).

Hindawi Publishing Corporation
Mathematical Problems in Engineering
Volume 2012, Article ID 790526, 11 pages
doi:10.1155/2012/790526

Research Article

Electrical Drive Radiated Emissions Estimation in Terms of Input Control Using Extreme Learning Machines

A. Wefky, F. Espinosa, L. de Santiago, P. Revenga, J. L. Lázaro, and M. Martínez

Electronics Department, Polytechnics School, University of Alcalà, Campus Universitario 28871, Alcalà de Henares, Spain

Correspondence should be addressed to F. Espinosa, espinosa@depeca.uah.es

Received 21 September 2012; Revised 9 November 2012; Accepted 9 November 2012

Academic Editor: Wuhong Wang

With the increase of electrical/electronic equipment integration complexity, the electromagnetic compatibility (EMC) becomes one of the key points to be respected in order to meet the constructor standard conformity. Electrical drives are known sources of electromagnetic interferences due to the motor as well as the related power electronics. They are the principal radiated emissions source in automotive applications. This paper shows that there is a direct relationship between the input control voltage and the corresponding level of radiated emissions. It also introduces a novel model using artificial intelligence techniques for estimating the radiated emissions of a DC-motor-based electrical drive in terms of its input voltage. Details of the training and testing of the developed extreme learning machine (ELM) are described. Good agreement between the electrical drive behavior and the developed model is observed.

1. Introduction

Because of the integration density increase and the assembly of electric/electronic circuits gathered in a confined space such as electrical vehicles, certain unwanted effects caused by EMC and electromagnetic interference (EMI) become unavoidable [1–3]. Electrical drives are the main source of electromagnetic emissions of electrical vehicles, including both electrical motor and the required power electronics. Indeed, the addition of equipment operating in fast switching is susceptible to cause harmful conducted and/or radiated interference that can spread through the onboard network [4]. These coupling effects may damage the electrical module in which they were integrated as can be found in digital and mixed-signal electronic circuits such as the RF devices and microcontrollers integrated in the command devices [5].

Applied Soft Computing 11 (2011) 2580–2599

Contents lists available at ScienceDirect

Applied Soft Computing

journal homepage: www.elsevier.com/locate/asoc

Comparison of neural classifiers for vehicles gear estimation

A. Wefky [a], F. Espinosa [a,*], A. Prieto [b], J.J. Garcia [a], C. Barrios [c]

[a] Department of Electronics, University of Alcala, Spain
[b] Automatic Department, Electrical Engineering Faculty, La Habana, Cuba
[c] CIEMAT, Madrid, Spain

ARTICLE INFO

Article history:
Received 7 July 2010
Received in revised form
19 November 2010
Accepted 7 January 2011
Available online 22 January 2011

Keywords:
ANN classifier
Vehicle gear estimation
Multi-layer perceptron
Radial basis function
Linear vector quantization
Probabilistic neural network

ABSTRACT

Nearly all mechanical systems involve rotating machinery with gearboxes used to transmit power or/and change speed. The gear position is an indication of the driver's behavior and it is also dependent on road conditions. That is why it presents an interesting problem to estimate its value from easily measurable variables. Concerning individual vehicles, there is a specific relationship between the size of the tires, vehicle speed, regime engine, and the overall gear ratio. Moreover, there are specific ranges for vehicle speed and regime engine for each gear. This paper evaluates the use of neural network classifiers to estimate the gear position in terms of two variables: vehicle velocity and regime engine. Numerous experiments were made using three different commercial vehicles in the streets of Madrid City. A comparative analysis of the classification efficiencies of different neural classifiers such as: multilayer perceptron, radial basis function, probabilistic neural network, and linear vector quantization, is presented. The best results in terms of classification efficiency were obtained using multilayer perceptron neural network (92.7%, 91.5%, and 85.9% for a Peugeot 205, a Seat Alhambra, and a Renault Laguna respectively). The maximum likelihood classifier is used as a benchmark to compare with the neural classifiers.

1. Introduction

An internal combustion engine uses a multigear transmission to transmit its power to the drive wheels. There are two basic types of automotive transmission systems: manual gear transmission and hydrodynamic transmission. Manual gear transmission consists of a clutch, gearbox, final drive, and drive shaft. The gearbox provides a number of gear ratios ranging from three to five for passenger cars [1].

The Electronics Department at the University of Alcala (UAH), in collaboration with the Thermal Engines Group of the ETSII-UPM in Madrid and the Research Center for Environmental Energy and Technology (CIEMAT) in Madrid are developing the MIVECO project (Methodology and instrumentation on board the vehicles to assess real effects of traffic pollutant emissions). This research project, in which the authors are involved, is focused on the measurement of gases, particles and electromagnetic pollutant emissions of vehicles as a result of the driver activity, vehicle state, and road conditions. Consequently, the knowledge of the gear value and its relationship with the emissions measured is required. However, in most engine control systems it is difficult to find an easy sensor for monitoring the transmission gear selector position for a variety of different types of vehicles.

Eq. (1) shows the formula relating the overall gear ratio (gr_o), the size of the tires (C_t), the vehicle speed (V_V), and the regime engine (R_E) [2]. The size of the tires is a constant depending on the type of the vehicle. The overall gear ratio includes a range of numbers for each gear. Consequently, the vehicle speed is linearly proportional to the regime engine for a specific gear.

$$gr_o = C_t * \frac{R_E}{V_V} \quad (1)$$

Fig. 1 illustrates that linear relationship and shows that given the vehicle speed and the regime engine, the corresponding gear can easily be deduced. It shows that the areas defining each gear can be linearly separated [1]. However, unfortunately the situation in reality is different. According to many experiments done on different types of cars, the linear boundaries between different gear zones cannot be clearly distinguished. In other words, practically there are not specific clear values for V_{C1}, V_{C2}, and V_{C3} shown in Fig. 1.

In many science branches, analysts are often faced with the task of classifying items based on measured data. A major difficulty faced by an analyst is that the data to be classified can often be quite complex, with numerous interrelated variables. Therefore, the time and effort required to develop a model to solve such classification problems can be significant. Neural networks are a proven

* Corresponding author. Tel.: +34 91 885 6546; fax: +34 91 885 6591.
E-mail address: espinosa@depeca.uah.es (F. Espinosa).

1568-4946/$ – see front matter © 2011 Elsevier B.V. All rights reserved.
doi:10.1016/j.asoc.2011.01.030

Sensors **2010**, *10*, 3798-3814; doi:10.3390/s100403798

OPEN ACCESS

sensors

ISSN 1424-8220

www.mdpi.com/journal/sensors

Article

Alternative Sensor System and MLP Neural Network for Vehicle Pedal Activity Estimation

Ahmed M. Wefky, Felipe Espinosa, José A. Jiménez *, Enrique Santiso, José M. Rodríguez and Alfredo J. Fernández

Electronics Department, Polytechnics, University of Alcalá, Campus Universitario s/n, 28871 Alcalá de Henares, Madrid, Spain; E-Mails: awefky@depeca.uah.es (A.M.W.); espinosa@depeca.uah.es (F.E.); santiso@depeca.uah.es (E.S.); jmra@depeca.uah.es (J.M.R.); alfredo.fernandezr@uah.es (A.J.F)

* Author to whom correspondence should be addressed; E-Mail: jimenez@depeca.uah.es; Tel.: +34-918-856-547; Fax: +34-918-856-591.

Received: 19 January 2010; in revised form: 21 February 2010 / Accepted: 22 March 2010 / Published: 14 April 2010

Abstract: It is accepted that the activity of the vehicle pedals (*i.e.*, throttle, brake, clutch) reflects the driver's behavior, which is at least partially related to the fuel consumption and vehicle pollutant emissions. This paper presents a solution to estimate the driver activity regardless of the type, model, and year of fabrication of the vehicle. The solution is based on an alternative sensor system (regime engine, vehicle speed, frontal inclination and linear acceleration) that reflects the activity of the pedals in an indirect way, to estimate that activity by means of a multilayer perceptron neural network with a single hidden layer.

Keywords: brake estimator; clutch estimator; throttle estimator; pedals activity estimation; multilayer perceptron; ANN estimator; on-board sensorial system

1. Introduction

Driving is one of the essentials in our daily life. Nowadays there are strong research efforts invested in the modeling of the driver behavior using driving signals by means of hidden Markov models (HMMs) [1,2] and dynamic belief networks (DBN) [3] as well as predicting the future status of the vehicle, drowsy or drunk driving detection with eye monitoring [4,5], and the cognitive modeling of

EEVC
Brussels, Belgium, November 19-22, 2012

Measurement Methodology for Radiated Emissions of Electrical Vehicles in Noisy Environments

Ahmed M. Wefky, Felipe Espinosa, Luis de Santiago, Alfredo Gardel, Pedro Revenga, Miguel Martínez

Electronics Department. Polytechnic School. University of Alcala. Spain. espinosa@depeca.uah.es

Abstract

Electromagnetic interferences (EMI) are the principal pollutant source in electrical vehicles. Current automotive electromagnetic compatibility (EMC) standards don't discuss the effect of the driving profile on real traffic vehicular radiated emissions. This paper introduces a methodology to evaluate the radiated emissions of electric motorcycles in terms of the driving profile signals in noisy environments. A time domain EMI measurement system with two antennas in the setup has been used to measure the temporal evolution of the radiated emissions in a semi-anechoic chamber. The velocity of the motorcycle was controlled by a remote laptop connected to the motorcycle via a CAN bus. The electromagnetic noise generated by the CAN bus has been cancelled using frequency domain adaptive filtering techniques.

Keywords: EMC, environment, electric vehicle, motorcycle, noise.

1 Introduction

In the next 50 years, the global population is expected to increase from 6 billion to 10 billion and thus the number of vehicles is estimated to increase from 700 million to 2.5 billion [1]. If all these vehicles are propelled by internal combustion engines, where will the oil come from? And where should the emissions be disseminated? Answers to these questions impose people to strive for sustainable road transportation for the 21st century [2]. In a world where energy conservation and environment protection are growing concerns, the development of electric vehicles has achieved an accelerated pace. From the energy point of view, electric vehicles can offer a secure and efficient energy option such as the utilization of various kinds of renewable energies. Concerning the environmental aspect, electric vehicles can provide gases and particles emission-free urban transportation, but on the other hand it's still considered as a strong source of electromagnetic emissions.

EMC issues related to the integration of an electric drive system into a conventional passenger car were investigated in [3]. Implementation difficulties encountered when measuring radiated electric and magnetic field emissions of experimental electric vehicles in the range 9 KHz to 30 MHz were described in [4]. Some EMI measurements including electric as well as magnetic field in two electric cars and a bus have been presented in [5]. Methods to control EMI noise generated in electric vehicle drive systems were studied using an electrical vehicle prototype in [6, 7].

The Electronics Department at the University of Alcala (UAH), in collaboration with the Thermal Engines Group of the ETSII-UPM in Madrid and the Research Center for Environmental Energy and

Effect of electrical vehicle-driver interaction on the radiated electromagnetic emissions: measurement methodology

Luis de Santiago[2], Felipe Espinosa[1], Miguel A. Ruiz[2], José A. Jiménez[1], Enrique Santiso[1], David Sanguino[2], Ahmed Wefky[1], Walter G. Fano[3]
[1] Electronics Department. Polytechnics. University of Alcala. Spain. espinosa@depeca.uah.es
[2] High Technology and Homologation Center. University of Alcala. Spain. luis.desantiago@uah.es
[3] Electronics Department. Engineering Faculty. Universidad Nacional de la Patagonia San Juan Bosco. Argentina.

Abstract- **This paper focuses on the developed methodology for the experimental evaluation of electrical vehicle-driver interaction and its effect on relative electromagnetic emissions, i.e. detecting in which way the driving style determines these pollutant emissions. Besides the theoretical aspects, specific instrumentation and set-up designed for this work, several results directly registered from electrical vehicles (fuel cell and battery powered) are shown. To made easier the results evaluation, maximum-average charts, spectrograms and 3D figures are included.**

The experimental tests allow deducing that the temporary association between the driver activity and the related electromagnetic emissions from electrical vehicles is more relevant at low frequencies (150 KHz-30MHz).

I. Introduction

Due to widespread use of electronic components in vehicles in the last 15 years, the aspects related to the electromagnetic compatibility (EMC) has become one of the critical parameters of vehicles from the initial design stage to its placement in the market [1],[2],[3]. So the manufacturers control the design and fabrication processes to comply with the existing automotive standards. However, the standard tests performed on vehicles so far have focused on measuring the interferences, radiated (EMI) and conducted (EMS), inherent in the vehicle itself and whose emission source is located on-board electrical and electronic devices.

Moreover, the continuous concern for the environment has led to a control and monitoring of vehicle emissions that is beyond the fabrication process, and not just from gases and particles resulting from combustion.

The authors join the research group of the MIVECO project (Methodology Onboard Instrumentation and Real Traffic to Evaluate Effects of Emissions Vehicles on Environmental Pollution [4]), whose objectives include studying the effect of the driver activity on the radiated electromagnetic emissions of the vehicle.

The problem is complex because an on-board measurement system cannot be developed that only records the emissions on-line from the vehicle, as in the case of gases and particles. To do so, a study had to be done in three phases: a) under conditions of isolated vehicle, measurement of the effect of vehicle-driver interaction on EMI-radiated emissions, b) obtaining electromagnetic emission model from the recorded experimental data, and c) in real traffic conditions, estimate the emissions using the developed model and the direct measurement of vehicle-driver interaction.

This work focuses on the phase a) proposal of a methodology for measuring, in the time and frequency domains, the effect of the driver behaviour on electromagnetic emissions from an isolated vehicle. However, under real traffic conditions, the captured emissions would have originated from the car exhaust, as well as many other sources.

The proposal is based on the CISPR12 [5] standard which establishes the measurement method for EMC emissions of a vehicle as DUT. The suitable modifications have been done to adapt the methodology to the requirements of the MIVECO project. It should be noted that, in addition to compliance with a particular standard, it is important to evaluate the relative levels of emissions in terms of vehicle operating conditions (speed, acceleration, engine speed, electrical devices connected to the vehicle, etc).

The proposed methodology includes a description of both the measurement set-up and the instrumentation used. Both aspects are addressed in the following sections.

II. Measurement Setup

The constraints of the MIVECO project require a proposal of a measurement methodology close to real traffic but avoiding all emission sources that would not be due to the vehicle itself.

Due to the unavailability of neither a Semi-Anechoic Chamber (SAC) nor an Open Air Test Site (OATS), a search for special measurements sites are done. Locations that emit low electromagnetic noise have been chosen for measurements. The location has been chosen such that the level of the ambient noise (TV, FM, mobile phone) is sufficiently low to allow discrimination of the vehicle emissions. However the external noise level is still so high in certain bands masking the signal to be recorded, so the study excludes this frequency range, as in the case of FM.

Figure 1 shows the registration of the ambient noise signal, with the engine stopped at various outdoor locations. The frequency range of the example covers 300 MHz to 1 GHz (band D).

978-1-4244-5697-0/10/$25.00 ©2010 IEEE

Sensorial System Minimization to Estimate the Driver Activity on the Vehicle's Pedals

Alexander Prieto
Electrical Engineering Faculty.
Automatic Department. ISPJAE.
C/ 114, nº 11901, Marianao 11500
La Habana (Cuba)
alexander@electrica.cujae.edu.cu

Felipe Espinosa, José L. Lázaro, Ahmed Wefky
Electronics Department. University of Alcala.
Polytechnics. University Campus, s/n.
28871 Alcala de Henares (Spain)
{espinosa, lazaro, awefky}@depeca.uah.es

Abstract

This work presents an alternative sensorial system, including the minimal number of devices, to register the driver activity on the control pedals. As it is known, sensors directly related to pedals are difficult to implement and require specific calibration for each tested vehicle. On the contrary, the new proposal based on the measurement of regime engine, frontal inclination, linear acceleration and vehicle speed, is easily on-board implemented.

After several tests with different vehicles and drivers, Mutual information, Principal component analysis, and Spearman correlation are applied to deduce the dependency analysis among variables.

The authors' study confirms that only two devices: inertial sensor to obtain frontal inclination and RPM meter to obtain regime engine, are enough to estimate the driver activity on brake and throttle pedals.

1. Introduction and objective

It is accepted that the activity of the vehicle pedals (i.e., throttle, brake, clutch) reflects the driver's behavior, which is at least directly related to the fuel consumption and the pollutant emissions.

Observable and measurable driving signals can be divided into three categories [4]: 1) driving activity signals, e.g., throttle, clutch and brake pedal activities or pressures and steering wheel angles; 2) vehicle state signals, e.g., vehicle speed and acceleration, regime engine; and 3) vehicle position signals, e.g., following distance, relative lane position, and relative angles (pitch and roll).

The instantaneous and simultaneous measurement of the three car pedals is a difficult task in the great majority of vehicles. In fact, there are 3 methods to directly measure the status of the car pedals: using position sensors [7], using pressure sensors [5], [19], [21], [25] and [32], and through the electronics system provided by the vehicle manufacturer (e.g., SMART and RAVEL-I [20], [26]).

The authors of this paper have the design experience of a universal and non-disturbing solution (Mireco Research Project [7]) to register the displacement of the pedals by means of potentiometers as shown in Fig. 1. However, four basic problems have been related to these pedal sensors. Firstly, it is difficult to place and fix the sensors near the pedals avoiding both errors resulting from accidental movement of the sensors as well as disturbing the driver while driving. Secondly, the connection of the sensors to the pedals by means of a flexible wire must be ad-hoc implemented for each car. Thirdly, the measured displacements of the pedals are inherently very small (few centimeters) which involves incorporating a special conditioning electronic system. Finally, it's necessary to indicate that the set-up utilized to mechanically fix this type of sensors depends on the model and type of the vehicle (car, van, lorry, industrial vehicle, etc). Because of the previously mentioned problems, this paper describes an alternative approach to the sensorial system shown in Figure 1 with the minimal possible number of devices incorporated in the vehicle. Consequently, this is easier to deploy and adjust, in order to register the driver's action on the control pedals.

This work starts by employing a set of minimally intrusive and easily installed sensors, on any type of vehicles, to record as accurately as possible the vehicle response to driver activity. With these assumptions, the fundamental objective is to analyze the dependency of variables that determine, with the minimum number of sensors, the driver action on the pedals. This will facilitate the study of the effects of driving mode in road traffic aspects such as pollution, traffic jams, accidents, etc.

The set of easily measurable driving variables (EMV) includes [36]: regime engine (RE), vehicle speed (VS), frontal inclination (FI), and linear acceleration (LA). Thus, instead of directly using sensors associated with pedal variables (PV) to provide the driver activity information, the authors propose in this paper the minimum alternative sensorial system including devices

978-1-4244-6849-2/10/$26.00 ©2010 IEEE

Gear predictor of manual transmission vehicles based on artificial neural network

A. M. Wefky, F. Espinosa, M. Mazo, J. A. Jiménez, E. Santiso, A. Gardel & D. Pérez
Department of Electronics, University of Alcala, Spain

Abstract

Nearly all mechanical systems involve rotating machinery (i.e., a motor or a generator), with gearboxes used to transmit power or/and change speed. Concerning vehicles, there is a specific *nonlinear* relationship between the size of the tires, linear velocity, engine RPM, gear ratio of the differential, and the gear ratio of the transmission. However, for each car there is a specific range of gear ratio of the transmission for each gear. On the other hand, the gear value is an indication of the driver behaviour and the road conditions, therefore it should be considered to establish non-pollutant driving guidelines. In this paper, two novel feed-forward artificial neural network (ANN) models have been developed and tested with the gear as the network output and the velocity of the engine (RPM) and the velocity of the car in (Km/h) as the network inputs. A lot of experiments were made using two commercial cars. The prediction efficiency of the proposed models is superior (i.e., the generalization mean square error is about 0.005). However after testing with two different vehicles, the conclusion is that on one hand the structure of the ANN model is suitable. On the other hand each vehicle has its specific model parameters. This paper shows that it is difficult to develop a universal model that predicts the gear based on the RPM and speed of any car.

Keywords: feed-forward artificial neural networks, gear predictor, manual transmission.

1 Introduction

The drivetrain system of the automobile engine consists of the following parts: engine, transmission, drive shaft, differential, and driven wheels. Firstly, the

WIT Transactions on Modelling and Simulation, Vol 48, © 2009 WIT Press
www.witpress.com, ISSN 1743-355X (on-line)
doi:10.2495/CMEM090041

Electronic application to evaluate the driver's activity on the polluting emissions of road traffic

D. Pérez, F. Espinosa, M. Mazo, J. A. Jiménez, E. Santiso, A. Gardel & A. M. Wefky
Department of Electronics, University of Alcalá, Spain

Abstract

The polluting emissions (gases and particles) produced by the traffic of automobiles are directly related to the activity of vehicle, but they are also affected by the route conditions and moreover, by the driver's behavior. However, PAMS commercial systems do not usually include elements to register this last component. This article presents an electronic system, specially designed to evaluate, ad-hoc, the effect of driver's activity on polluting emissions. This electronic application integrates a hardware and a software component, both designed concerning MIVECO research project. From the hardware component the sensorial part stands out, formed by potentiometers connected to the pedals that control the vehicle and the inertial device, which allows one to evaluate the instantaneous accelerations in the x-y-z-axes as well as the turns with respect to these axes. Once the signals are conditioned and acquired, the software component processes them for on-line monitoring in a GUI and stores them in a database to facilitate its evaluation off-line. This electronic application has two important properties: it can be incorporated in any vehicle of the market (light or heavy, diesel or gasoline, pre or post-eobd) and it allows the capture and registration of information about the driver's activity synchronously with PEMS (gases and/or particles) systems. The work includes experimental results obtained in an urban circuit in the city of Madrid.

Keywords: driver's behavior, PAMS, eco-driving, multi-sensorial system, onboard electronic system.

WIT Transactions on Ecology and the Environment, Vol 123, © 2009 WIT Press
www.witpress.com, ISSN 1743-3541 (on-line)
doi:10.2495/AIR090231

REFERENCES

1. Chan, C.C., *The state of the art of electric and hybrid vehicles.* Proceedings of the IEEE, 2002. **90**(2): p. 247-275.
2. Becker, T.A., I. Sidhu, and B. Tenderich, *Electric vehicles in the United States: a new model with forecasts to 2030.* Center for Entrepreneurship & Technology (CET) Technical Brief, 2009(2009.1).
3. Nemry, F. and M. Brons, *Plug-in hybrid and battery electric vehicles. Market penetration scenarios of electric drive vehicles*, 2010, Institute for Prospective and Technological Studies, Joint Research Centre.
4. Olden, K., *NIEHS Report on health effects from exposure to power-line frequency electric and magnetic fields*. 1999: DIANE Publishing.
5. Grandolfo, M., *Worldwide standards on exposure to electromagnetic fields: an overview.* The Environmentalist, 2009. **29**(2): p. 109-117.
6. Recommendation, C., *519/EC of 12 July 1999 on the limitation of exposure of the general public to electromagnetic fields (0 Hz to 300 GHz).* Official Journal L, 1999. **197**: p. 1999.
7. Directive, E., *Directive 2004/40/EC of the European Parliament and of the Council of 29 April 2004 on the minimum health and safety requirements regarding the exposure of workers to the risks arising from physical agents (electromagnetic fields). Eighteenth individual Directive within the meaning of Article 16 (1) of Directive 89/391/EEC.* Off J Eur Union, 2004. **159**: p. 1-26.
8. *IEEE Standard for Safety Levels With Respect to Human Exposure to Electromagnetic Fields, 0-3 kHz.* IEEE Std C95.6-2002, 2002: p. 0_1.
9. Ahlbom, A., et al., *Guidelines for limiting exposure to time-varying electric, magnetic, and electromagnetic fields (up to 300 GHz). International Commission on Non-Ionizing Radiation Protection.* Health Phys, 1998. **74**(4): p. 494-522.
10. ICNIRP, *ICNIRP guidelines on limits of exposure to static magnetic fields* in *Health Physics*2009. p. 504 - 514.
11. ICNIRP, *ICNIRP guidelines for limiting exposure to time-varying electric and magnetic fields (1 Hz - 100 KHz)*, 2010. p. 818-836.
12. Berisha, S., et al., *Magnetic Field Generated From Different Electric Vehicles.* SAE Technical Paper, 1995. **951934**.
13. Dietrich, F.M. and W.L. Jacobs, *Survey and assessment of electric and magnetic field (EMF) public exposure in the transportation environment*, 1999. p. Medium: X; Size: Pages: (248 p).
14. Schmid, G., R. Überbacher, and P. Göth. *ELF and LF magnetic field exposure in hybrid- and electric cars*. in *Bio-electromagnetics*. 2009. Davos, Switzerland: Curran Associates, Inc.
15. Überbacher, R., G. Schmid, and P. Göth. *ELF magnetic field exposure during an inner-city hybridbus ride*. in *Bio-electroamgnetics*. 2009. Davos, Switzerlands.
16. Karabetsos, E., et al. *EMF Measurements In Hybrid Technology Cars*. in *Proceedings of 6th International Workshop on Biological Effects of Electromagnetic Fields, Istambul*. 2010.
17. Halgamuge, M.N., C.D. Abeyrathne, and P. Mendis, *Measurement and analysis of electromagnetic fields from trams, trains and hybrid cars.* Radiation protection dosimetry, 2010. **141**(3): p. 255-268.
18. Mizuno, Y., K. Tanaka, and K. Naito. *Quantification of low frequency magnetic field in living environment*. in *EMC Europe 2011 York*. 2011. IEEE.
19. Pous, M., A. Atienza, and F. Silva. *EMI radiated characterization of an hybrid bus*. in *EMC Europe 2011 York*. 2011. IEEE.
20. Ptitsyna, N. and A. Ponzetto. *Magnetic fields encountered in electric transport: Rail systems, trolleybus and cars*. in *Electromagnetic Compatibility (EMC EUROPE), 2012 International Symposium on*. 2012.

21. Concha Moreno-Torres, P., et al., *Evaluation of the Magnetic Field Generated by the Inverter of an Electric Vehicle.* Magnetics, IEEE Transactions on, 2013. **49**(2): p. 837-844.
22. Tell, R., et al., *ELF magnetic fields in electric and gasoline-powered vehicles.* Bioelectromagnetics, 2013. **34**(2): p. 156-161.
23. Health, N.I.o., *Electric and magnetic fields associated with the use of electric power*, 2002. p. 42.
24. ICNIRP, *ICNIRP guidelines for limiting exposure to time varying electric, magnetic, and electromagnetic fields (up to 300 GHz)*, 1998, Health Physics. p. 494 - 522.
25. Tynes, T. and A. Andersen, *Electromagnetic fields and male breast cancer.* Lancet, 1990. **336**(Dec. 22/29).
26. Blanchard, L. and D. Whitehead, *A study to assess the possible effects on radio based services of electromagnetic emissions from the proposed increase of electrically powered public and private transport.* Final Report, UK Transport Research Laboratory, 2000.
27. Ruddle, A.R., D.A. Topham, and D.D. Ward. *Investigation of electromagnetic emissions measurements practices for alternative powertrain road vehicles*. in *Electromagnetic Compatibility, 2003 IEEE International Symposium on*. 2003.
28. Su, G.-J., J.W. McKeever, and K.S. Samons, *Design of a PM Brushless Motor Drive for Hybrid Electrical Vehicle Application.* PCIM 2000, 2005.
29. Serrao, V., et al. *EMI characterization and communication aspects for power electronics in hybrid vehicles*. in *Power Electronics and Applications, 2007 European Conference on*. 2007.
30. Silva, F. and M. Aragon. *Electromagnetic interferences from electric/hybrid vehicles*. in *General Assembly and Scientific Symposium, 2011 XXXth URSI*. 2011.
31. agency, N.s., *allied environmental conditions and tests publication AECTP 500 Edition 4*, January 2011.
32. Wefky, A., et al., *ON-ROAD MAGNETIC EMISSIONS PREDICTION OF ELECTRIC CARS IN TERMS OF DRIVING DYNAMICS USING NEURAL NETWORKS.* Progress In Electromagnetics Research, 2013. **139**: p. 671-687.
33. Wefky, A., et al., *Electrical Drive Radiated Emissions Estimation in Terms of Input Control Using Extreme Learning Machines.* Mathematical Problems in Engineering, 2012. **2012**: p. 11.
34. Baofeng, G., M.S. Nixon, and T.R. Damarla. *Acoustic information fusion for ground vehicle classification*. in *Information Fusion, 2008 11th International Conference on*. 2008.
35. Bing, L., A. Dibazar, and T.W. Berger. *Perimeter Security on Detecting Acoustic Signature of Approaching Vehicle Using Nonlinear Neural Computation*. in *Technologies for Homeland Security, 2008 IEEE Conference on*. 2008.
36. x, et al. *Vehicle identification using acoustic and seismic signals*. in *Signal Processing and Communications Applications Conference (SIU), 2010 IEEE 18th*. 2010.
37. Ji, J.-w., et al. *An Approach of Automatic Vehicle Classification by Acoustic Wave Based on PCA-RBF*. in *Information Engineering and Computer Science, 2009. ICIECS 2009. International Conference on*. 2009.
38. Cevher, V., R. Chellappa, and J.H. McClellan, *Vehicle Speed Estimation Using Acoustic Wave Patterns.* Signal Processing, IEEE Transactions on, 2009. **57**(1): p. 30-47.
39. ALI, N.N.B.M., *AUTOMOTIVE ENGINE FAULT DIAGNOSIS USING ACOUSTIC EMISSION TECHNIQUE*, in *Mechanical Engineering*2010, MALAYSIA PAHANG.
40. Hansen, J.Q., M. Winther, and S.C. Sorenson, *The influence of driving patterns on petrol passenger car emissions.* Science of The Total Environment, 1995. **169**(1–3): p. 129-139.
41. Joumard, R., et al., *Hot passenger car emissions modelling as a function of instantaneous speed and acceleration.* Science of The Total Environment, 1995. **169**(1–3): p. 167-174.

42. Sjödin, Å. and M. Lenner, *On-road measurements of single vehicle pollutant emissions, speed and acceleration for large fleets of vehicles in different traffic environments.* Science of The Total Environment, 1995. **169**(1–3): p. 157-165.
43. Barth, M., et al., *Analysis of Modal Emissions From Diverse In-Use Vehicle Fleet.* Transportation Research Record: Journal of the Transportation Research Board, 1997. **1587**(-1): p. 73-84.
44. Nesamani, K.S. and K.P. Subramanian, *Impact of Real-World Driving Characteristics on Vehicular Emissions.* JSME International Journal Series B Fluids and Thermal Engineering, 2006. **49**(1): p. 19-26.
45. Washington, S., J. Wolf, and R. Guensler, *Binary Recursive Partitioning Method for Modeling Hot-Stabilized Emissions From Motor Vehicles.* Transportation Research Record: Journal of the Transportation Research Board, 1997. **1587**(-1): p. 96-105.
46. Barth, M.J., et al., *Development of a comprehensive modal emissions model*, 2000.
47. Sorenson, S.C., et al., *Individual and public transportation - Emissions and energy consumption models*. 1992, Lyngby.
48. Ahn, K., et al., *Estimating vehicle fuel consumption and emissions based on instantaneous speed and acceleration levels.* Journal of Transportation Engineering, 2002. **128**(2): p. 182-190.
49. Holmén, B.A. and D.A. Niemeier, *Characterizing the effects of driver variability on real-world vehicle emissions.* Transportation Research Part D: Transport and Environment, 1998. **3**(2): p. 117-128.
50. Tong, H., W. Hung, and C. Cheung, *On-road motor vehicle emissions and fuel consumption in urban driving conditions.* Journal of the Air & Waste Management Association, 2000. **50**(4): p. 543-554.
51. Espinosa, F., et al., *Design and implementation of a portable electronic system for vehicle–driver–route activity measurement.* Measurement, 2011. **44**(2): p. 326-337.
52. Pérez, D., et al., *Electronic application to evaluate the driver's activity on the polluting emissions of road traffic*, 2009, WIT Press, Ashurst Lodge Ashurst Southampton SO 40 7 AA UK.
53. Guttowski, S., et al. *EMC issues in cars with electric drives*. in *Electromagnetic Compatibility, 2003 IEEE International Symposium on*. 2003.
54. Chingchi, C. and X. Xingyi. *Modeling the conducted EMI emission of an electric vehicle (EV) traction drive*. in *Electromagnetic Compatibility, 1998. 1998 IEEE International Symposium on*. 1998.
55. Gaul, H.W., T. Huettl, and C. Powers. *Radiated emissions testing of an experimental electric vehicle*. in *Electromagnetic Compatibility, 1996. Symposium Record. IEEE 1996 International Symposium on*. 1996.
56. Labrousse, D., B. Revol, and F. Costa, *Common-Mode Modeling of the Association of N-Switching Cells: Application to an Electric-Vehicle-Drive System.* Power Electronics, IEEE Transactions on, 2010. **25**(11): p. 2852-2859.
57. Guo, Y., L. Wang, and C. Liao, *Systematic analysis of conducted electromagnetic interferences for the electric drive system in electric vehicles.* Progress In Electromagnetics Research, 2013. **134**: p. 359-378.
58. Mutoh, N., et al., *EMI noise control methods suitable for electric vehicle drive systems.* Electromagnetic Compatibility, IEEE Transactions on, 2005. **47**(4): p. 930-937.
59. Shuo, W. *Improve vehicle's function safety with an approach investigating vehicle's electromagnetic interference with its function safety*. in *Vehicle Power and Propulsion Conference (VPPC), 2011 IEEE*. 2011.
60. Ltd, M.A.C., *Time Domain EMC Emissions Measurement System*, 2004, Multiple Access Communications Ltd.
61. Keller, C. and K. Feser, *Fast emission measurement in time domain.* Electromagnetic Compatibility, IEEE Transactions on, 2007. **49**(4): p. 816-824.

62. Krug, F. and P. Russer, *The time-domain electromagnetic interference measurement system.* Electromagnetic Compatibility, IEEE Transactions on, 2003. **45**(2): p. 330-338.
63. Winter, W. and M. Herbrig. *Time Domain Measurements in automotive applications*. in *Electromagnetic Compatibility, 2009. EMC 2009. IEEE International Symposium on*. 2009.
64. Winter, W. and M. Herbrig. *Time Domain Measurements a novel method for qualification of electronics*. in *Microwave Techniques (COMITE), 2010 15th International Conference on*. 2010.
65. De Santiago, L., et al. *Effect of electrical vehicle-driver interaction on the radiated electromagnetic emissions: Measurement methodology*. in *Industrial Technology (ICIT), 2010 IEEE International Conference on*. 2010. IEEE.
66. Ruddle, A.R., D.A. Topham, and D.D. Ward. *Investigation of electromagnetic emissions measurements practices for alternative powertrain road vehicles*. in *Electromagnetic Compatibility, 2003 IEEE International Symposium on*. 2003. IEEE.
67. Ruddle, A., *Investigation of electromagnetic emissions from alternative powertrain road vehicles (01-845060).* Nuneaton, UK: MIRA Ltd, 2002.
68. Paul, C.R., *Introduction to Electromagnetic Compatibility*. 2006: Wiley.
69. Paul, C.R., *A comparison of the contributions of common-mode and differential-mode currents in radiated emissions.* Electromagnetic Compatibility, IEEE Transactions on, 1989. **31**(2): p. 189-193.
70. Hockanson, D.M., et al., *FDTD modeling of common-mode radiation from cables.* Electromagnetic Compatibility, IEEE Transactions on, 1996. **38**(3): p. 376-387.
71. Smith, W.T. and R.K. Frazier. *Prediction of anechoic chamber radiated emissions measurements through use of empirically-derived transfer functions and laboratory common-mode current measurements*. in *Electromagnetic Compatibility, 1998. 1998 IEEE International Symposium on*. 1998.
72. Chinchi, C. *Predicting vehicle-level radiated EMI emissions using module-level conducted EMIs and harness radiation efficiencies*. in *Electromagnetic Compatibility, 2001. EMC. 2001 IEEE International Symposium on*. 2001.
73. Geping, L., et al. *Anticipating full vehicle radiated EMI from module-level testing in automobiles*. in *Electromagnetic Compatibility, 2002. EMC 2002. IEEE International Symposium on*. 2002.
74. Ala, G., et al., *Evaluation of Radiated EMI in 42-V Vehicle Electrical Systems by FDTD Simulation.* Vehicular Technology, IEEE Transactions on, 2007. **56**(4): p. 1477-1484.
75. Cajan, H., L. Pichon, and C. Marchand, *Finite element method for radiated emissions in EMC analysis.* Magnetics, IEEE Transactions on, 2000. **36**(4): p. 964-967.
76. Changyi, S. and T.H. Hubing, *Calculating Radiated Emissions Due to I/O Line Coupling on Printed Circuit Boards Using the Imbalance Difference Method.* Electromagnetic Compatibility, IEEE Transactions on, 2012. **54**(1): p. 212-217.
77. Troudet, T., S. Garg, and W.C. Merrill. *Neural network application to aircraft control system design*. in *AIAA Guidance, Navigation and Control Conference, New Orleans, LA, Technical Papers.* 1991.
78. Venugopal, K.P., R. Sudhakar, and A.S. Pandya, *On-line learning control of autonomous underwater vehicles using feedforward neural networks.* Oceanic Engineering, IEEE Journal of, 1992. **17**(4): p. 308-319.
79. Khashman, A., *Neural networks for credit risk evaluation: Investigation of different neural models and learning schemes.* Expert Systems with Applications, 2010. **37**(9): p. 6233-6239.
80. Castelaz, P.F. *Neural networks in defense applications*. in *Neural Networks, 1988., IEEE International Conference on*. 1988. IEEE.
81. Hollis, P.W. and J.J. Paulos, *Artificial neural networks using MOS analog multipliers.* Solid-State Circuits, IEEE Journal of, 1990. **25**(3): p. 849-855.

82. Hong, P., Z. Wen, and T.S. Huang, *Real-time speech-driven face animation with expressions using neural networks.* Neural Networks, IEEE Transactions on, 2002. **13**(4): p. 916-927.
83. Azoff, E.M., *Neural network time series forecasting of financial markets*. 1994: John Wiley & Sons, Inc.
84. Radhakrishnan, V. and A. Mohamed, *Neural networks for the identification and control of blast furnace hot metal quality.* Journal of process control, 2000. **10**(6): p. 509-524.
85. Brockett, P.L., et al., *A neural network method for obtaining an early warning of insurer insolvency.* Journal of Risk and Insurance, 1994: p. 402-424.
86. Zhang, H.-C. and S. Huang, *Applications of neural networks in manufacturing: a state-of-the-art survey.* THE INTERNATIONAL JOURNAL OF PRODUCTION RESEARCH, 1995. **33**(3): p. 705-728.
87. Brameier, M. and W. Banzhaf, *A comparison of linear genetic programming and neural networks in medical data mining.* Evolutionary Computation, IEEE Transactions on, 2001. **5**(1): p. 17-26.
88. Yu, S., K. Zhu, and F. Diao, *A dynamic all parameters adaptive BP neural networks model and its application on oil reservoir prediction.* Applied Mathematics and Computation, 2008. **195**(1): p. 66-75.
89. Fierro, R. and F.L. Lewis, *Control of a nonholonomic mobile robot using neural networks.* Neural Networks, IEEE Transactions on, 1998. **9**(4): p. 589-600.
90. Morgan, D.P. and C.L. Scofield, *Neural networks and speech processing*. 1991: Springer.
91. Kimoto, T., et al. *Stock market prediction system with modular neural networks*. in *Neural Networks, 1990., 1990 IJCNN International Joint Conference on*. 1990. IEEE.
92. Egmont-Petersen, M., D. de Ridder, and H. Handels, *Image processing with neural networks—a review.* Pattern recognition, 2002. **35**(10): p. 2279-2301.
93. Dougherty, M., *A review of neural networks applied to transport.* Transportation Research Part C: Emerging Technologies, 1995. **3**(4): p. 247-260.
94. Demuth, H. and M. Beale, *Neural network toolbox for use with MATLAB.* 1993.
95. Xiaopeng, D., et al., *Detection and Identification of Vehicles Based on Their Unintended Electromagnetic Emissions.* Electromagnetic Compatibility, IEEE Transactions on, 2006. **48**(4): p. 752-759.
96. Tsai, C.Y., E.J. Rothwell, and K.M. Chen, *Target discrimination using neural networks with time domain or spectrum magnitude response.* Journal of Electromagnetic Waves and Applications, 1996. **10**(3): p. 341-382.
97. Atkins, R.G., R.T. Shin, and J.A. Kong, *A neural network method for high range resolution target classification.* Progress In Electromagnetics Research, 1991. **4**: p. 255-292.
98. Koroglu, S., et al., *An approach to the calculation of multilayer magnetic shielding using artificial neural network.* Simulation Modelling Practice and Theory, 2009. **17**(7): p. 1267-1275.
99. K. Aunchaleevarapan, K.P., W. Khan-Ngern, and S. Nitta, *Novel Method for Predicting PCB Configurations for Near Field and Far Field Radiated EMI Using a Neural Network.* IEICE Trans. Commun., 2003. **E86**(B): p. 1364 - 1376.
100. Chahine, I., et al., *Characterization and Modeling of the Susceptibility of Integrated Circuits to Conducted Electromagnetic Disturbances Up to 1 GHz.* Electromagnetic Compatibility, IEEE Transactions on, 2008. **50**(2): p. 285-293.
101. P. Dangkham, P.S., S. Chaichana, K. Aunchaleevarapan, and P. Teekaput, *Recognition and Identification of Radiated EMI for Shielding Aperture using Neural Network.* PIERS Online, 2007. **3**(4): p. 444 - 447.
102. Luo, M. and K.-M. Huang, *Prediction of the electromagnetic field in metallic enclosures using artificial neural networks.* Progress In Electromagnetics Research, 2011. **116**: p. 171-184.

103. Zaharis, Z.D., K.A. Gotsis, and J.N. Sahalos, *Comparative study of neural network training applied to adaptive beamforming of antenna arrays.* Progress In Electromagnetics Research, 2012. **126**: p. 269-283.
104. Zaharis, Z.D., K.A. Gotsis, and J.N. Sahalos, *Adaptive beamforming with low side lobe level using neural networks trained by mutated boolean PSO.* Progress In Electromagnetics Research, 2012. **127**: p. 139-154.
105. Li, X. and J. Gao, *Pad modeling by using artificial neural network.* Progress In Electromagnetics Research, 2007. **74**: p. 167-180.
106. Al Salameh, M.S. and E.T. Al Zuraiqi, *Solutions to electromagnetic compatibility problems using artificial neural networks representation of vector finite element method.* Microwaves, Antennas & Propagation, IET, 2008. **2**(4): p. 348-357.
107. Bermani, E., S. Caorsi, and M. Raffetto, *An inverse scattering approach based on a neural network technique for the detection of dielectric cylinders buried in a lossy half-space.* Progress in Electromagnetic Research, 2000. **PIER 26**: p. 69-90.
108. Khare, M. and S.M.S. Nagendra, *Artificial neural networks in vehicular pollution modelling*. 2007: Springer.
109. Cybenko, G., *Approximation by superpositions of a sigmoidal function.* Mathematics of control, signals and systems, 1989. **2**(4): p. 303-314.
110. Mazroua, A.A., M. Salama, and R. Bartnikas, *PD pattern recognition with neural networks using the multilayer perceptron technique.* Electrical Insulation, IEEE Transactions on, 1993. **28**(6): p. 1082-1089.
111. Attali, J.-G. and G. Pagès, *Approximations of functions by a multilayer perceptron: a new approach.* Neural Networks, 1997. **10**(6): p. 1069-1081.
112. Yan, H., et al., *A multilayer perceptron-based medical decision support system for heart disease diagnosis.* Expert Systems with Applications, 2006. **30**(2): p. 272-281.
113. Bounds, D.G., et al. *A multilayer perceptron network for the diagnosis of low back pain*. in *Neural Networks, 1988., IEEE International Conference on*. 1988. IEEE.
114. Vidal, E., M. Castro, and M. Perceptron, *Classification of banded chromosomes using error-correcting grammatical inference (ECGI) and multilayer perceptron (MLP).* 1997.
115. Pandey, P. and S. Barai, *Multilayer perceptron in damage detection of bridge structures.* Computers & Structures, 1995. **54**(4): p. 597-608.
116. Agirre-Basurko, E., G. Ibarra-Berastegi, and I. Madariaga, *Regression and multilayer perceptron-based models to forecast hourly O< sub> 3</sub> and NO< sub> 2</sub> levels in the Bilbao area.* Environmental Modelling & Software, 2006. **21**(4): p. 430-446.
117. Moore, S., et al., *A modified multilayer perceptron model for gas mixture analysis.* Sensors and Actuators B: Chemical, 1993. **16**(1): p. 344-348.
118. Koskela, T., et al. *Time series prediction with multilayer perceptron, FIR and Elman neural networks*. in *Proceedings of the World Congress on Neural Networks*. 1996.
119. Watterson, J., *An optimum multilayer perceptron neural receiver for signal detection.* Neural Networks, IEEE Transactions on, 1990. **1**(4): p. 298-300.
120. Colombet, I., et al. *Models to predict cardiovascular risk: comparison of CART, multilayer perceptron and logistic regression*. in *Proceedings of the AMIA Symposium*. 2000. American Medical Informatics Association.
121. Hontoria, L., J. Aguilera, and P. Zufiria, *An application of the multilayer perceptron: solar radiation maps in Spain.* Solar energy, 2005. **79**(5): p. 523-530.
122. Xu, Y., et al., *Adaptive multilayer perceptron networks for detection of cracks in anisotropic laminated plates.* International Journal of Solids and Structures, 2001. **38**(32): p. 5625-5645.
123. Moulin, L., et al. *Support vector and multilayer perceptron neural networks applied to power systems transient stability analysis with input dimensionality reduction*. in *Power Engineering Society Summer Meeting, 2002 IEEE*. 2002. IEEE.

124. Morgan, N. and H. Bourlard. *Continuous speech recognition using multilayer perceptrons with hidden Markov models*. in *Acoustics, Speech, and Signal Processing, 1990. ICASSP-90., 1990 International Conference on*. 1990. IEEE.
125. Verma, B. *Handwritten Hindi character recognition using multilayer perceptron and radial basis function neural networks*. in *Neural Networks, 1995. Proceedings., IEEE International Conference on*. 1995. IEEE.
126. Sivakumar, K. and U. Desai, *Image restoration using a multilayer perceptron with a multilevel sigmoidal function.* Signal Processing, IEEE Transactions on, 1993. **41**(5): p. 2018-2022.
127. Gibson, G.J., S. Siu, and C. Cowen. *Multilayer perceptron structures applied to adaptive equalisers for data communications*. in *Acoustics, Speech, and Signal Processing, 1989. ICASSP-89., 1989 International Conference on*. 1989. IEEE.
128. Wasserman, P.D. and T. Schwartz, *Neural networks. II. What are they and why is everybody so interested in them now?* IEEE Expert, 1988. **3**(1): p. 10-15.
129. Gardner, M. and S. Dorling, *Artificial neural networks (the multilayer perceptron)--a review of applications in the atmospheric sciences.* Atmospheric environment, 1998. **32**(14-15): p. 2627-2636.
130. Shirvany, Y., M. Hayati, and R. Moradian, *Multilayer perceptron neural networks with novel unsupervised training method for numerical solution of the partial differential equations.* Applied Soft Computing, 2009. **9**(1): p. 20-29.
131. Pal, S.K. and S. Mitra, *Noisy fingerprint classification using multilayer perceptron with fuzzy geometrical and textural features.* Fuzzy sets and systems, 1996. **80**(2): p. 121-132.
132. Li, G. and Y. Gui-sheng. *Application of double hidden layer process neural network on wood drying modeling*. in *Industrial Engineering and Engineering Management (IE&EM), 2011 IEEE 18Th International Conference on*. 2011.
133. Niska, H., et al., *Evolving the neural network model for forecasting air pollution time series.* Engineering Applications of Artificial Intelligence, 2004. **17**(2): p. 159-167.
134. Kanellopoulos, I. and G.G. Wilkinson, *Strategies and best practice for neural network image classification.* International Journal of Remote Sensing, 1997. **18**(4): p. 711-725.
135. Goyal, S., *Advanced computing research on cascade single and double hidden layers for detecting shelf life of kalakand: An artificial neural network approach.* International Journal of Computer Science & Emerging Technologies, 2011. **2**(5).
136. Surkan, A.J. and J.C. Singleton. *Neural networks for bond rating improved by multiple hidden layers*. in *Neural Networks, 1990., 1990 IJCNN International Joint Conference on*. 1990.
137. Chan, H.-P., et al., *Computer-aided detection of mammographic microcalcifications: pattern recognition with an artificial neural network.* Medical Physics, 1995. **22**: p. 1555.
138. Goyal, S. and G.K. Goyal, *Study on single and double hidden layers of cascade artificial neural intelligence neurocomputing models for predicting sensory quality of roasted coffee flavoured sterilized drink.* International Journal of Applied Information Systems, 2012. **1**(3): p. 1-4.
139. Kawato, M., et al., *Trajectory formation of arm movement by cascade neural network model based on minimum torque-change criterion.* Biological Cybernetics, 1990. **62**(4): p. 275-288.
140. Seong-Whan, L. and K. Sang-Yup, *Integrated segmentation and recognition of handwritten numerals with cascade neural network.* Systems, Man, and Cybernetics, Part C: Applications and Reviews, IEEE Transactions on, 1999. **29**(2): p. 285-290.
141. Nechyba, M.C. and X. Yangsheng. *Cascade neural networks with node-decoupled extended Kalman filtering*. in *Computational Intelligence in Robotics and Automation, 1997. CIRA'97., Proceedings., 1997 IEEE International Symposium on*. 1997.

142. Schetinin, V., *A learning algorithm for evolving cascade neural networks.* Neural Processing Letters, 2003. **17**(1): p. 21-31.
143. Htike, K.K. and O.O. Khalifa. *Rainfall forecasting models using focused time-delay neural networks*. in *Computer and Communication Engineering (ICCCE), 2010 International Conference on*. 2010.
144. Wintoft, P. and L.R. Cander, *Short-term prediction of fof2 using time-delay neural network.* Physics and Chemistry of the Earth, Part C: Solar, Terrestrial & Planetary Science, 1999. **24**(4): p. 343-347.
145. Lang, K.J., A.H. Waibel, and G.E. Hinton, *A time-delay neural network architecture for isolated word recognition.* Neural Networks, 1990. **3**(1): p. 23-43.
146. Rawat, M., K. Rawat, and F.M. Ghannouchi, *Adaptive Digital Predistortion of Wireless Power Amplifiers/Transmitters Using Dynamic Real-Valued Focused Time-Delay Line Neural Networks.* Microwave Theory and Techniques, IEEE Transactions on, 2010. **58**(1): p. 95-104.
147. Wo, et al., *An adaptable time-delay neural-network algorithm for image sequence analysis.* Neural Networks, IEEE Transactions on, 1999. **10**(6): p. 1531-1536.
148. Reese, M.G., *Application of a time-delay neural network to promoter annotation in the Drosophila melanogaster genome.* Computers & Chemistry, 2001. **26**(1): p. 51-56.
149. Wöhler, C., et al. *A time delay neural network algorithm for real-time pedestrian recognition*. in *International Conference on Intelligent Vehicle*. 1998. Citeseer.
150. Xie, J.-X., et al., *A hybrid adaptive time-delay neural network model for multi-step-ahead prediction of sunspot activity.* International journal of environment and pollution, 2006. **28**(3): p. 364-381.
151. Zhu, J., et al., *An on-line wastewater quality predication system based on a time-delay neural network.* Engineering Applications of Artificial Intelligence, 1998. **11**(6): p. 747-758.
152. Waibel, A., et al., *Phoneme recognition using time-delay neural networks.* Acoustics, Speech and Signal Processing, IEEE Transactions on, 1989. **37**(3): p. 328-339.
153. Wan, E.A. *Time series prediction by using a connectionist network with internal delay lines*. in *SANTA FE INSTITUTE STUDIES IN THE SCIENCES OF COMPLEXITY-PROCEEDINGS VOLUME-*. 1993. ADDISON-WESLEY PUBLISHING CO.
154. Micu, D.D., et al. *Layer recurrent neural network solution for an electromagnetic interference problem*. in *Electromagnetic Field Computation (CEFC), 2010 14th Biennial IEEE Conference on*. 2010.
155. Siegelmann, H.T., B.G. Horne, and C.L. Giles, *Computational capabilities of recurrent NARX neural networks.* Systems, Man, and Cybernetics, Part B: Cybernetics, IEEE Transactions on, 1997. **27**(2): p. 208-215.
156. Ardalani-Farsa, M. and S. Zolfaghari, *Chaotic time series prediction with residual analysis method using hybrid Elman–NARX neural networks.* Neurocomputing, 2010. **73**(13–15): p. 2540-2553.
157. Maier, H.R. and G.C. Dandy, *Neural networks for the prediction and forecasting of water resources variables: a review of modelling issues and applications.* Environmental Modelling & Software, 2000. **15**(1): p. 101-124.
158. Patel, A. and J. Dunne, *NARX neural network modelling of hydraulic suspension dampers for steady-state and variable temperature operation.* Vehicle system dynamics, 2003. **40**(5): p. 285-328.
159. Dzielinski, A. *Neural networks based NARX models in nonlinear adaptive control*. in *Neural Networks, 1999. IJCNN'99. International Joint Conference on*. 1999. IEEE.
160. Lee, Y.-W. and T.-L. Chang, *Application of NARX neural networks in thermal dynamics identification of a pulsating heat pipe.* Energy Conversion and Management, 2009. **50**(4): p. 1069-1078.

161. Wang, J.-S. and Y.-P. Chen, *A fully automated recurrent neural network for unknown dynamic system identification and control.* Circuits and Systems I: Regular Papers, IEEE Transactions on, 2006. **53**(6): p. 1363-1372.
162. Lu, T. and M. Viljanen, *Prediction of indoor temperature and relative humidity using neural network models: model comparison.* Neural Computing and Applications, 2009. **18**(4): p. 345-357.
163. Miyajima, C., et al. *Cepstral Analysis of Driving Behavioral Signals for Driver Identification*. in *Acoustics, Speech and Signal Processing, 2006. ICASSP 2006 Proceedings. 2006 IEEE International Conference on*. 2006.
164. Wefky, A.M., et al., *Alternative Sensor System and MLP Neural Network for Vehicle Pedal Activity Estimation.* Sensors, 2010. **10**(4): p. 3798-3814.
165. Prieto, A., et al. *Sensorial system minimization to estimate the driver activity on the vehicle's pedals*. in *Emerging Technologies and Factory Automation (ETFA), 2010 IEEE Conference on*. 2010.
166. Wefky, A.M., et al., *Gear predictor of manual transmission vehicles based on artificial neural network*, 2009, WIT Press Publications: Southampton, UK. p. 37-46.
167. Wefky, A., et al., *Comparison of neural classifiers for vehicles gear estimation.* Applied Soft Computing, 2011. **11**(4): p. 3580-3599.
168. Jimenez-Palacios, J.L., *Understanding and quantifying motor vehicle emissions with vehicle specific power and TILDAS remote sensing*, 1998, Massachusetts Institute of Technology.
169. Frey, H.C., et al., *Comparing real-world fuel consumption for diesel-and hydrogen-fueled transit buses and implication for emissions.* Transportation Research Part D: Transport and Environment, 2007. **12**(4): p. 281-291.
170. Wang, H., et al., *Modelling of the fuel consumption for passenger cars regarding driving characteristics.* Transportation Research Part D: Transport and Environment, 2008. **13**(7): p. 479-482.
171. Zegeye, S., et al. *Model-based traffic control for the reduction of fuel consumption, emissions, and travel time*. in *mobil. TUM 2009-International Scientific Conference on Mobility and Transport-ITS for larger Cities*. 2009.
172. Krug, F., D. Mueller, and P. Russer, *Signal processing strategies with the TDEMI measurement system.* Instrumentation and Measurement, IEEE Transactions on, 2004. **53**(5): p. 1402-1408.
173. Wefky, A.M., et al., *Measurement Methodology for Radiated Emissions of Electrical Vehicles in Noisy Environments.*
174. Thales. http://www.thalesgroup.com/Countries/Netherlands/What_we_do/ECC/ECC_EMC/.
175. Ptitsyna, N., et al. *Analysis of magnetic fields onboard electric transport systems in regard to human exposure*. in *Electromagnetic Compatibility (EMC EUROPE), 2012 International Symposium on*. 2012.
176. Kopytenko, Y.A., et al. *Monitoring and Analysis of Magnetic Fields Onboard Transport Systems: Waveforms and Exposure Assessment*. in *Electromagnetic Compatibility and Electromagnetic Ecology, 2007 7th International Symposium on*. 2007.
177. Hornik, K., M. Stinchcombe, and H. White, *Multilayer feedforward networks are universal approximators.* Neural Networks, 1989. **2**(5): p. 359-366.
178. Haykin, S.S., *Neural networks: a comprehensive foundation*. 1994: Macmillan.
179. Hagan, M.T., H.B. Demuth, and M.H. Beale, *Neural Network Design*. 1996: Pws Pub.
180. Hagan, M.T. and M.B. Menhaj, *Training feedforward networks with the Marquardt algorithm.* Neural Networks, IEEE Transactions on, 1994. **5**(6): p. 989-993.
181. Møller, M.F., *A scaled conjugate gradient algorithm for fast supervised learning.* Neural networks, 1993. **6**(4): p. 525-533.
182. Battiti, R., *First-and second-order methods for learning: between steepest descent and Newton's method.* Neural computation, 1992. **4**(2): p. 141-166.

183. Setiono, R. and L.C.K. Hui, *Use of a quasi-Newton method in a feedforward neural network construction algorithm.* Neural Networks, IEEE Transactions on, 1995. **6**(1): p. 273-277.
184. Huang, G.-B., D. Wang, and Y. Lan, *Extreme learning machines: a survey.* International Journal of Machine Learning and Cybernetics, 2011. **2**(2): p. 107-122.
185. Guang-Bin, H., C. Lei, and S. Chee-Kheong, *Universal approximation using incremental constructive feedforward networks with random hidden nodes.* Neural Networks, IEEE Transactions on, 2006. **17**(4): p. 879-892.
186. Huang, G.-B., Q.-Y. Zhu, and C.-K. Siew, *Extreme learning machine: Theory and applications.* Neurocomputing, 2006. **70**(1–3): p. 489-501.
187. Yan, X., et al., *A Reliable Intelligent System for Real-Time Dynamic Security Assessment of Power Systems.* Power Systems, IEEE Transactions on, 2012. **27**(3): p. 1253-1263.
188. Samet, S. and A. Miri, *Privacy-preserving back-propagation and extreme learning machine algorithms.* Data & Knowledge Engineering, 2012. **79–80**(0): p. 40-61.
189. Song, Y., J. Crowcroft, and J. Zhang, *Automatic epileptic seizure detection in EEGs based on optimized sample entropy and extreme learning machine.* Journal of Neuroscience Methods, 2012. **210**(2): p. 132-146.
190. Decherchi, S., et al., *Circular-ELM for the reduced-reference assessment of perceived image quality.* Neurocomputing, (0).
191. Decherchi, S., et al., *Efficient Digital Implementation of Extreme Learning Machines for Classification.* Circuits and Systems II: Express Briefs, IEEE Transactions on, 2012. **59**(8): p. 496-500.
192. Choi, K., K.-A. Toh, and H. Byun, *Incremental face recognition for large-scale social network services.* Pattern Recognition, 2012. **45**(8): p. 2868-2883.
193. Minhas, R., A.A. Mohammed, and Q.M. Wu, *Incremental Learning in Human Action Recognition Based on Snippets.* Circuits and Systems for Video Technology, IEEE Transactions on, 2011. **PP**(99): p. 1-1.
194. Guang-Bin, H., et al., *Extreme Learning Machine for Regression and Multiclass Classification.* Systems, Man, and Cybernetics, Part B: Cybernetics, IEEE Transactions on, 2012. **42**(2): p. 513-529.
195. Bjorck, A., *Numerical methods for least squares problems*. 1996: Society for Industrial and Applied Mathematics.
196. Wefky, A.M., et al., *Modeling Radiated Electromagnetic Emissions of Electric Motorcycles in Terms of Driving Profile Using Mlp Neural Networks.* Progress In Electromagnetics Research, 2013. **135**: p. 231-244.
197. Haykin, S.S., *Adaptive filter theory*. 2002: Prentice Hall.
198. Bishop, C.M. and G. Hinton, *Neural Networks for Pattern Recognition*. 1995: Clarendon Press.